Linköping Studies in Science and Technology
Thesis, No 1528

Diagnosis and Supervision of Industrial Gas Turbines

Emil Larsson

Linköping University
INSTITUTE OF TECHNOLOGY

Department of Electrical Engineering
Linköping University, SE-581 83 Linköping, Sweden

Linköping 2012

Linköping Studies in Science and Technology
Thesis, No 1528

Emil Larsson
lime@isy.liu.se
www.vehicular.isy.liu.se
Division of Vehicular Systems
Department of Electrical Engineering
Linköping University
SE–581 83 Linköping, Sweden

Larsson, Emil
Diagnosis and Supervision of Industrial Gas Turbines
ISBN 978-91-7519-914-6
ISSN 0280-7971
LIU-TEK-LIC-2012:13

Typeset with LaTeX 2ε
Printed by LiU-Tryck, Linköping, Sweden 2012

Abstract

Monitoring of industrial gas turbines is of vital importance, since it gives valuable information for the customer about maintenance, performance, and process health. The performance of an industrial gas turbine degrades gradually due to factors such as environment air pollution, fuel content, and ageing to mention some of the degradation factors. The compressor in the gas turbine is especially vulnerable against contaminants in the air since these particles are stuck at the rotor and stator surface. The loss in compressor performance, due to fouling, can partially be restored by an on-line/off-line compressor wash. If the actual health state of the gas turbine is known, it is possible to efficiently plan the service and maintenance and thereby reduce the environmental impact and the fuel cost for the customer.

A thermodynamic gas turbine modeling package, called GTLib, is developed in the equation-based object-oriented modeling language Modelica. Using the GTLib package, a gas turbine model can be constructed. The gas turbine model can be used for performance calculation and as a base when diagnosis tests are generated. These tests can be used in a diagnosis and supervision system to detect compressor fouling and abrupt sensor faults. One of the benefits with using GTLib is the ability to model a lean stoichiometric combustion at different air/fuel ratio. Using the air/fuel ratio concept, an arbitrary number of gas species in the in-coming air can be considered. The number of equations is reduced if the air/fuel ratio concept is considered instead of modeling each gas species separately. The difference in the number of equations is significant if many gas species are considered.

When the gas turbine components deteriorate, a mismatch between the nominal performance model and the measurements increase. To handle this, the gas turbine model is augmented with a number of estimation parameters. These estimation parameters are used to detect slow deterioration in the gas turbine components and are estimated with a Constant Gain Extended Kalman Filter (CGEKF). The state estimator is chosen using structural methods before an index reduction of the model is performed. Experimental data is investigated and it is shown that the performance degradation due to compressor fouling can be estimated. After the compressor is washed, the performance of the compressor is partially restored. An abrupt sensor fault of 1 % of the nominal value is introduced in the discharge temperature of the compressor. The sensor fault can be detected using the CUSUM algorithm for change detection.

Finally, the overall thesis contribution is the calculation chain from a simulation model used for performance calculation to a number of test quantities used in a diagnosis and supervision system. Since the considered gas turbine model is a large non-linear DAE model that has unobservable state variables, the test construction procedure is automatically performed with developed parsers.

Acknowledgments

This work has been carried out at the Division of Vehicular Systems at the department of Electrical Engineering, Linköping University. The research has been funded by the Swedish Energy Agency, Siemens Industrial Turbomachinery AB, Volvo Aero Corporation, and the Royal Institute of Technology through the Swedish research program TURBOPOWER, the support of which is gratefully acknowledged.

First of all I would like to express my gratitude to my supervisors Jan Åslund, Erik Frisk, and Lars Eriksson for all their support during these years as a Ph.D. Student at the research group at the Vehicular Systems.

All colleagues at the Vehicular Systems are acknowledged for maintaining a pleasant research atmosphere. Christofer Sundström is acknowledged for proofreading a part of the licentiate thesis manuscript with valuable inputs and regarding specific diagnosis issues. My former room-mate Andreas Thomasson is thanked for interesting thermodynamic discussions. Erik Hellström is thanked for C and Matlab implementation issues regarding functions known as MapCalc.

Mats Sjödin, chairman of the Processes and Diagnostics steering committee, is thanked for sharing his expertise according to industrial gas turbine applications. Jesper Waldfelt, Lennart Näs, Åsa Lovén, and Christer von Wowern from Siemens Industrial Turbomachinery AB in Finspång are all acknowledged regarding issues according to measurement data and developed models by the company.

Finally, I would like to express my gratitude to Marie for her support and encouragement.

Emil Larsson
Linköping, March 2012

Contents

1 Introduction **1**

1.1 Modelica . . . 1
1.1.1 Connectors . . . 2
1.2 Simulation Environment . . . 2
1.2.1 The Reference Gas Turbine Model . . . 4
1.3 Problem Statement . . . 5
1.4 Thesis Contributions . . . 5
1.5 Thesis Outline . . . 6

2 Thermodynamic Concepts **9**

2.1 Thermodynamic System . . . 10
2.1.1 Thermodynamic Quantities . . . 10
2.1.2 Thermodynamic Laws . . . 11
2.2 Thermodynamic Properties of Species . . . 12
2.2.1 Specific Heat Capacity of Species . . . 14
2.2.2 Enthalpy of Species . . . 14
2.2.3 Entropy of Species . . . 15
2.2.4 Gibbs Free Energy . . . 16
2.3 Combustion . . . 16
2.3.1 Stoichiometry . . . 17
2.3.2 Chemical Equilibrium . . . 20
2.3.3 Comparison of the Heat Capacity Between the Stoichiometric Gas Description and the Chemical Equilibrium Calculation . . . 24
2.3.4 Mixing of Exhaust Gases with Different Lambda . . . 25
2.4 Ideal Gas Model . . . 25
2.4.1 Thermodynamics Properties for Frozen Mixtures . . . 26
2.4.2 Mass Concentration Differential dX . . . 26
2.5 Energy Conservation of Thermodynamic Systems . . . 27
2.5.1 Thermodynamic Differentials dU, dW, and dQ . . . 27
2.5.2 Energy of the Mixture of Frozen Ideal Gases . . . 28
2.6 Control Volume Model . . . 29
2.6.1 Lambda Concentration Differential $d\lambda$ . . . 29

2.6.2 State Equations . . . 30
2.7 Conclusion . . . 31

3 GTLib – Thermodynamic Gas Turbine Modeling Package 33
3.1 Background . . . 34
3.1.1 The Gas Turbine Cycle . . . 35
3.1.2 Performance Characteristics . . . 35
3.2 Gas Turbine Library – GTLib . . . 38
3.2.1 Variation in Ambient Air Composition . . . 39
3.2.2 Gas Turbine Model . . . 41
3.3 Implementation of GTLib . . . 43
3.3.1 Connectors . . . 43
3.3.2 Medium Model Package . . . 43
3.3.3 Components . . . 48
3.4 Conclusion . . . 52

4 Diagnosability Analysis and Test Selection Procedure 53
4.1 Gas Turbine Monitoring . . . 54
4.1.1 Gas Path Analysis . . . 54
4.1.2 Engine Health Monitoring . . . 56
4.2 Gas Turbine Diagnosis Model . . . 56
4.2.1 Input and Output signals . . . 57
4.2.2 Health Parameters . . . 57
4.2.3 Sensor Faults . . . 59
4.2.4 Differential Algebraic Equation Form . . . 60
4.3 Diagnosability Analysis . . . 61
4.3.1 Structural Analysis . . . 62
4.4 DAE-Index Analysis . . . 65
4.4.1 DAE-Index Reduction . . . 67
4.4.2 Algebraic Manipulation of the $\tilde{E}$ matrix . . . 68
4.4.3 Semi-Explicit Index-1 DAE . . . 70
4.4.4 DAE-index 1 Conservation in the Over-Determined M^+ Part . . . 71
4.5 Observability Analysis . . . 72
4.5.1 Structural Observability . . . 73
4.5.2 Removing of Unobservable Modes . . . 74
4.5.3 Number of Health Parameters in the Model . . . 75
4.6 Diagnosis Test Equations . . . 76
4.7 Parsers for an Automatic Extraction of Sub Systems . . . 77
4.7.1 Dymola Parser – Automatic Extraction of the DAE Model . . . 78
4.7.2 Structural Model Parser . . . 79
4.7.3 Index Reduction Parser . . . 79
4.7.4 Ordinary Differential Equation Construction Parser . . . 79
4.8 Conclusion . . . 81

5 Estimation of Health Degradation in Industrial Gas Turbines **83**
5.1 Background . . . 84
5.1.1 Experiment Setup . . . 85
5.2 Introductory Methods to Determine Compressor Fouling . . . 86
5.2.1 Bell-Mouth Based Estimation . . . 87
5.2.2 Pressure Ratio Based Mass Flow Estimation . . . 88
5.2.3 Performance Model Based Mass Flow Estimation . . . 88
5.2.4 Power versus Mass Flow of Fuel . . . 88
5.3 Measurement Delta Calculation . . . 90
5.4 Constant Gain Extended Kalman Filters . . . 93
5.4.1 Observer Design . . . 94
5.4.2 Evaluation of the CGEKF Based Test Quantity . . . 99
5.5 Overall Results of the Performance Estimation Techniques . . . 105
5.5.1 Bell-Mouth Based Estimation . . . 105
5.5.2 Measurement Delta Calculation . . . 105
5.5.3 Constant Gain Extended Kalman Filters . . . 109
5.6 Conclusion . . . 109

6 Conclusion **111**

References **113**

A Mole/Mass Conversions **119**
A.1 Mole/Mass Fraction Calculation . . . 119
A.2 Stoichiometry Matrix Expressed in Mass . . . 120
A.3 Determination of Stoichiometric Air/Fuel Ratio . . . 120

B Measurement Plots **121**
B.1 Ambient Temperature T_0 . . . 122
B.2 Ambient pressure p_0 . . . 123
B.3 Shaft Speed n_{C1} of the Gas Generator . . . 124
B.4 Generated Power by the Application . . . 125

C Health Parameter Plots **127**
C.1 $\Delta\Gamma_{C1}$ – Flow Deviation of *C1* . . . 128
C.2 $\Delta\eta_{T1}$ – Efficiency Deviation of *T1* . . . 129
C.3 $\Delta\Gamma_{T1}$ – Flow Deviation of *T1* . . . 130
C.4 $\Delta\eta_{To}$ – Efficiency Deviation of *To* . . . 131

Chapter 1

Introduction

Monitoring of industrial gas turbines is of vital importance, since it gives valuable information for the customer about maintenance, performance, and process health. The performance of an industrial gas turbine degrades gradually due to factors such as environment air pollution, fuel content, and ageing to mention some of the degradation factors. The compressor in the gas turbine is especially vulnerable against contaminants in the air since these particles are stuck at the rotor and stator surface. The loss in compressor performance, due to fouling, can partially be restored by an on-line/off-line compressor wash. If the actual health state of the gas turbine is known, it is possible to efficiently plan the service and maintenance and thereby reduce the environmental impact and the fuel cost for the customer.

For the work in this thesis, a real world simulation platform is provided by the industry partner Siemens Industrial Turbomachinery AB in Finspång, Sweden. The simulation platform is built from an in-house thermodynamic library called *SiemensLib* which is implemented in the modeling language Modelica. The simulation platform is mainly used for performance calculation and other in-house tools are considered for diagnosis and supervision statements. Therefore, an overall idea with this work is to integrate the Modelica performance model also in the design of the diagnosis and supervision system of the gas turbine. The motive for the introduction of a systematically design of the diagnosis and supervision system is the ability to have one combined model instead of two separate models. In two separate models, parameters and components have to be updated in both models which can result in unnecessary mistakes.

1.1 Modelica

Modelica is an equation based object oriented modeling language where the focus on reusing component and model libraries is applied. In an equation based language the relationships between variables are specified by the user simultaneously the causality

is left open. An open causality means that the order to calculate the variables does not have to be specified by the user. An example where a model of an ideal resistor should be designed, the user specifies the relation of the involved variables according to Ohm's law, i.e., the equation $U = IR$ in the model component. In this simple example, the voltage U, the current I, or the resistance R can be calculated depending on the available input signals or the surrounding variables. This, together with the object oriented nature of the language simplifies the construction of component libraries since models can be reused where the same base class model can be used in all the three cases.

Another advantage with the Modelica language is the concept of multi-domain modeling which means that different kinds of physical domains can be encapsulated in the same model. In the available simulation platform, shown in Figure 1.1, the considered domains are; the thermodynamic, the mechanical, and the electrical domain. In Modelica, state equations and algebraic constraints can be mixed which results in a model that is in a differential algebraic equation (DAE) form. For a differential algebraic equation model, the DAE-index of the model is an important property. For simulation purposes, a state-space form of the system model is desirable and the DAE-index is one measure of how easy/hard it is to obtain a state-space form. In general, higher index problems are often more complicated than lower index problems to simulate. Simulations of DAE-system are well described in Hairer et al. (1991).

For a comprehensive description of the Modelica language, see the language specification at the webpage in Modelica Association (2007), or the textbooks by Fritzson (2004); Tiller (2001). In Casella et al. (2006), the Media library available in the standard Modelica package is presented.

1.1.1 Connectors

It is desirable, in a physical model based framework, that components exchange information only through special connection points. In Modelica, these connection points are called *connectors*. There are basically two kinds of variables in a connector, and these variables are either defined as a *flow*, or a *non-flow* variable. In a connection point, flow variables are summed to zero and non-flow variables are set equal.

1.2 Simulation Environment

The available simulation platform consists of a controller, a fuel system, a starter motor, a transmission, and a two shafted gas turbine. The simulation platform and its components are shown in Figure 1.1. All of these components are written in the modeling language Modelica, and the platform is simulated through the tool *Dynamic Modeling Laboratory* (Dymola). The experimental platform can be used for start/stop trip simulations, and other dynamic and static operational cases. During the simulation, environment conditions such as pressure, temperature, and relative humidity of the incoming air can be varied. A modification in these ambient conditions changes the composition of species in the incoming air. The ambient component adjusts the amount of water steam in the incoming air which can affect, e.g., the efficiency and mass flow of the gas turbine.

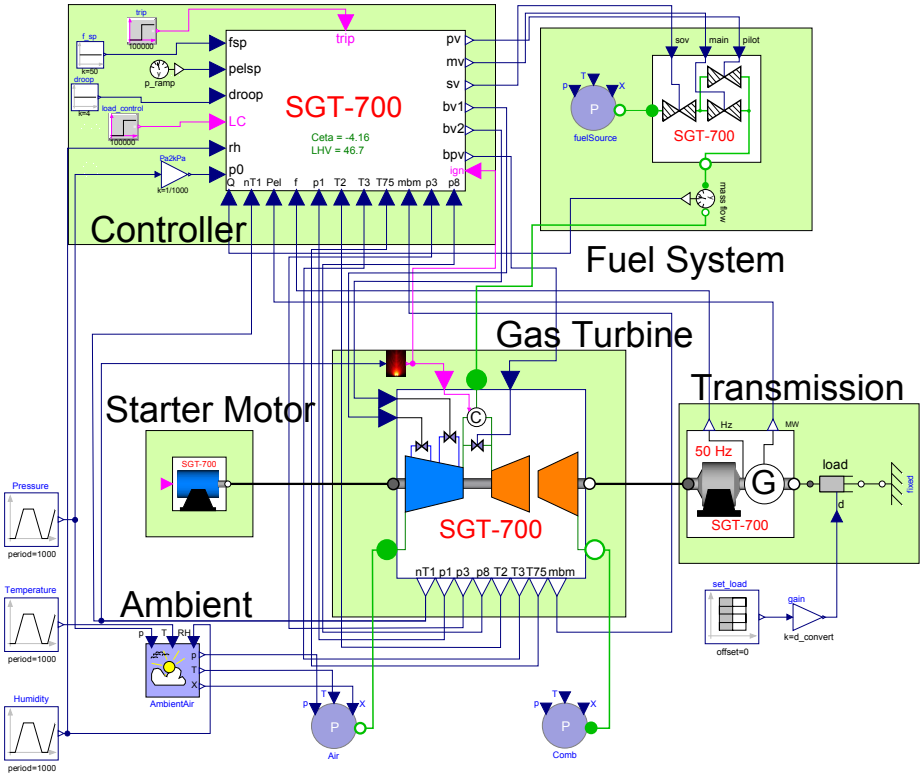

Figure 1.1: The simulation platform, used for performance calculation, consists of a controller, a fuel system, a starter motor, a transmission, and a two shafted gas turbine. All of these components are implemented in Modelica and are simulated through the tool Dymola. The input signals are the ambient pressure, the ambient temperature, the relative humidity of ambient air, and the desired application power.

Pressure and temperature have a direct impact on the efficiency and the mass flow, even if the air composition is fixed. Thus, in the simulation platform it is possible to have the air composition fixed but change the pressure and the temperature of the incoming air.

The advantage with the simulation platform is the ability to evaluate reliable performance estimation of parameters throughout the gas path, due to different operational conditions. The input signals to the simulation platform are the ambient pressure, the ambient temperature, the relative humidity of ambient air, and the desired generator power. In the simulation platform, the speed of the power turbine is fixed since here the application is a 50 Hz electrical generator. It is easy to modify the platform to also handle variable speed of the power turbine, i.e., a simulation of a mechanical drive application instead of an electrical generator.

1.2.1 The Reference Gas Turbine Model

One of the components in the simulation platform, shown in Figure 1.1, is the gas turbine model. The gas turbine model utilizes the Modelica Media package, included in the standard Modelica library, to describe the thermodynamic properties of the fluid. A medium model, which can be constructed with the Modelica Media is flexible since mixtures of ideal gases can be modeled. This approach gives a number of equations in the gas turbine model that increases drastically with the number of species in the described gas. The number of equations is increased since each species in the gas is described by a separate state in each control volume in the model. This results in a linear relationship between the number of species in the gas and the number of equations in the overall gas turbine model. The reference model has about 2500 equations and 60 states which are considered large. More details about the reference gas turbine model, in an early stage, can be found in Idebrant and Näs (2003). The reference model has been used as a reference for the gas turbine model presented in Chapter 3. The validation of the gas turbine model also relies on the reference model.

Input and Output signals

All industrial gas turbines are equipped with a number of actuators and instrumentation sensors that measure temperatures, pressures, and shaft speeds. The instrumentation sensor positions of the measured quantities temperature and pressure are located at different cross-sectional areas throughout the gas path, while the speed sensors measure the rotational speed of the gas generator n_{C_I} and the rotational speed of the power turbine n_{To}. The measured temperatures are the compressor inlet temperature T_2, the compressor discharge temperature T_3, and the exhaust gas temperature T_{75} after the power turbine. The measured pressures are the compressor inlet pressure p_1, the compressor discharge pressure p_3, and the exhaust gas pressure p_8. The index number notation in the sensor describes the cross-sectional area position of the actual sensor, where low index number is for the air entrance and high index number is for the exhaust gas that leaves the gas turbine. The sensor position in the gas turbine model will be shown in Figure 3.7.

In some of the cross-sectional areas, the quantity is measured with more than one sensor. For example, the discharge pressure p_3 is measured with the three sensors $p_{3,1}$,

$p_{3,2}$, and $p_{3,3}$. The exhaust temperature T_{75} is measured with sensors in three rings where each ring has 16 thermocouples. The total number of sensors that measure the temperature T_{75}, at different location around the circumference of the three rings, is 48. The large number of thermocouples in the exhaust gas is used, e.g., to monitor the burners in the combustion chamber to discover if any burner has a poor flame.

The instrumentation sensor signals are primarily used by the control system to maintain correct actuator values. In the reference gas turbine model, the actuators are used to control; the bleed valves, the combustor bypass valve, and the combustor flame. The bleed valves are usually used during start-up phases to avoid surge in the compressor, and the bypass valve is usually used during partial base loads. In the fuel system, the actuators are used to maintain correct fuel flow.

1.3 Problem Statement

The aim of this work is to investigate a model based approach for diagnosis and supervision of industrial gas turbines. Since the available gas turbine fleet consists of a large number of individuals, where all of them have their own properties and are running under different ambient conditions, it is desirable that the design of the diagnosis and supervision system is systematic. The intention with a systematic design is: (1) the diagnosis tests for different gas turbine hardware configurations should be generated easily, (2) the equations, which are necessary to consider in the diagnosis tests, should be selected carefully from the performance model. The systematic design is especially important since the available reference gas turbine model, used for performance calculation, is a large differential algebraic equation (DAE) model which is non-linear. Early investigations show that the reference model has unobservable state variables which need to be removed if observer based diagnosis tests are constructed.

1.4 Thesis Contributions

The contribution of the work is mainly divided into the two papers:

- In Larsson et al. (2010) the contribution is the gas turbine thermodynamic library GTLib, implemented in Modelica. One of the benefits with using GTLib is the ability to model a lean stoichiometric combustion at different lambda. With the GTLib package, a gas turbine model is constructed which has similar accuracy as the reference model but utilizes fewer equations. Models constructed in GTLib can be used for performance calculation and in the construction procedure of diagnosis tests. Therefore, another contribution with the GTLib package is the ability to generate observer based diagnosis tests directly from the constructed model in Modelica.

- In Larsson et al. (2011), the first contribution is the extension of GTLib to also handle changes in the amount of water steam in the incoming air. This topic is studied since a variation in absolute humidity affects the estimation parameters

used for compressor fouling detection. The change of absolute humidity in GTLib occur *quasi-static* in all involved model components, which means that all thermodynamic properties referred to the absolute humidity change simultaneously in all components. The second contribution in the paper is the investigation of the so-called health parameters which are used to estimate performance deterioration. The health parameters are introduced in the performance equations in the diagnosis model. The systematic method to construct diagnosis tests, developed in the previous paper, is used to generate a Constant Gain Extended Kalman Filter (CGEKF) which is used to estimate the health parameters. The generated filter is then utilized on experimental data from a mechanical drive site during a sequence length of one year. In the estimation of the compressor efficiency, it is possible to see a degradation in the health parameter due to compressor fouling. After the compressor is washed the efficiency is partially restored.

1.5 Thesis Outline

The thesis is divided into two main parts, where the two first chapters consist of the modeling work of the gas turbine. The following two chapters describe the design of the diagnosis and supervision system.

In Chapter 2, thermodynamic concepts that are used in the media model are presented. The media model is a part of the GTLib package and is used everywhere in the gas turbine model where a gas is described. The combustion of air and fuel is introduced in the chapter, and the combustion is based on a stoichiometric combustion. The state of the gas in a control volume is specified through the three state variables; pressure p, temperature T, and air/fuel ratio λ. When the state variable λ is known, the mass fraction of species in the exhaust gas can be calculated. Here, the gas species argon (Ar), oxygen (O_2), nitrogen (N_2), carbon dioxide (CO_2), and water (H_2O) are considered. With the air/fuel ratio description, pure atmospheric air can be described with an infinitely large air/fuel ratio λ.

In Chapter 3, the implementation of the gas turbine components in the GTLib-package, described in Chapter 2, is presented. These components are then used in an introductory control volume example where the focus is on variation in ambient conditions. The constructed gas turbine model used for performance calculation is also shown in this chapter.

In Chapter 4, a diagnosability analysis of the diagnosis gas turbine model is performed. In the diagnosis model, a number of extra estimation parameters, i.e., so-called health parameters is introduced. These parameters should capture deviation in performance due to fouling, and other factors that can affect the performance. The equations, which are used in each diagnosis test, are selected by structural methods. Since observer based tests are derived in Chapter 5, the derived test equations must be observable. An observability analysis, together with an index reduction are performed of the test equations. A number of parsers is presented in the chapter. These parsers are used to convert the diagnosis model into runnable Matlab code. The Matlab environment is used here because of the available tools for diagnosis analysis that are implemented in Matlab.

In Chapter 5, three studies are presented where techniques of performance deterioration estimations are investigated. In the first study, a simple approach to calculate deterioration due to compressor fouling is presented. In the next two studies, the gas turbine model is used as a base for the estimation techniques. In the second study, the estimations are based on so-called measurement deltas, which are generally the difference between the simulated, and the measured gas path quantity. In the third study, a non-linear Kalman observer is evaluated on two test cases. In the first test case, simulated data from the reference platform is evaluated for different operational points and different atmospheric weather conditions. In the second test case, experimental data from a gas turbine mechanical drive site in the Middle East is evaluated. Finally, to see how the monitoring system reacts on a faulty sensor, an abrupt bias change is added to one of the measurement signals and a change detection algorithm is used to detect the injected sensor fault.

Chapter 2

Thermodynamic Concepts

The objective of this chapter is to study important thermodynamic concepts that are useful in the development of a physical based gas turbine model used for: (1) performance calculation, (2) supervision of components, and (3) diagnosis statements. An important part of a gas turbine model is the description of the gas used throughout the gas path. Here, the gas description is encapsulated in a medium model where all the thermodynamic calculations are performed. In the gas turbine application, two types of gas medium are used; air and fuel. These two fluids consist of a number of gas species specified by the user. The thermodynamic properties of the species are based on the well known NASA polynomials.

In the chapter, the main focus is on a combustion process where two types of combustion are presented. These two types of combustion are based on (1) a chemical equilibrium calculation, and (2) a combustion based on stoichiometry. A comparison study between these two combustion models for different temperatures and air/fuel ratios is performed. The concept of a stoichiometric combustion is then incorporated in the gas model through the air/fuel ratio variable λ, which is the main difference against the available reference Modelica Media package. The benefit with using the λ state variable is the reduction of model equations in the gas turbine model, which gives a model that is easier to handle in practice. The disadvantage is that only pure air and exhaust gas with $\lambda \geq 1$ can be used throughout the gas path. This means that an arbitrary gas species cannot be injected, e.g., pure oxygen, which should destroy the air/fuel ratio. It is not a problem to inject cooling air in the exhaust gas that can be used to cool the first blades in the turbine.

In Section 2.5, the energy conservation for a mixture of ideal gases is derived, which leads to the specification of the state equations in the control volume model presented in Section 2.6.

2.1 Thermodynamic System

The purpose with the present chapter is to introduce important thermodynamic relationships that are used when a gas process in a gas turbine application is modeled. A gas turbine is a thermodynamic system, and a thermodynamic system is defined as an amount of space with a surrounding boundary against its environment. The thermodynamic system can either be *open* or *closed*. In an open system, the boundary lets mass, heat, and work passing through. In a closed system, the boundary only allows heat and work to be transferred. Since the gas turbine application is an open system, only this case is considered in the sequel. The thermodynamic system itself is called a *control volume* in the thesis. The control volume model is a central component in the developed gas turbine library GTLib since it works as a bridge between the thermodynamic calculations performed in the medium model with the remaining part of the gas turbine model. The GTLib package will be presented in Chapter 3. The intention with the present chapter is to give an introductory insight for thermodynamic models that can be used when a gas turbine should be modeled and later on simulated. For a more comprehensive thermodynamic survey, see, e.g., Eastop and McConkey (1993); Heywood (1988); Borman and Ragland (1998); Turns (2000); Öberg (2009).

2.1.1 Thermodynamic Quantities

The state of a thermodynamic system can be described by a number of quantities. The most commonly occurring quantities are; temperature T, pressure p, volume V, mass m, enthalpy h, and internal energy u. For a gas that occupy a volume V, the state of the gas can be described with an independent pair of thermodynamic quantities. Depending on this choice, the appearance of the described system equations are different, and an example of an independent pair of variables is the states pressure p and temperature T for a known gas volume. From the state variables, all the other thermodynamic quantities can be derived, e.g., mass m and enthalpy h. In a thermodynamic system it is often possible to measure both the pressure and the temperature and therefore are these quantities often called *measured* quantities since they are measurable. When a thermodynamic system has to be analyzed, it can be convenient to introduce quantities that are not directly measurable, and these variables are called *intermediate* quantities. Internal energy u and enthalpy h are examples of such quantities. The enthalpy h is defined:

$$h = u + pv \tag{2.1}$$

where v is the specific volume of the gas. In open systems, Eq. (2.1) is suitable to consider since it simplifies the model equations where the enthalpy encapsulates both the internal energy and the mechanical work applied to the system which is affected by a flowing fluid into the control volume.

Mass specific quantities are denoted with lower case letters in the sequel and specific quantities do not vary with the size of the system. Upper case letters are usually applied to denote the total amount of a certain quantity of the system. In some cases it is more suitable to consider the mole specific quantities, and here is the tilde convention over

the corresponding mass specific quantity used. The total energy can for example be expressed, either in masses or in moles, according to:

$$U = mu = n\tilde{u} \tag{2.2}$$

where m is the total mass, and n is the total number of moles in the gas.

Specific Heat Capacities

To describe the amount of energy that is needed to increase the temperature of a fluid one degree, for a unit mass, the specific heat capacities are used. Since the amount of energy that is required for a system that undergoes a constant-volume or a constant-pressure thermodynamic process is different, two specific heat capacities c_v and c_p are defined according to:

$$c_v = \left(\frac{\partial q}{\partial T}\right)_v, \; c_p = \left(\frac{\partial q}{\partial T}\right)_p \tag{2.3}$$

where q is the amount of energy, v denotes a constant-volume process, and p denotes a constant-pressure process. An example of a constant-volume process is a fluid in a bomb calorie meter, and an example of a fluid that undergoes a constant-pressure combustion process is the fluid in a bunsen burner. Combustion chambers in the gas turbines are typically bunsen burners.

The heat capacities of a reversible process can be written:

$$c_v = \left(\frac{\partial u}{\partial T}\right)_v, \; c_p = \left(\frac{\partial h}{\partial T}\right)_p \tag{2.4}$$

where the first law of thermodynamics (2.6) for a reversible thermodynamic process together with the enthalpy definition (2.1) are considered.

The ratio of the specific heat capacities is defined:

$$\gamma = \frac{c_p}{c_v} \tag{2.5}$$

The gamma ratio is frequently used when an isentropic compression or expansion processes are considered.

2.1.2 Thermodynamic Laws

The first law of thermodynamics states that the energy in a system that undergoes a closed thermodynamic cycle cannot either be created, or destroyed. The energy is merely converted between thermal energy (heat) and mechanical energy (work). For a thermodynamic cycle that is open, the intrinsic energy of the fluid can increase or decrease. The first law of thermodynamics is written:

$$dU = dQ + dW \tag{2.6}$$

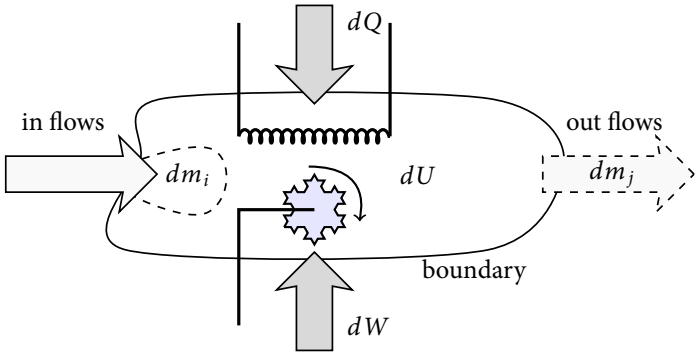

Figure 2.1: Sign conventions for an open thermodynamic system are shown in the figure. Positive flow directions are into the control volume. For a time interval dt, the amount of heat dQ and the work done on the system is dW. At the same time, the mass dm_i is added to the system while the mass dm_j is removed from the system.

where U is the internal energy, Q is the supplied heat, and W is the supplied work. The sign conventions of the energy flows are shown in Figure 2.1.

If the system undergoes a *reversible* thermodynamic process, the supplied work is $dW = -pdV$ and the first law of thermodynamic can be rewritten:

$$dU = dQ - pdV \tag{2.7}$$

where p is the pressure and V is the volume. The second law of thermodynamics can be written:

$$\frac{dQ}{T} \leq dS \tag{2.8}$$

where S is the entropy, and T is the temperature. The equality (2.8) holds for all reversible processes.

2.2 Thermodynamic Properties of Species

A gas media, used in a thermodynamic system, can either consist of pure substances or a mixture of substances. These substances are called species. For example, the atmosphere air media consists of the species: nitrogen, oxygen, argon, etc. Once the composition of the gas mixture is known, thermodynamic properties such as enthalpy, entropy, and heat capacity can be determined either on a mass basis, or on a mole basis as shown in:

$$h = \Sigma x_i h_i, \qquad \tilde{h} = \Sigma \tilde{x}_i \tilde{h}_i \tag{2.9a}$$

$$s = \Sigma x_i s_i, \qquad \tilde{s} = \Sigma \tilde{x}_i \tilde{s}_i \tag{2.9b}$$

$$c_p = \Sigma x_i c_{p,i}, \qquad \tilde{c}_p = \Sigma \tilde{x}_i \tilde{c}_{p,i} \tag{2.9c}$$

where x_i is the mass concentration, and $\tilde{x}_i$ is the mole concentration of species i.

In this section, the thermodynamic properties for the species in (2.9) will be presented. To describe these thermodynamic properties of an ideal gas, tabulated data can be used. The NIST-JANAF thermochemical tables in Chase (1998) consist of tabulated data of many different species. The NIST-JANAF tables are well known, and the thermodynamic data is available in a wide range of pressure and temperature with high accuracy. Since the data is in a tabular form, it can be necessary to interpolate between the points depending on the application.

Another method to describe gas properties is to use polynomial curve fitting techniques. The main advantage with using polynomials is the ability to encapsulate a large amount of thermodynamic data with only a few polynomial coefficients. Since polynomials are continuous, they can be differentiated easily which can reduce the simulation time.

An early chemical equilibrium program (CEC71) contribution is presented in Gordon and McBride (1971) where the heat capacity is described by a fourth-order polynomial with constant coefficients $a_1, \ldots, a_5$. These coefficients are approximated with a least-square technique (McBride and Gordon, 1992). To describe enthalpy and entropy the heat capacity coefficients are extended with a_6 and a_7. For every species, two sets of coefficients are available. These sets are divided into a low temperature 200 – 1 000 K range and a high temperature 1 000 – 6 000 K range. The chemical equilibrium program (CEA) presented in Gordon and McBride (1994) is an extension of the previous developed CEC71 program. In the new program, the thermodynamic heat capacity data is represented by two more coefficients. An additional temperature interval 6 000 to 20 000 K is added for some species. A summary of the NASA Glenn least-square coefficients and the tabulated thermodynamic data are shown in McBride et al. (2002). In the paper, the enthalpy of formation $\Delta_f h^o$ and the difference in enthalpy $H0$ between the datum state temperature T_o and temperature at 0 K are tabulated.

Datum State

The reference state of the NASA Glenn polynomials is; datum temperature $T_o = 298.15$ K and datum pressure $p_o = 1$ bar. The datum states do not affect the performance calculations so instead is $p_o = 1.01325$ bar chosen for datum state of the pressure since $p_o = 1$ atm. In this section, the reference datum state is denoted with the super-script ^{o}. In other parts of the thesis, the datum state notation is omitted for simplicity.

Reference Elements and Enthalpy of Formation $\Delta_f h^o$

To each tabulated molecule, a value called enthalpy of formation $\Delta_f h^o$ is assigned. The enthalpy of formation is defined to be the energy that is released when the molecule is split to its reference elements in the datum state. An example of reference elements are; argon Ar (g), carbon C (c), hydrogen H_2 (g), nitrogen N_2 (g), and oxygen O_2 (g). The symbol (g) indicates that the element is in a gaseous phase and the symbol (c) indicates that the element is in a condensed phase. For a reference gas the enthalpy of formation is equal to zero:

$$\Delta_f h^o(T_o) = 0$$

for the datum state temperature T_o.

Assigned Enthalpy Values

The enthalpy $h_o(T)$ relative to the datum state T_o can be written:

$$h^o(T) = h^o(T_o) + [h^o(T) - h^o(T_o)] \tag{2.10}$$

For all species at datum state, the enthalpy of formation is arbitrary assigned the same value as the enthalpy:

$$\Delta_f h^o(T_o) = h^o(T_o) \tag{2.11}$$

This expression can be inserted into (2.10) to get:

$$h^o(T) = \Delta_f h^o(T_o) + \int_{T_o}^{T} c_p(\tau) d\tau \tag{2.12}$$

where the definition (2.3) of c_p is introduced. Since the reference elements have an enthalpy of formation that is zero for the datum state, also the the enthalpies of the reference elements are zero at the datum state. If another reference state is used, e.g., the reference state $T_o = 0\,K$ it is possible to adjust (2.10) with the tabulated constant bias term $H0$:

$$H0 = h^o(T_o) - h^o(0)$$

to get:

$$h^{\hat{o}}(T) \equiv h^o(T) + H0 = \Delta_f h^o(298.15) + \int_{0}^{T} c_p(\tau) d\tau \tag{2.13}$$

2.2.1 Specific Heat Capacity of Species

The NASA polynomials for the specific heat capacity $\tilde{c}_p$ of a gas species i have the structure:

$$\frac{\tilde{c}_{p,i}}{\tilde{R}} = a_{i1}\frac{1}{T^2} + a_{i2}\frac{1}{T} + a_{i3} + a_{i4}T + a_{i5}T^2 + a_{i6}T^3 + a_{i7}T^4 \tag{2.14}$$

where the constants a_{ij} are the tabulated NASA Glenn Coefficients. The left hand side of (2.14) is a dimensionless quantity, so it is possible to formulate it as:

$$\frac{\tilde{c}_{p,i}}{\tilde{R}} = \frac{c_{p,i}}{R} \tag{2.15}$$

where R is the universal gas constant, and $\tilde{R}$ is the specific gas constant. The relation between the gas constants is: $\tilde{R} = \tilde{m}R$. Eq. (2.15) shows that both the mass and the molar specific quantities can be calculated from the same polynomial coefficients.

2.2.2 Enthalpy of Species

The enthalpy is related thermodynamically to the heat capacity as follows:

$$\frac{h^o(T)}{RT} = \frac{\int c_p(\tau) d\tau}{RT} + \frac{b_1}{T} \tag{2.16}$$

where b_1 is an integration constant. The heat capacity c_p is integrated with respect to the temperature T. To obtain the enthalpy of a species, the integration is performed to get:

$$\frac{h_i^o}{RT} = -a_{i1}\frac{1}{T^2} + a_{i2}\frac{\ln(T)}{T} + a_{i3} + \frac{a_{i4}}{2}T + \frac{a_{i5}}{3}T^2 + \\ + \frac{a_{i6}}{4}T^3 + \frac{a_{i7}}{5}T^4 + b_{i1}\frac{1}{T} \tag{2.17}$$

where the constant b_{i1} is chosen to match (2.12) for the temperature $T = T_o$. Since the constant b_{i1} is chosen to match (2.12), the enthalpy of formation is included in the NASA polynomials as default. If the sensible enthalpy is needed, the enthalpy of formation is subtracted from the NASA polynomial calculations. The coefficients a_{ij} are the same as for the heat capacity.

2.2.3 Entropy of Species

The entropy is related thermodynamically to the heat capacity as follows:

$$\frac{s^o(T)}{R} = \int \frac{c_p(\tau)d\tau}{RT} + b_2 \tag{2.18}$$

where b_2 is an integration constant. To obtain the entropy of a species, the integration of c_p/T is performed to get:

$$\frac{s_i^o}{R} = -\frac{a_{i1}}{2}\frac{1}{T^2} - a_{i2}\frac{1}{T} + a_{i3}\ln(T) + a_{i4}T + \frac{a_{i5}}{2}T^2 + \\ + \frac{a_{i6}}{3}T^3 + \frac{a_{i7}}{4}T^4 + b_{i2} \tag{2.19}$$

where b_{i2} is an integration constant. The coefficients a_{ij} are the same as for the heat capacity.

Entropy for an Ideal Gas

For an ideal gas, the entropy depends on the temperature and the pressure. If the first and second laws of thermodynamics are combined, together with the enthalpy definition (2.1) and an assumption of a reversible thermodynamic process (2.7), the entropy differential can be written:

$$ds = \frac{c_p}{T}dT - \frac{R}{p}dp \tag{2.20}$$

where also the relation $dh = c_p dT$ of an ideal gas is introduced. To get an expression for the entropy, the differential (2.20) is integrated to get:

$$s(T,p) = \int_{T^o}^{T} \frac{c_p(\tau)}{\tau}d\tau - R\ln\left(\frac{p}{p^o}\right) = s^o(T) - R\ln\left(\frac{p}{p^o}\right) \tag{2.21}$$

where the entropy is calculated by the integration of c_p/T, i.e., the expression (2.19).

2.2.4 Gibbs Free Energy

When the temperature T and the pressure p are given, Gibbs free energy is feasible to consider in the determination of mixture concentration of species which are in chemical equilibrium. Gibbs free energy is minimized when the species is in chemical equilibrium and is defined as:

$$g(T, p) = h(T) - Ts(T, p) \tag{2.22}$$

where h is the enthalpy, and s is the entropy defined previously.

If instead the temperature T and the volume V are given, Helmholtz free energy should be considered instead of Gibbs free energy.

2.3 Combustion

In a gas turbine model, the combustion process is important to consider. The combustion products depend on the heat that is released when the two reactants fuel and air are burned. The composition of molecules in the exhaust gas is different from the composition of the unburned mixture, which results in different thermodynamic properties of the gas before and after the combustion.

A main goal here, with the developed thermodynamic relations, is the potential to introduce combustion in the gas processes. In a general case, the composition of the species in the exhaust gas reacts with each other. The reacting rate depends on the temperature and the pressure of the fluid, i.e., so-called dissociation. Usually, a higher temperature and a higher pressure give a higher reacting rate. The number of dissociation products that have to be considered is also larger for higher temperatures and pressures. For example, nitrogen oxide NO_x molecules appear in a lean exhaust gas ($\lambda > 1$) when the temperature is high. The dissociation products have a significant effect on the heat capacities, but a disadvantage with the consideration of a dissociation term in the gas model is the increasing complexity. For lower temperatures, < 1500 K, a good simplification is to assume that the exhaust gas composition is frozen, i.e., independent of pressure and temperature so the dissociation terms can be neglected. This gives an assumption of a stoichiometric combustion.

In the medium model, developed in the GTLib package, properties of the exhaust gases are described by the air/fuel ratio λ and the combustion temperature T which will be presented in the sub-section 2.3.1. In the medium model, dissociation effects are not described which result in an absence of NO_x molecules. It will be shown that the dissociation effect for higher temperatures have a significant influence on the heat capacities. The advantages, with the stoichiometric modeling approach, are that the combustion can be described relatively easily and it is simple to change the concentration of the air/fuel gases.

Adiabatic Flame Temperature of a Constant-Pressure Combustion Process

The pressure during a combustion process, in an ideal gas turbine, is assumed to be adiabatic and constant. For an adiabatic constant-pressure combustion process, it holds

that the enthalpy h_u before the combustion and the enthalpy h_b after the combustion are equal. At least locally, h_b is invertible which gives a solution for the flame temperature:

$$T_b = h_b^{-1}\Big(h_u(T_u)\Big) \tag{2.23}$$

where T_u is the temperature of the unburned mixture, and T_b are the temperature of the exhaust gas. Depending on the chosen pair of independent thermodynamic state variables the expression (2.23) needs to be solved in each control volume. If the temperature is chosen as a state variable, the enthalpy needs to be calculated in each control volumes and Eq. (2.23) has to be solved with a numerical solver. If the enthalpy is chosen instead as a state variable, it is not necessary to find an explicit solution of the temperature in each control volume and therefore it is not necessary to solve (2.23) explicitly. To solve (2.23) can be time consuming which can be avoided if the enthalpy, instead of temperature, is chosen as a state variable.

2.3.1 Stoichiometry

If sufficient oxygen is available in the air, a hydrocarbon fuel can be completely oxidized with the rest products of carbon dioxide and water. For the amount of air that just converts all hydrocarbons to carbon dioxide and water it is possible to define a stoichiometric air/fuel ratio. The stoichiometric air/fuel ratio can either be expressed in moles $(A/F)_{\bar{s}}$ or in masses $(A/F)_s$. The actual air/fuel ratio λ, expressed in mole basis of a mixture is defined:

$$\lambda = \frac{n_a/n_f}{(A/F)_{\bar{s}}} \tag{2.24}$$

where n_a is the mole number of air, and n_f is the mole number of fuel. The air/fuel ratio, corresponding to an expression in mass basis, is defined:

$$\lambda = \frac{m_a/m_f}{(A/F)_s} \tag{2.25}$$

where m_a is the mass of air, and m_f is the mass of fuel. A simple reaction formula for a hydrocarbon fuel, with emphasis on combustion, is presented in the following example.

Example 2.1

A hydrocarbon fuel C_3H_8 is combusted with air that consists of oxygen and nitrogen. A simple air model assumption is that for each oxygen molecule (O_2), 3.773 nitrogen molecules (N_2) are available. This gives the following reaction formula, in mole basis, for the combustion:

$$\overbrace{C_3H_8}^{Fuel} + n\overbrace{(O_2 + 3.773N_2)}^{Air} \longrightarrow 3CO_2 + 4H_2O + (n-5)O_2 + n3.773N_2$$

where $n \geq 5$ is the number of available oxygen molecules in the unburned mixture where 1 propane molecule is available. If $n = 5$ the oxidization is complete, i.e., all

hydrocarbons have been converted to carbon dioxide and water. If $n > 5$, there are not enough hydrocarbons in the combustion so the formula has an excesses of oxygen. In the present example, it is assumed that $n \geq 5$, but for the case with a $n < 5$, it is not enough oxygen molecules for the carbon dioxide molecule formations. Instead, the formula has to be extended with carbon oxide molecules (CO) to preserve the number of atoms in the chemical reaction. Since the combustion in a gas turbine has excesses of oxygen, this case is not considered in the GTLib package.

To simplify the presentation of the chemical reaction, it can be written in a matrix form according to:

$$\overbrace{C_3H_8}^{Fuel} + n\overbrace{(O_2 + 3.773N_2)}^{Air} \longrightarrow \Bigg(\underbrace{\begin{bmatrix} 0 \\ 0 \\ n \\ 3.773n \end{bmatrix}}_{n_{air}} + \underbrace{\begin{bmatrix} 3 \\ 4 \\ -5 \\ 0 \end{bmatrix}}_{\tilde{S}} \Bigg)^T \begin{bmatrix} CO_2 \\ H_2O \\ O_2 \\ N_2 \end{bmatrix} \tag{2.26}$$

where the stoichiometric matrix $\tilde{S}$ consists of the coefficients of the hydrocarbon molecule combustion. The advantage with the introduced stoichiometric matrix is the ability to use fuels with several hydrocarbon molecules in a compact manner. The right hand side of (2.26) describes the number of constructed molecules in the combustion.

For $n = 5$, the oxidation is complete and the stoichiometric air/fuel ratio can be calculated (1) in mole: $(A/F)_{\tilde{s}} = 23.87$, and (2) in mass: $(A/F)_s = 15.68$ according to the definition of air/fuel ratio (2.24) and (2.25).

The chemical reaction formula in Example 2.1 can be extended to capture more general hydrocarbon fuel and air descriptions. Here, it is assumed that the fuel consists of the following molecules: methane (CH_4), ethane (C_2H_6), propane (C_3H_8), carbon dioxide (CO_2), and nitrogen (N_2). The chemical reaction for these species can be written:

$$\begin{aligned} CH_4 + 2O_2 &\rightarrow CO_2 + 2H_2O \\ C_2H_6 + 3.5O_2 &\rightarrow 2CO_2 + 3H_2O \\ C_3H_8 + 5O_2 &\rightarrow 3CO_2 + 4H_2O \\ CO_2 &\rightarrow CO_2 \\ N_2 &\rightarrow N_2 \end{aligned} \tag{2.27}$$

where the species of CO_2 and N_2 are unaffected by the combustion. The corresponding species for the air are the following: argon (Ar), carbon dioxide (CO_2), water (H_2O), nitrogen (N_2), and oxygen (O_2). To get a more flexible description, also the concentrations of respective species in the gases are considered. The mole concentration vectors of

air $\tilde{x}_a$ and fuel $\tilde{x}_f$ are expressed according to:

$$\tilde{x}_a = \begin{pmatrix} \tilde{x}_{a,Ar} \\ \tilde{x}_{a,CO_2} \\ \tilde{x}_{a,H_2O} \\ \tilde{x}_{a,N_2} \\ \tilde{x}_{a,O_2} \end{pmatrix}, \; \tilde{x}_f = \begin{pmatrix} \tilde{x}_{f,CH_4} \\ \tilde{x}_{f,C_2H_6} \\ \tilde{x}_{f,C_3H_8} \\ \tilde{x}_{f,CO_2} \\ \tilde{x}_{f,N_2} \end{pmatrix} \tag{2.28}$$

where the sums of the elements are $\sum_i \tilde{x}_{a,i} = \sum_i \tilde{x}_{f,i} = 1$. If the stoichiometric reaction formula in (2.27) is combined with the method described in Example 2.1, the following combustion formula can be written:

$$\tilde{x}_f + n\tilde{x}_a \longrightarrow \left(n\tilde{x}_a + \tilde{S}\tilde{x}_f\right)^T \begin{bmatrix} Ar \\ CO_2 \\ H_2O \\ N_2 \\ O_2 \end{bmatrix} \tag{2.29}$$

where the stoichiometric matrix is:

$$\tilde{S} = \begin{pmatrix} 0 & 0 & 0 & 0 & 0 \\ 1 & 2 & 3 & 1 & 0 \\ 2 & 3 & 4 & 0 & 0 \\ 0 & 0 & 0 & 0 & 1 \\ -2 & -3.5 & -5 & 0 & 0 \end{pmatrix} \tag{2.30}$$

The stoichiometric matrix (2.30) is expressed in moles. The element (i, j) in the matrix symbolize the number of air species $\tilde{x}_{a,i}$ that are created/depleted from each species $\tilde{x}_{f,j}$ in the fuel. In practice, it is more suitable to have the description in masses instead of moles. The conversion procedure is shown in Appendix A. The stoichiometric matrix can be rewritten:

$$S = \begin{pmatrix} 0 & 0 & 0 & 0 & 0 \\ \frac{M_{CO_2}}{M_{CH_4}} & 2\frac{M_{CO_2}}{M_{C_2H_6}} & 3\frac{M_{CO_2}}{M_{C_3H_8}} & 1 & 0 \\ 2\frac{M_{H_2O}}{M_{CH_4}} & 3\frac{M_{H_2O}}{M_{C_2H_6}} & 4\frac{M_{H_2O}}{M_{C_3H_8}} & 0 & 0 \\ 0 & 0 & 0 & 0 & 1 \\ -2\frac{M_{O_2}}{M_{CH_4}} & -3.5\frac{M_{O_2}}{M_{C_2H_6}} & -5\frac{M_{O_2}}{M_{C_3H_8}} & 0 & 0 \end{pmatrix} \tag{2.31}$$

where M_i is the mole mass of molecule i. The chemical reaction between the two gases air and fuel, can now be written:

$$m_a x_a + m_f x_f \rightarrow m_a x_a + m_f S x_f \tag{2.32}$$

where m_a is the mass of air, and m_f is the mass of fuel. The mass fraction of the burned gas arise if the right hand side of (2.32) is normalized. This gives an expression of the mass fraction of species in the exhaust gas x_b according to:

$$x_b(\lambda) = \frac{m_a x_a + m_f S x_f}{m_a \sum_i x_{a,i} + m_f \sum_i S x_f|_{\text{row}=i}} = \frac{(A/F)_s \lambda x_a + S x_f}{(A/F)_s \lambda + 1} \equiv X(\lambda) \tag{2.33}$$

where $\sum x_{a,i} = 1$, and $\sum Sx_f|_{\text{row}=i} = 1$ because normalized mass flow concentrations are used, and the number of atoms are conserved. The mass fraction in the exhaust gas x_b is defined as $X(\lambda)$ in the sequel. To receive the final expression (2.33), the lambda definition (2.25) is considered in the determination. The stoichiometric air/fuel ratio $(A/F)_s$ is calculated according to:

$$(A/F)_s = \left(\frac{m_a}{m_f}\right)_s = \frac{2\frac{x_{f,CH_4}}{M_{CH_4}} + 3.5\frac{x_{f,C_2H_6}}{M_{C_2H_6}} + 5\frac{x_{f,C_3H_8}}{M_{C_3H_8}}}{\frac{x_{a,O_2}}{M_{O_2}}} \tag{2.34}$$

where the concentration of oxygen in the exhaust gas in (2.32) is equal to zero. Eq. (2.33) states that the mass fraction of the exhaust gas can be expressed only in the scalar variable λ if the two gases air and fuel are considered. In Figure 2.3, the exhaust mass fraction of a combustion of a hydrocarbon fuel is shown at different air/fuel ratios.

2.3.2 Chemical Equilibrium

For performance calculation, a good approximation is to assume that the species produced by the combustion is in equilibrium. Equilibrium here means that the *dissociation* between the species occurs with equal rate, e.g., the same number of O_2 molecules dissociated into O atoms as the number of O_2 molecules that are constructed from O atoms, i.e., $O_2 \leftrightharpoons 2O$. This dissociation rate depends highly on the temperature, and increases with the increased temperature (Heywood, 1988). To calculate the chemical equilibrium for a specific exhaust gas at a given combustion temperature, a chemical equilibrium program can be used. A well known program is the NASA equilibrium program, presented in Gordon and McBride (1994). Here, the chemical equilibrium program CHEPP developed in Eriksson (2004) is utilized with some modification. In the original CHEPP version, hydrocarbons in the form: C_aH_bOH, together with atmospheric air in the form: $(O_2 + 3.773N_2)$ are considered as reactants. In the present work, the interface to CHEPP is modified to handle hydrocarbons, and atmospheric air in the form showed in (2.28). The modified CHEPP is used to check how well the thermodynamic properties of a chemical reaction in (2.32) harmonize with an exhaust gas in chemical equilibrium. In Figure 2.2, a demonstration of CHEPP's ability to calculate the mole concentration in the exhaust gas for an isooctane fuel (C_8H_{18}) at three different temperatures is shown. As the figure indicates, the dominant species for $\lambda > 1$ are: nitrogen (N_2), carbon dioxide (CO_2), water (H_2O), and oxygen molecule (O_2) when the temperature is low. For higher temperatures, the species of nitrogen oxide (NO) increase in concentration. For $\lambda < 1$, the shortage of oxygen molecules results in a reduction in carbon monoxide (CO).

An introduction of how the equilibrium is calculated will follow in the remaining sub-section. For a more comprehensive explanation about equilibrium calculation see, e.g., Heywood (1988). First step in the process is to select which product species in the exhaust gas that should be considered. This means that the structure of the x_b vector has to be specified. In the second step, the constraints of atom conservations are specified. In the conservation n_a different atoms and n_s different species in the exhaust gas is considered. On a mole basis, these constraints are written:

$$\tilde{b} = \tilde{A}n \tag{2.35}$$

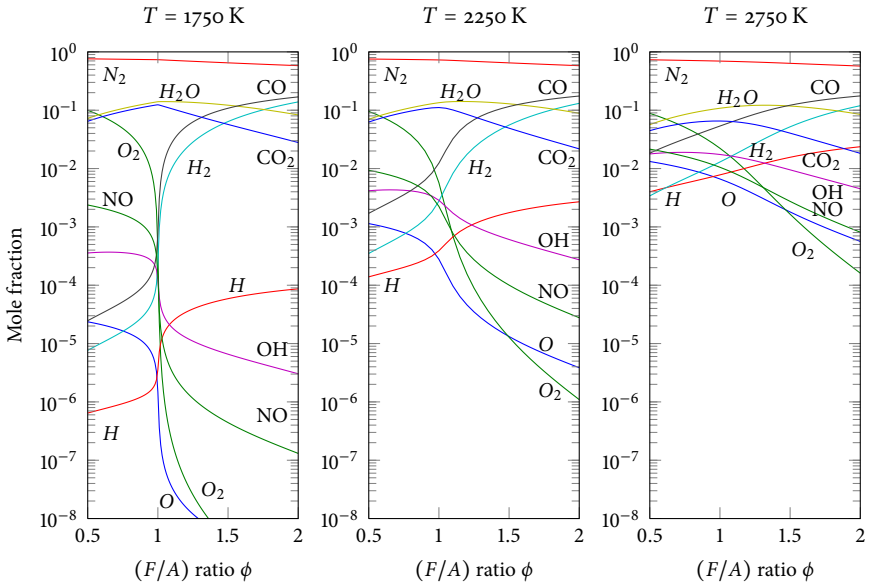

Figure 2.2: In the figure, the combustion products of an isooctane (C_8H_{18}) fuel at chemical equilibrium for the temperatures 1750 K, 2250 K, and 2750 K is showed. The figure is generated in the chemical equilibrium program CHEPP, where the ten most affectable product species are considered. The species are plotted against the fuel/air ratio ϕ, where $\phi = \lambda^{-1}$. For a lean combustion at temperature 1750 K the dominated species are oxygen (O_2), carbon dioxide (CO_2), water (H_2O), and nitrogen (N_2). For a lean combustion at higher temperatures the nitrogen oxide NO species increases in concentration.

where $\tilde{b} \in \mathbb{R}^{n_a}$, $n \in \mathbb{R}^{n_s}$, and $\tilde{A} \in \mathbb{R}^{\epsilon n_b \times n_s}$. Vector $\tilde{b}$ consists of all the available atoms in the unburned mixture, i.e., the mixture of air and fuel. Vector n consists of the produced product species for the equilibrium calculation. Finally, $\tilde{A}$ is the matrix that describes how many atoms each combustion product consists of. Often, $n_b > n_s$, which results in an over-determined equations system, so an optimization procedure is sought. The optimization problem is to minimize the Gibbs free energy (2.22), $G = \sum_i \tilde{g}_i n_i$, under the constraints in (2.35). The solution to the optimization problem is the equilibrium gas composition, and the exhaust gas concentration vector is simply: $\tilde{x}_b = \frac{n}{|n|}$.

An evaluation of an equilibrium calculation, for a hydrocarbon fuel performed in CHEPP, is investigated in Example 2.2. The result from this study is then compared with the corresponding calculation for a hydrocarbon fuel where a stoichiometric combustion is considered.

Example 2.2

A hydrocarbon fuel with a concentration vector $\tilde{x}_f$, is combusted with atmospheric air with a concentration vector $\tilde{x}_a$. These two vectors have been introduced in (2.28). The exhaust gas concentration vector $\tilde{x}_b$ is calculated using the chemical equilibrium program CHEPP. Vector $\tilde{x}_b$ is the solution to the optimization problem presented in (2.35). The product species in $\tilde{x}_b$ are chosen to be: hydrogen (H), nitrogen (N_2), oxygen (O), carbon monoxide (CO), carbon dioxide (CO_2), water (H_2O), oxygen molecule (O_2), nitrogen monoxide (NO), hydroxyl (OH), hydrogen molecule (H_2), and argon (Ar). These species are summarized in the exhaust vector:

$$\tilde{x}_b = \left(\tilde{x}_H,\, \tilde{x}_{N_2},\, \tilde{x}_O,\, \tilde{x}_{CO},\, \tilde{x}_{CO_2},\, \tilde{x}_{H_2O},\, \tilde{x}_{O_2},\, \tilde{x}_{NO},\, \tilde{x}_{OH},\, \tilde{x}_{H_2},\, \tilde{x}_{Ar}\right)^T \tag{2.36}$$

The chemical reaction formula between air and fuel can in this case be written:

$$\begin{gathered}\overbrace{\tilde{x}_{Ar}Ar + \tilde{x}_{CO_2}CO_2 + \tilde{x}_{O_2}O_2 + \ldots}^{\text{Air}} + \overbrace{\tilde{x}_{CH_4}CH_4 + \tilde{x}_{C_2H_6}C_2H_6 + \ldots}^{\text{Fuel}} \longrightarrow \\ \underbrace{n_1H + n_2N_2 + n_3O + \ldots + n_{11}Ar}_{\text{Exhaust Gas}}\end{gathered} \tag{2.37}$$

where the n_i depends on the temperature, and the pressure. To get the concentration vector $\tilde{x}_b$, the n vector is normalized. In this case, unique atoms in the reactants are: hydrogen (H), nitrogen (N), oxygen (O), carbon (C), and argon (Ar). The constraint matrix $\tilde{A}$ in (2.35) is constructed according to:

$$A = \begin{array}{c} \\ H \\ N \\ O \\ C \\ Ar \end{array} \begin{array}{c} \begin{array}{ccccccccccc} H & N_2 & O & CO & CO_2 & H_2O & O_2 & NO & OH & H_2 & Ar \end{array} \\ \begin{pmatrix} 1 & 0 & 0 & 0 & 0 & 2 & 0 & 0 & 1 & 2 & 0 \\ 0 & 2 & 0 & 0 & 0 & 0 & 0 & 1 & 0 & 0 & 0 \\ 0 & 0 & 1 & 1 & 2 & 1 & 2 & 1 & 1 & 0 & 0 \\ 0 & 0 & 0 & 1 & 1 & 0 & 0 & 0 & 0 & 0 & 0 \\ 0 & 0 & 0 & 0 & 0 & 0 & 0 & 0 & 0 & 0 & 1 \end{pmatrix} \end{array}$$

and the vector $\tilde{b}$ is constructed according to:

$$\tilde{b}(\tilde{x}_a, \tilde{x}_f) = \left(n_H,\, n_N,\, n_O,\, n_C,\, n_{Ar}\right)^T$$

where the number of moles in $\tilde{b}$ depends on the actual air and the fuel. The ratio between the air and fuel is controlled by the λ parameter which gives a $\tilde{b}(\lambda)$. In Figure 2.3, the result of the CHEPP calculation is shown where the most dominant species are viewed. In the figure, the species according to the stoichiometric calculation in (2.32) are viewed in the same subfigure.

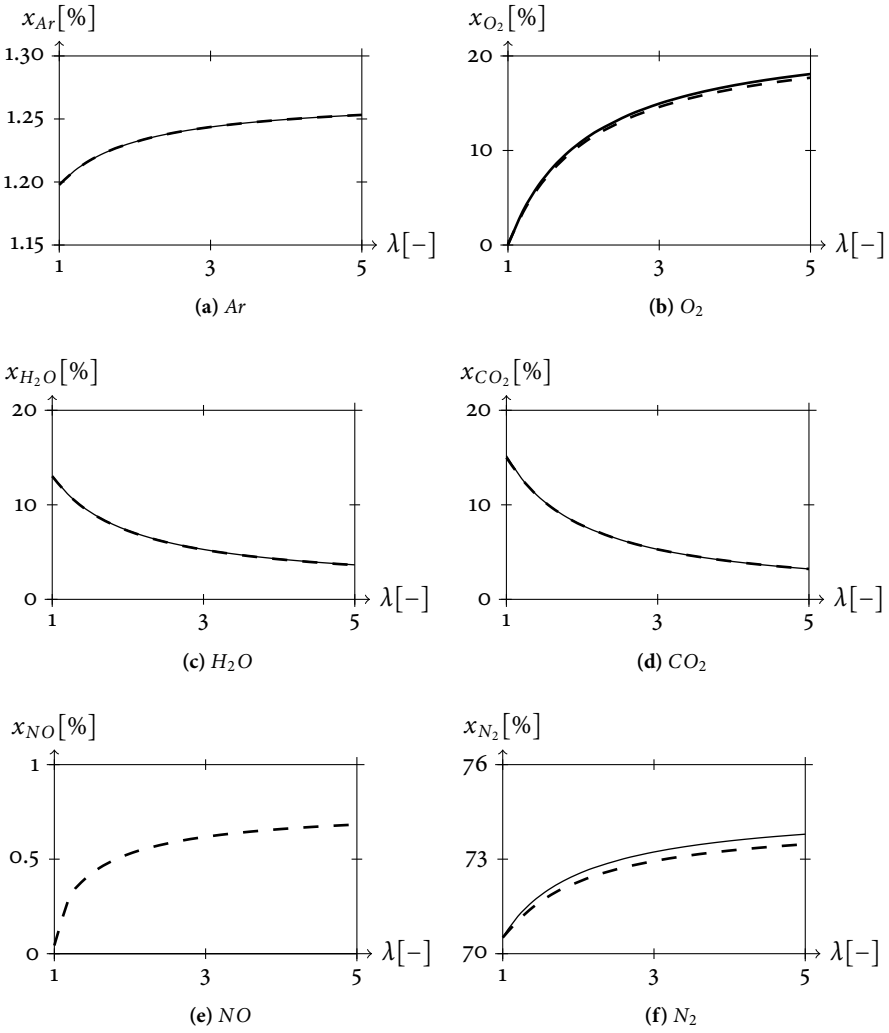

(a) Ar **(b)** O_2 **(c)** H_2O **(d)** CO_2 **(e)** NO **(f)** N_2

Figure 2.3: Mass fraction of the species argon (Ar), oxygen (O_2), water (H_2O), carbon dioxide (CO_2), nitrogen oxide (NO), and nitrogen (N_2) in the exhaust gas when the combustion is lean, and the temperature is 2000 K. The dashed lines in respective subfigure represent species for equilibrium calculations performed in CHEPP, and described in Example 2.2. Solid lines represent calculations made according to stoichiometric combustion presented in (2.32). For these two cases, the same air x_a, and fuel x_f mass concentration vectors are used. The nitrogen oxide NO is not considered in the stoichiometric combustion, and is not shown here. The other species that $\tilde{x}_b$ consists of, showed in (2.36) are not showed here since they are too small. The main difference between these two cases is the appearance, and the increase of nitrogen oxide in the CHEPP calculation.

2.3.3 Comparison of the Heat Capacity Between the Stoichiometric Gas Description and the Chemical Equilibrium Calculation

The most commonly occurring thermodynamic properties of a gas are, e.g., the enthalpy h, the entropy s, the internal energy u, the density ρ, the gas constant R, and the heat capacities c_p and c_v. An idea is to check how well these properties are described for different gas description approaches. Here, the behaviour of the stoichiometric combustion (2.33) and the chemical equilibrium calculation (2.37) in the previous sections, is investigated for the heat capacity c_p. In Figure 2.3, the mass concentrations of species in the two modeling approaches are shown. The main difference between these two approaches is the increase in concentration of the nitrogen oxide molecules. The chemical equilibrium calculation is strongly connected to the increase in temperature which leads to a higher amount of nitrogen oxide molecules. The change in mass concentration of species affects the thermodynamic properties mentioned previously, and in Figure 2.4 the heat capacity is compared for the two approaches. In the figure, three different combustion temper-

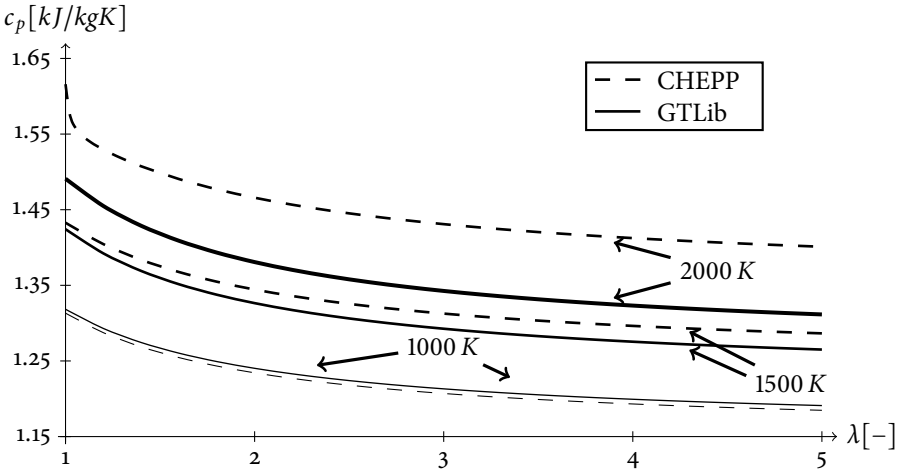

Figure 2.4: In the figure, the heat capacity c_p is calculated for the two calculation methods: stoichiometric combustion, and chemical equilibrium calculation. For these two methods, the combustion is lean and three temperatures are studied. The temperatures are: T = 1000 K, T = 1500 K, and T = 2000 K. As the figure indicates, the difference between these two cases appears to increase for high temperatures. For temperatures above 2000 K, the mismatch between the two calculation methods is larger than 8 %. For temperatures below ≈ 1500 K, the stoichiometric description agrees with the chemical equilibrium calculation.

atures: T = 1000 K, T = 1500 K, and T = 2000 K are compared for the two modeling approaches. The study indicates that the mismatch between the two cases appears to increase for large temperatures, and for temperatures above 2000 K the mismatch is larger than 8 %. For temperatures below ≈ 1500 K, the stoichiometric description agrees with the chemical equilibrium calculation. In all three cases the results are as expected.

2.3.4 Mixing of Exhaust Gases with Different Lambda

It is important to have the potential to mix two (or more) gases with different air/fuel ratio. For example, the combustion temperature in a modern gas turbine is too high for the material in the first turbine blades. To handle this, cooling air is injected through small holes in the turbine blades, and the air is distributed as a thin cooling film at the blades. After a while, the injected air and the exhaust gas are mixed which changes the thermodynamic gas properties of the fluid. Therefore it is important to have a model library that can handle the mixture between burned gases with different air/fuel ratios and pure cooling air.

The mass concentration of a gas, that is a mixture of the two gases with masses m_1, m_2 and air/fuel ratio λ_1, λ_2 is:

$$X(\lambda) = \frac{m_1 X(\lambda_1) + m_2 X(\lambda_2)}{m_1 + m_2} \tag{2.38}$$

Solving (2.38) gives an analytic solution of the air/fuel ratio λ in the mixed gas as:

$$\lambda = \frac{(m_1\lambda_1 + m_2\lambda_2) + \lambda_1\lambda_2(A/F)_s(m_1 + m_2)}{(m_1\lambda_2 + m_2\lambda_1)(A/F)_s + (m_1 + m_2)} \tag{2.39}$$

where the mass concentration vector in (2.33) is used. This expression is used in the turbine component in the GTLib package when the cooling air is mixed with the exhaust gas. The masses in (2.39) can directly be translated to masses per unit time, i.e., mass flows.

2.4 Ideal Gas Model

In this sub-section, the relation between the independent differentials; pressure and temperature of an ideal gas is presented. Since the considered gas is described by a number of gas species, also the mass fraction differential has to be considered when the ideal gas model is specified. The definition of an ideal gas is:

$$pV = n\tilde{R}T = mRT \tag{2.40}$$

where p is the pressure, V is the volume, n is the number of moles, $\tilde{R}$ the universal gas constant, T is the temperature, m is the mass and R the gas constant. For an ideal gas, the enthalpy (2.1) can be written:

$$h = u + RT \tag{2.41}$$

where the ideal gas law (2.40) is utilized. The differentials of the ideal gas law are:

$$Vdp = RT\sum_i dm_i + mTdR + mRdT \tag{2.42}$$

where it is assumed that the size of the container is fixed, i.e., $pdV = 0$. All differentials, except dR are either requested or available. The differential dR is calculated as follows:

$$dR(p, T, X) = \frac{\partial R}{\partial p}dp + \frac{\partial R}{\partial T}dT + (\nabla_X R)^T dX \tag{2.43}$$

where ∇_X is the gradient of the mass concentration vector X. It is assumed that no reaction occurs in the container, i.e., the gas composition is *frozen* so the differential (2.43) is simply:

$$dR = (\nabla_X R)^T dX \tag{2.44}$$

2.4.1 Thermodynamics Properties for Frozen Mixtures

The thermodynamic properties such as enthalpy h, internal energy u, gas constant R, and heat capacities can be expressed with help of the mass fraction vector X in (2.33) as:

$$h(T, \lambda) = h_s(T)^T X(\lambda) \tag{2.45a}$$

$$u(T, \lambda) = u_s(T)^T X(\lambda) \tag{2.45b}$$

$$R(\lambda) = R_s^T X(\lambda) \tag{2.45c}$$

$$c_p(T, \lambda) = c_{p,s}(T)^T X(\lambda) \tag{2.45d}$$

where it is possible to separate the temperature and air/fuel ratio dependencies. Indices s denote a vector with gas properties according to the actual gas species.

2.4.2 Mass Concentration Differential dX

Since fluids with different mass concentrations can be mixed, it is important to develop an expression of the mass concentration differential vector dX in control volume V. For a number of fluids that is flowing into the control volume, a schematic view of the process is shown in Figure 2.5 where $X_i dm_i$ is the mass amount of species that is flowing

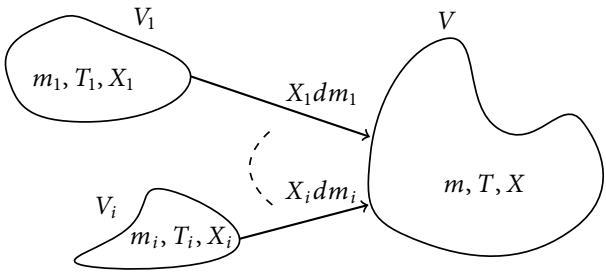

Figure 2.5: Mass flow of species into a control volume V.

into the control volume. This gives an expression of the *species of mass change* in the perfectly mixed control volume according to:

$$d(mX) = \sum_i X_i dm_i \tag{2.46}$$

where the left hand side is the differential vector that consists of specie masses. The mass change of respective mass element is just the sum of the in-coming/out-going mass

flows of the specific species, i.e., the right hand side. The differential $d(mX)$ can also be written:

$$d(mX) = X\sum_i dm_i + mdX \tag{2.47}$$

when the chain rule is applied, and the summation of all in-coming masses $dm = \sum_i dm_i$ is introduced. If the expressions (2.46) and (2.47) above are combined, the mass concentration differential vector dX for a number of species in a perfectly mixed container is:

$$dX = \sum_i \frac{\hat{X}_i - X}{m} dm_i \tag{2.48}$$

where index i represents the gas stream i. The gas composition is not affected by the out-flowing gas streams so $\hat{X}_i$ can be expressed:

$$\hat{X}_i = \begin{cases} X_i & \text{When gas stream } i \text{ flows into the mixer } (dm_i > 0) \\ X & \text{When gas stream } i \text{ flows out from the mixer } (dm_i \leq 0) \end{cases}$$

where X_i is the mass fraction of gas stream i. The mass concentration differential (2.48) can be combined with the mass concentration vector (2.33). Rewriting (2.48) in lambda gives:

$$dX = \sum_i \frac{X(\hat{\lambda}_i) - X(\lambda)}{m} dm_i \tag{2.49}$$

where

$$\hat{\lambda}_i = \begin{cases} \lambda_i & \text{When gas stream } i \text{ flows into the mixer } (dm_i > 0) \\ \lambda & \text{When gas stream } i \text{ flows out from the mixer } (dm_i \leq 0) \end{cases}$$

2.5 Energy Conservation of Thermodynamic Systems

The first law of thermodynamics (2.6) states that energy cannot be created or destroyed. The energy can only be transformed between different states of the fluid. In open thermodynamic systems, the transformation is between thermal energy dQ, mechanical work dW, and intrinsic energy dU of the fluid. The goal with this sub-section is to derive a relation between differentials of the considered fluid.

2.5.1 Thermodynamic Differentials dU, dW, and dQ

The thermodynamic differentials are summarized in the following sub-sections.

Internal Energy Differential dU

The internal energy of the gas before and after a mixing occurs can be denoted U_0 and U_Δ according to:

$$\begin{aligned} U_0 &= mu(T_0, \lambda_0) + \Delta m_i u(T_i, \lambda_i) \\ U_\Delta &= (m + \Delta m_i) u(T_\Delta, \lambda_\Delta) \end{aligned} \tag{2.50}$$

where Δ denotes the mixing properties and indices i denotes the incoming fluid properties. The difference between the two states can be described by a Taylor series expansion at the point (p_0, T_0, λ_0). The Taylor series expansion of U_Δ is:

$$U_\Delta = (m + \Delta m_i)\Big(u(T_0, \lambda_0) + \frac{\partial u}{\partial T}\Delta T + \frac{\partial u}{\partial \lambda}\Delta\lambda + O(\Delta^2)\Big) \tag{2.51}$$

where $O(\Delta^2)$ captures all the second order, and higher terms. The change in internal energy $\Delta U = U_\Delta - U_0$ can now be written:

$$\Delta U = m\Big(\frac{\partial u}{\partial T}\Delta T + \frac{\partial u}{\partial \lambda}\Delta\lambda\Big) + \Big(u(T_0, \lambda_0) - u(T_i, \lambda_i)\Big)\Delta m_i \tag{2.52}$$

The definition of the differential dU, together with (2.52), gives:

$$dU = \lim_{h\to 0}\Big(\frac{\Delta U}{h}\Big) = m\Big(\frac{\partial u}{\partial T}dT + \frac{\partial u}{\partial \lambda}d\lambda\Big) + \Big(u(T_0, \lambda_0) - u(T_i, \lambda_i)\Big)dm_i \tag{2.53}$$

Work Energy Differential dW

The gas stream that is flowing into the control volume does work on the thermodynamic system, so the differential dW had to be split into two different work contributions:

$$dW = d\tilde{W} + pv_i dm_i \tag{2.54}$$

where $d\tilde{W}$ is the external mechanical work, and $pv_i dm_i$ is the work performed by the mass differential dm_i. If no external work is applied, $d\tilde{W} = 0$.

Thermal Energy Differential dQ

The thermal energy differential dQ is assumed to be known and if the container is perfectly insulated, $dQ = 0$.

2.5.2 Energy of the Mixture of Frozen Ideal Gases

The first law of thermodynamics can be written together with (2.53) and (2.54):

$$m\Big(c_v(T, \lambda)dT + \frac{\partial u(T, \lambda)}{\partial \lambda}d\lambda\Big) + u(T, \lambda)dm_i = dQ + d\tilde{W} + h(T_i, \lambda_i)dm_i \tag{2.55}$$

where the enthalpy $h = u + pv$ for the incoming flow and the specific heat capacity $c_v = \frac{\partial u}{\partial T}$ are introduced. When open systems are studied, it is convenient to consider the enthalpy since it encapsulates both the internal energy and the mechanical work of the inflowing masses.

2.6 Control Volume Model

To describe the state of a gas in a perfectly mixed container, the differentials that are derived from the ideal gas law (2.42), and the differentials that are derived from the energy conservation equation (2.55) can be used. To completely specify the gas properties, also the mass concentration vector is needed. An idea is to use a chemical equilibrium program that calculate the concentration of products for a given temperature and pressure. In this work, it is assumed that the gas composition is frozen so (2.49) can be used.

2.6.1 Lambda Concentration Differential $d\lambda$

The differential of the mass fraction vector can be written:

$$dX = \frac{dX}{d\lambda} d\lambda \tag{2.56}$$

where the derivative with respect to lambda is:

$$\frac{dX}{d\lambda} = \frac{a - b(A/F)_s}{((A/F)_s \lambda + 1)^2} \tag{2.57}$$

where $a = (A/F)_s x_a$ and $b = S x_f$ are introduced for easier notation. The differential for the mass fraction, that was derived previously in (2.49), can be combined with (2.56) and (2.57) to get:

$$\frac{1}{m} \sum_i \left[\frac{a\hat{\lambda}_i + b}{(A/F)_s \hat{\lambda}_i + 1} - \frac{a\lambda + b}{(A/F)_s \lambda + 1} \right] dm_i = \frac{a - b(A/F)_s}{((A/F)_s \lambda + 1)^2} d\lambda \tag{2.58}$$

which can be simplified to:

$$d\lambda = \frac{1}{m} \sum_i \left[\frac{(A/F)_s \lambda + 1}{(A/F)_s \hat{\lambda}_i + 1} \left(\hat{\lambda}_i - \lambda \right) \right] dm_i \tag{2.59}$$

where

$$\hat{\lambda}_i = \begin{cases} \lambda_i & \text{When gas stream } i \text{ flows into the mixer } (dm_i > 0) \\ \lambda & \text{When gas stream } i \text{ flows out from the mixer } (dm_i \leq 0) \end{cases} \tag{2.60}$$

as before. In this case, the mass fraction differential which is a vector can be replaced with the lambda differential that is a scalar. It can also be noted that the mass concentration vectors for the air a and for the fuel b do not appear in (2.59). It is only the stoichiometric air/fuel ratio $(A/F)_s$ that is included in (2.59).

Partial Derivatives of Gas Property Functions

The derivative of the mass concentration vector with respect to lambda (2.57) can instead be written:

$$\begin{aligned}\frac{dX}{d\lambda} &= \frac{(A/F)_s}{(A/F)_s\lambda+1}\Big(x_a - \frac{(A/F)_s\lambda x_a + Sx_f}{(A/F)_s\lambda+1}\Big) \\ &= \lim_{h\to\infty}\frac{(A/F)_s}{(A/F)_s\lambda+1}\Big(X(h) - X(\lambda)\Big)\end{aligned} \tag{2.61}$$

where pure air has a lambda that is "infinitely" large.

The partial derivatives with respect to lambda of gas property functions for the frozen mixture described in sub-section 2.4.1 can be written:

$$\frac{\partial h}{\partial\lambda} = h_{air}^T\frac{dX}{d\lambda}, \qquad \frac{\partial u}{\partial\lambda} = u_{air}^T\frac{dX}{d\lambda} \tag{2.62a}$$

$$\frac{\partial R}{\partial\lambda} = R_{air}^T\frac{dX}{d\lambda}, \qquad \frac{\partial c_p}{\partial\lambda} = c_{p,air}^T\frac{dX}{d\lambda} \tag{2.62b}$$

where h_{air} is the enthalpy, u_{air} is the internal energy, R_{air} is the gas constant, and $c_{p,air}$ is the heat capacity of the ambient air. All partial derivatives are scalars and depend on the ambient air temperature T and relative humidity RH.

2.6.2 State Equations

The differentials for the ideal law, the energy conservation, and the air/fuel concentration can be summarized in the following state equation differentials:

$$\begin{aligned}Vdp - mT\frac{\partial R}{\partial\lambda}d\lambda - mRdT &= RTdm \\ m\Big(c_v dT + \frac{\partial u}{\partial\lambda}d\lambda\Big) &= dE - udm \\ d\lambda &= \frac{1}{m}d\Lambda\end{aligned} \tag{2.63}$$

where

$$dm = \sum_i dm_i \tag{2.64a}$$

$$dE = \sum_i h_i dm_i \tag{2.64b}$$

$$d\Lambda = \sum_i\left[\frac{(A/F)_s\lambda+1}{(A/F)_s\hat{\lambda}_i+1}\Big(\hat{\lambda}_i - \lambda\Big)\right]dm_i \tag{2.64c}$$

are introduced for simplicity. Differential dE is the energy contribution of the incoming fluids, $d\Lambda$ is the air/fuel ratio contribution, and dm is the total change of mass in the volume. The air/fuel ratio is, as previously defined:

$$\hat{\lambda}_i = \begin{cases}\lambda_i & \text{When gas stream } i \text{ flows into the mixer } (dm_i > 0) \\ \lambda & \text{When gas stream } i \text{ flows out from the mixer } (dm_i \le 0)\end{cases} \tag{2.65}$$

In Eq (2.63), dQ and $d\tilde{W}$ are assumed to be zero, i.e., a perfectly insulated container with no applied external work. State variables for the control volume can be chosen as pressure, temperature and air/fuel ratio. In Figure 2.6 the exchange of mass, energy, and lambda according to (2.64) are showed.

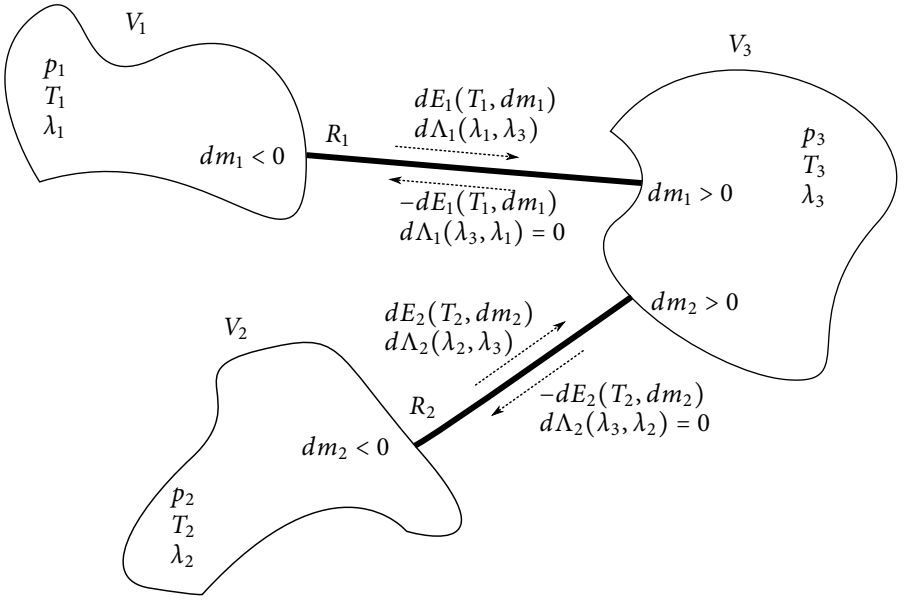

Figure 2.6: In the figure, three control volumes, together with two flow restrictions are presented. The mass flows through the restrictions have the directions from volumes V_1, and V_2 to volume V_3. The flow variables through the restrictions are the mass flow, the enthalpy flow, and the lambda flow according to (2.64).

2.7 Conclusion

In the chapter, fundamental thermodynamic concepts are presented that can be used when a gas turbine model is developed. In the present study, these concepts are implemented in the gas turbine package – GTLib, which will be presented further in Chapter 3. The central part of the chapter is the development of a control volume model, where an exhaust gas is specified with the three states pressure p, temperature T, and air/fuel ratio λ. The ambient air, which is used in the combustion, can handle different amounts of humidity through an adjustment of the mass fraction of water. The framework handles hydrocarbon fuel with a number of individual species. To model atmospheric air in a control volume, the λ variable needs to be specified large, i.e, preferably "infinitely", but a large number is sufficient in practice.

The advantage with using the presented thermodynamic concept is the ability to integrate combustion in the model. During the combustion, the mass concentrations

of species in the incoming air are changed, since species of carbon dioxide and water are produced under the consumption of oxygen. The number of these constructed species depends on the actual hydrocarbon species in the fuel and this reaction formula is specified in the stoichiometric matrix. The mass fraction of species in the exhaust gas is specified with the state variable air/fuel ratio λ. For this procedure, the assumptions are: (1) the combustion is lean, i.e., $\lambda > 1$, and (2) the exhaust gas is frozen in composition, i.e., no dissociation effects between the species occur. The first assumption is not a problem in a gas turbine application, since an excess of oxygen is available. The second assumption can be a problem if the flame temperature is too high. It is shown that for temperatures above 1500 K, the thermodynamic properties of the fluid start to change. For a temperature of 2000 K, the error in heat capacity c_p is about 8 % against a calculation where dissociation effects are considered. For the temperature of 1500 K, the error is only 2 %.

Chapter 3

GTLib – Thermodynamic Gas Turbine Modeling Package

The objective of the chapter is to introduce the gas turbine package – GTLib, which can be used when a gas turbine model is constructed. A gas turbine model constructed in GTLib can be used for performance calculation and as a base for further investigations when a diagnosis and supervision system is constructed. An important part of GTLib is the medium model which is used in the thermodynamic gas turbine components. In the medium model, the implemented thermodynamic relationships are fundamentally based on the presented equations in the previous chapter. The benefit with using GTLib is an overall reduction in the gas turbine model equations compared to the reference gas turbine model and the ability to automatically construct test quantities used for diagnosis and supervision in a systematic manner.

In Section 3.1, background theory and information of the considered gas turbine are presented. An important part of the performance calculation is the performance characteristic and an overview of a typical appearance of these maps will also be presented in the chapter. The performance characteristics, for the compressor and the turbine, utilize the concept of corrected parameters which will be explained in sub-section 3.1.2. In Section 3.2, the GTLib package is presented together with a control volume example. The purpose with the Example 3.1 is to evaluate the behaviour of the gas properties between the GTLib package and the Media library contained in the standard Modelica package. In the control volume example, a transient in the ambient air composition of species is investigated. In Section 3.3, the implementation of GTLib at a high level is presented. Here, the medium model and its implemented thermodynamic functions together with the gas turbine components are shown. These presented gas turbine components are; the control volume, the compressor, the turbine, and the combustor.

3.1 Background

The gas turbine considered here is a 1-spool and 2-shafted gas turbine which is shown in Figure 3.1. In these kinds of gas turbines a gas generator, which consists of a compressor

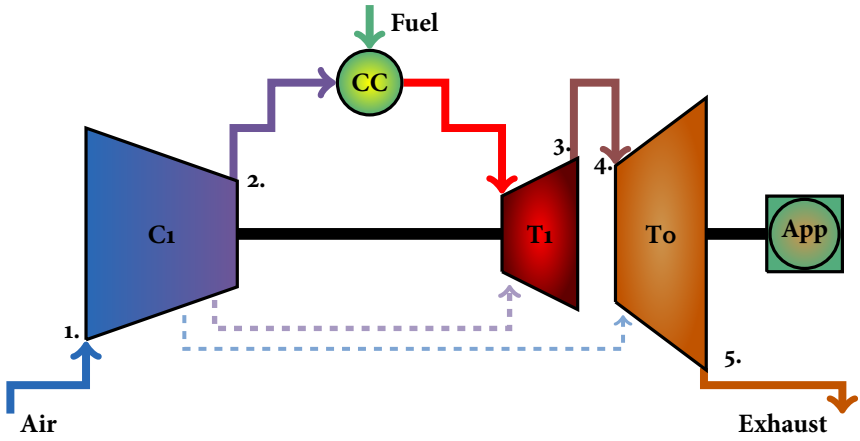

Figure 3.1: An overview of a 2-shafted gas turbine with cooling air is shown in the figure. This gas turbine consists of a gas generator (consists of a compressor and a compressor-turbine), a power turbine, and an external application. The gas generator supplies the power turbine with hot gases and the power turbine delivers the work demanded by the application. The cooling air, tapped from the compressor is shown with dashed arrows in the figure.

and a turbine, is used to generate hot gases for the power turbine. The temperature of the hot gases is too high for the material in the first turbine blades. To protect the first blades of the turbine, cooling air is injected which creates a thin film of air around the blades. The work that is delivered to the application is taken from the power turbine. In a 2-shafted gas turbine, a mechanical connection between the gas generator and the power turbine is absent. Therefore, a transformation between rotational speed and delivered torque is possible for a given amount of output power. This is suitable for *mechanical drive* sites where the external application is, e.g., a pump or an external compressor. The driven component can for example be used to pump gas in a pipeline with a variable speed.

One of the objective with this work is to construct a framework where tests used for supervision of components and diagnosis statements can be generated in an systematic manner. The supervised components can for example be the compressor where the efficiency is monitored due to fouling. The diagnosis statements can for example be that a specific measurement sensor has an unknown bias error. A more general diagnosis statement is that the sensor is broken with an unknown faulty mode. The gas turbine fleet that is supervised today consists of about two hundred individuals at different locations around the world. The individuals have different hardware configurations and are used in several types of applications. The ambient conditions at the site locations can be

different and the ambient conditions can also change with time, i.e., summer and winter. Therefore, a systematic method to handle these challenges is desirable to obtain which should reduce the overall work needed for supervision. The systematic method should also give reliable monitoring results.

In Chapter 1, the available performance model written in Modelica was introduced. Since a lot of work has been spent on the development of the performance model, a good idea is to re-use a big part of the performance model also in the diagnosis and supervision system. A challenging task with the available reference gas turbine model is the complexity according to the number of variables and equations. A lot of these equations can be associated with the using of the Modelica media package. The generality, that Modelica media represents, are paid in the number of equations. Modelica media is complex, so it can be challenging to make a parser that can handle the complexity. Therefore, a new package called Gas Turbine Library – GTLib is constructed where the gas property descriptions are based on the air/fuel ratio λ instead of the mass fraction of each gas species. The GTLib is constructed in a way that makes it possible to automatically extract model properties with a developed Modelica parser presented in Chapter 4.

3.1.1 The Gas Turbine Cycle

The gas turbine cycle is best described by the Brayton cycle see, e.g., Giampaolo (2009); Horlock (2007); Saravanamuttoo et al. (2001). In the ideal Brayton cycle, expressed in temperature and entropy, the entropy is constant during the compression and the expansion phases. A Brayton cycle, with two turbines, is shown in Figure 3.2. In the figure, a *non ideal* gas turbine cycle (dotted lines) is also viewed where the entropy increases during the compression and the expansion phases. This means that more work needs to be supplied in the compression phase and less heat is converted to work in the expansion which leads to lower efficiency. During the combustion, the pressure is constant and the supplied heat is Q_{in} and heat which is leaving the gas turbine is denoted Q_{out}.

3.1.2 Performance Characteristics

A simple approach to describe the performance of a gas turbine component is to assume that the isentropic efficiency η_{is} is constant. In, e.g., Hadik (1990), the isentropic efficiency is considered to be $\eta_{is} = 0.87$. A more sophisticated method to describe the performance of gas turbine components, such as compressors and turbines, is to use look-up tables of *corrected parameters*. The advantage with using corrected parameters in the look-up tables is the ability to describe the performance in other operating conditions than at the measured reference conditions. The corrected parameters are collected in non-dimensional groups which have a background in dimensional analysis (Buckingham, 1914). A relation between the non-dimensional groups is presented in, e.g., Dixon and Hall (2010); Saravanamuttoo et al. (2001); Heywood (1988); Volponi (1999), and is re-

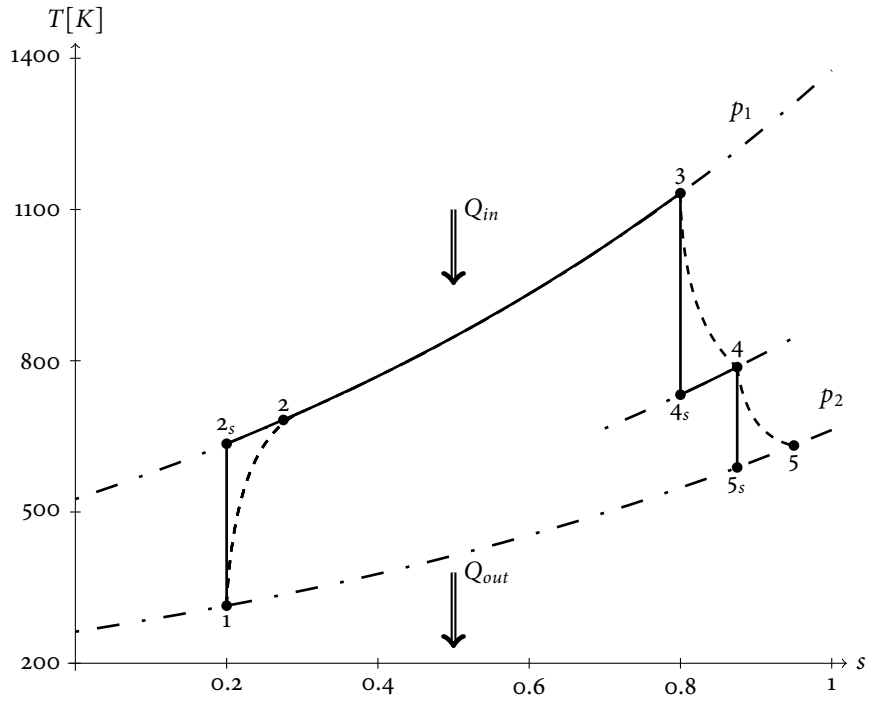

Figure 3.2: An ideal (solid lines), and a non ideal (dotted lines) Brayton cycle of a 2-shafted gas turbine is shown in the figure. In the non ideal cycle, the entropy in the compression and the expansion phase is not constant. This means that more work needs to be supplied in the compression phase and less heat is converted to work in the expansion phase, i.e., the entropy increases. In the non ideal gas turbine cycle, no pressure losses in components are considered. The numbers in the figure represent the gas path positions which are shown in Figure 3.1.

viewed here:

$$\Big[\Pi, \underbrace{\eta_{is}}_{\eta^*_{is}}\Big] = f\Big(\underbrace{\frac{m_{flow}\sqrt{T_{01}R\gamma}}{D^2 p_{01}}}_{m^*_{flow}}, \underbrace{\frac{nD}{\sqrt{T_{01}R\gamma}}}_{n^*}\Big) \tag{3.1}$$

where n is the shaft speed, D is the impeller diameter, Π is the pressure ratio, m_{flow} is the mass flow of air, R is the specific gas constant, γ is the heat capacity ratio, T is the temperature, p is the pressure, and η_{is} is the isentropic efficiency. The indices in, e.g., T_{01} denotes stagnation temperature at the inlet of the component and the indices will be removed in the following section to get simpler notation. The function arguments are corrected parameters and will be denoted with $(*)$ in the sequel. For a specific gas turbine, the impeller diameter is fixed so D in (3.1) can be neglected. Normalized quantities of the corrected parameters can be constructed by multiplication of a non-dimensional constant to get:

$$m^*_{flow,norm} = 100\frac{m_{flow}}{m_{flow,ref}}\frac{p_{ref}}{p}\sqrt{\frac{T}{T_{ref}}\frac{R}{R_{ref}}\frac{\gamma}{\gamma_{ref}}} \tag{3.2a}$$

$$n^*_{norm} = \frac{n}{n_{ref}}\sqrt{\frac{T_{ref}}{T}\frac{R_{ref}}{R}\frac{\gamma_{ref}}{\gamma}} \tag{3.2b}$$

$$\eta^*_{is,norm} = \frac{\eta_{is}}{\eta_{is,ref}} \tag{3.2c}$$

$$C^*_{norm} = \frac{C}{C_{ref}}\sqrt{\frac{R}{R_{ref}}\frac{\gamma}{\gamma_{ref}}} \tag{3.2d}$$

where (ref) denotes the reference value at the datum state. In the last expression, the *flow capacity* notation is introduced where $C = \frac{m_{flow}\sqrt{T}}{p}$. The reference parameters must be given together with the look-up tables which are described in the following sub-section.

Compressor Map

The performance of the compressor is described by a look-up table of corrected and normalized parameters. The variables, given by the map, are the normalized mass flow of air, and the isentropic efficiency according to:

$$m^*_{flow,norm} = g_1(\Pi, n^*_{norm}, \alpha) \tag{3.3a}$$

$$\eta^*_{is,norm} = g_2(\Pi, m^*_{flow,norm}, \alpha) \tag{3.3b}$$

where the function in (3.1) is extended with the angle α of the inlet guide vanes (IGV). The IGV:s are used to change the surge line in the compressor map which can be useful when the gas turbine starts up. With an IGV, the compressor can cover a wider operating range since the surge line is moved. In Figure 3.3, the isentropic efficiency is plotted versus the normalized corrected mass flow. In the figure, also the normalized speed lines are plotted versus the normalized mass flow.

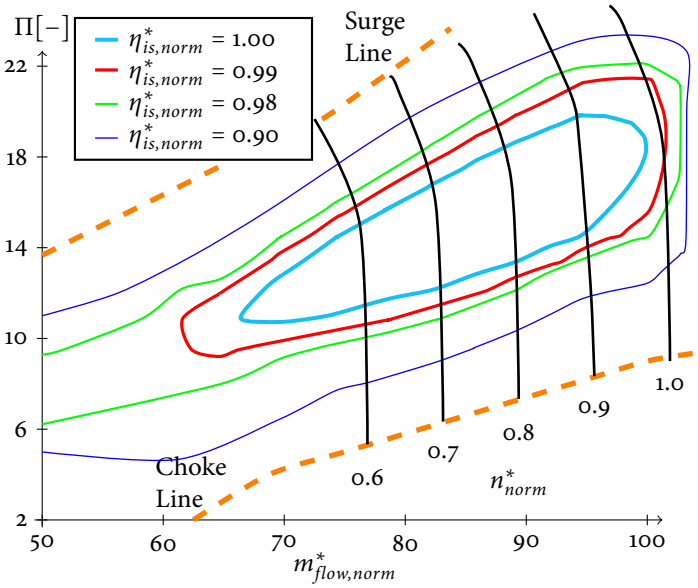

Figure 3.3: In the figure, a typical appearance of the performance characteristic of a compressor is viewed. In the compressor map, the efficiency and the normalized mass flow are calculated for different pressure ratios and speeds. The surge line and the choke line are also viewed in the figure.

Turbine Map

The performance of the turbine is described in the same way as for the compressor, i.e., using of normalized variables and look-up tables. Here, the calculated variables are turbine flow capacity C_T and isentropic efficiency according to

$$C^*_{T,norm} = h_1(\Pi, n^*_{norm}\frac{n_{ref}}{\sqrt{T_{ref}}}) \tag{3.4a}$$

$$\eta^*_{is,norm} = h_2(\Pi, n^*_{norm}\frac{n_{ref}}{\sqrt{T_{ref}}}) \tag{3.4b}$$

where T_{ref} and n_{ref} from (3.2b) are neglected. In Figure 3.4, an example of a turbine map is viewed. In the figure, typical appearances of corrected and normalized isentropic efficiency, and turbine flow capacity are plotted versus the pressure ratio.

3.2 Gas Turbine Library – GTLib

The gas turbine package GTLib can be used when a gas turbine model is constructed. The advantage with GTLib is the ability to build up a model which can be used for performance calculation and as a base when diagnosis tests are constructed. The GTLib is

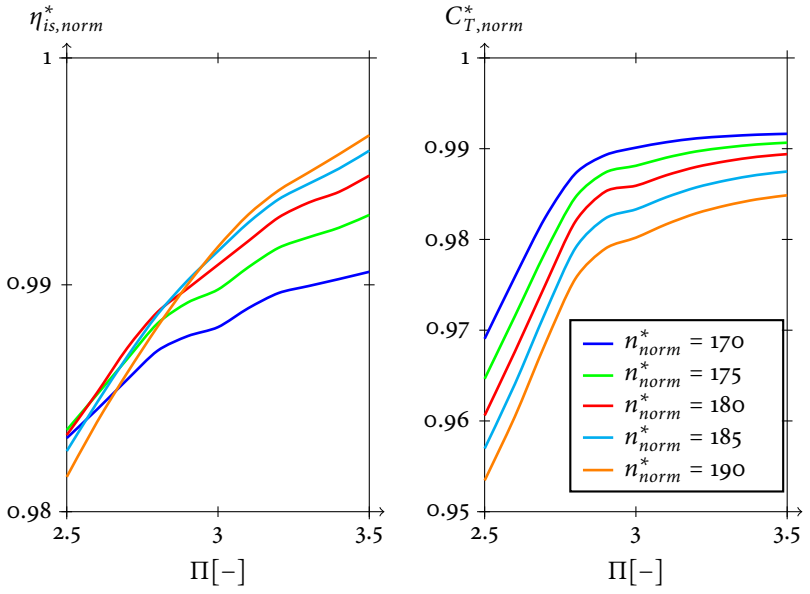

(a) Turbine efficiency. **(b)** Turbine flow capacity.

Figure 3.4: In the figure, a typical appearance of the performance characteristic of a power turbine for different normalized speeds, is viewed.

mainly divided in two parts; (1) a medium model library, and (2) a gas turbine component library. In the medium model, the thermodynamic relationships presented in Chapter 2 are implemented. In the component library, gas turbine components that utilize the medium model are implemented.

3.2.1 Variation in Ambient Air Composition

The gas model, in its original design, can only handle fuel and air gases with a fix concentration of respective species. If the properties of the ambient air are changed, a number of constants need to be updated in the medium model. These constants are the stoichiometric air/fuel ratio $(A/F)_s$, the internal energy of air u_{air}, the enthalpy of air h_{air}, and the gas constant of air R_{air}. These constants appear, e.g., in Eq. (2.33), (2.62), and (3.28) where the last expression is presented in the next sub-section. Thus, if the gas model should compensate for variation in the ambient air composition, these constants need to be updated. In GTLib, these constants are a direct function of the ambient conditions such as temperature T, pressure p, and relative humidity RH and can be calculated using a moist air model (Buck, 1981). The calculation performed in the moist air model is shown in Table 3.2 and is used when the mass concentration air vector of the ambient air is determined. In the implementation, the ambient conditions are declared as global (inner/outer concept in Modelica) which allows a simultaneous

update of the considered constants. The simultaneous update procedure of the constants can be summarized in the following steps:

1. Calculate the concentration of species in the ambient air, i.e., use the moist air model with inputs: pressure, temperature, and relative humidity.
2. Calculate the air specific constants such as: $(A/F)_s$, u_{air}, h_{air}, and R_{air}.
3. Update $(A/F)_s$ in the control volume, in the combustor, and in the turbine components.
4. Update all thermodynamic functions such as $h(T, \lambda)$, $u(T, \lambda)$, and $R(\lambda)$ with constants in step 2.
5. The air/fuel ratio λ gives now the actual concentration of species in the exhaust gas.

With this procedure, the gas properties are updated instantaneous in all gas turbine components. This results in an error during transients in the ambient air composition which Example 3.1 should symbolize. For the gas turbine application, this phenomenon is negligible because of the high throughput speed compared to the changes in the ambient conditions. The ratio between the control volumes and the mass flow is small, i.e., the gas exchange is fast in the control volumes. The update of the gas property constants is called a *quasi-static* change of ambient conditions in the thesis.

Example 3.1

Before the gas turbine performance model is presented, it is a good idea to introduce a small simulation example that shows the main difference in gas properties between a model which uses the GTLib package and a model which uses Modelica Media package. In Figure 3.5, a model that consists of a source S_1, a sink S_2, a control volume V_{10}, and two pressure losses dp_1, dp_2, is shown. The same type of models is used in the two simulation

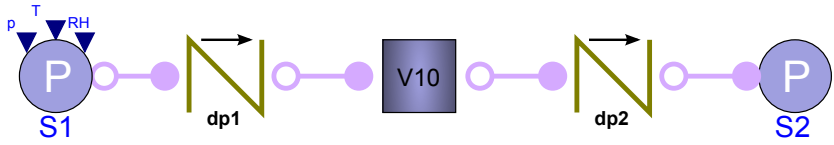

Figure 3.5: In the figure, a sub-system with a control volume V_{10}, a gas source S_1, a gas sink S_2, and two pressure losses dp_1, dp_2 is presented. The input signals to the system are the pressure p, the temperature T, and the relative humidity RH of the ambient air. It is assumed that the pressure in the gas source is higher than in the gas sink which gives a mass flow direction to the right in the figure.

cases, and a step is injected in the ambient conditions such as temperature T and relative humidity RH. In the example, it is interesting to compare how the gas properties in the volume V_{10} are affected when the temperature, and relative humidity have changed. To

show this phenomenon, it is assumed that the incoming volume mass is much less then the available control volume mass in V_{10}, i.e., it takes long time to change all the mass in the control volume. In Figure 3.6, the temperature T, the pressure p, the specific gas constant R, the specific enthalpy h, the density d, and the relative humidity RH of the control volume V_{10} are viewed for the two simulation cases.

In the figure, it can be seen that during transients in ambient conditions, gas properties such as specific gas constant, specific enthalpy, and density change instantaneously in GTLib, except for the temperatures in subfigure 3.6a. This is because $(A/F)_s$ and x_a in (2.33) are changed directly according to the ambient conditions, so they are updated instantaneously in all components in the model. When the transients have declined, the gas properties converge to the same values for the two simulation cases.

In the example, the incoming mass is much less than the mass in the control volume which can be seen as an extreme case. For the real gas turbine application, the throughput speed for the gas turbine is high so the error due to transients in ambient conditions is not a problem. The ratio between the control volumes and the mass flow is small.

3.2.2 Gas Turbine Model

The main difference between the gas turbine model (described in the present chapter) and the reference gas turbine model (described in Chapter 1) is the description of the gas used in the medium model. In the present gas turbine model, the gas is specified through the air/fuel ratio λ and in the reference model the gas is specified through the mass fraction of species in the air and fuel gases. A benefit with this model is the reduction of equations and states according to the lambda description. The reduction in model size reduces the demanded simulation time.

The goal with the modeling work is to get a gas turbine model that can be used in performance calculation and as a base for diagnosis test generation. To make a gas turbine model which fulfill these two conditions, the GTLib package is introduced. Why the gas turbine model and not the reference model can be used for this purpose depends on the parsers which are developed. These parsers can only parse a subset of the Modelica language. The components in GTLib fulfill the specification of the parsers and can therefore be used to generate diagnosis tests. More about the test selection and construction procedure will be described in Chapter 4. Since the Modelica Media package used in the reference model is very general, it can be a challenge to develop parsers for this model.

The gas turbine model consists of a number of standard components, such as control volumes, valves, turbines, etc. The gas turbine model and the reference model have the same environment connections which means that both models can be evaluated in the same simulation platform. The available instrumentation sensors measure pressure and temperatures throughout the gas path, and angular velocities of the shafts. Between the output of the compressor *C1* and the output of the power turbine *To* there are no available measured gas path parameters. This results in gas path parameters that have to

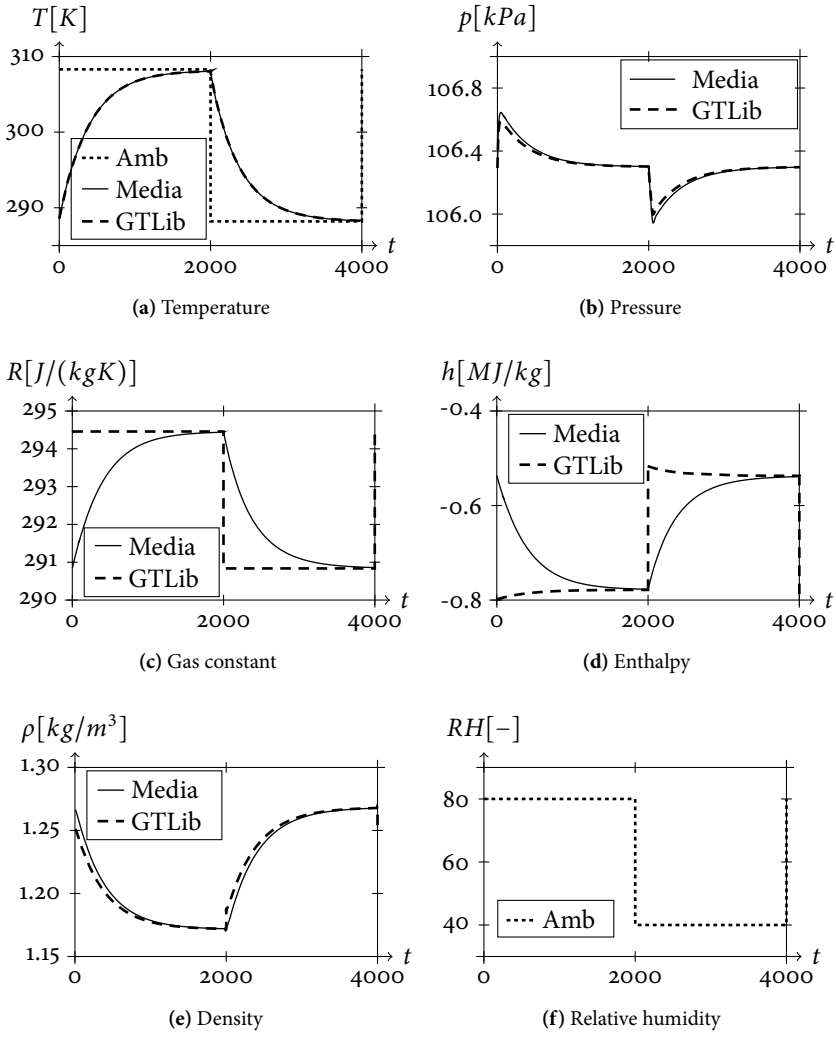

(a) Temperature **(b)** Pressure

(c) Gas constant **(d)** Enthalpy

(e) Density **(f)** Relative humidity

Figure 3.6: In subfigure a, a step in temperature T and relative humidity RH of the ambient air is introduced at time 0 and 2000. The experiment is performed for the two test cases where GTLib (dashed line) and Modelica Media (solid line) are used in the sub-system presented in Figure 3.5. In the subfigures, the thermodynamic properties of the gas enclosed in the control volume V_{10} are shown. The gas properties in all subfigures mismatch during the transient but the effect on the temperature is very small. The mismatch during a transient depends on an instantaneous change in the gas properties in GTLib, e.g., the gas constant R goes from ≈ 294 to 291 immediately. In the real gas turbine application, this phenomenon is not a problem since the mass flow is large compared to the size of the control volumes.

be estimated, since these quantities are important to supervise in the diagnosis tests. The gas turbine model and the actual measurement sensors are shown in Figure 3.7.

3.3 Implementation of GTLib

In this section, the implementation of the gas turbine modeling package GTLib is presented. The GTLib package consists of two parts: (1) a medium model library, and (2) a gas turbine component library. In this section, these two libraries will be described. In the medium model library, the gas media model is specified and the thermodynamic properties of the media are calculated. In the component library, the gas turbine components that utilize the media library are implemented.

3.3.1 Connectors

In Modelica, information between components is shared through connection points that are called connectors. In a connection point, there are basically two kinds of variables which are either defined as a flow or a non-flow variable. In a connection point, flow variables are summed to zero, and non-flow variables are set equal.

With this approach, the flow variables are identified from Eq. (2.64) and Figure 2.6 to be; dm, dE, and $d\Lambda$. The summation in (2.64) is performed for the number of flows in each connection point which is the same as the number of connected components. In general, each non-flow variable is specified in the control volume and each flow variable is calculated in the restrictions between the control volumes. The considered variables, which are used in the connectors are summarized in Table 3.1.

Table 3.1: In the table, the connector variables used in the GTLib package are presented. These variables are either defined as a flow or a non-flow variable. The flow variables are summed to zero and the non-flow variables are set equal in each connector point.

type	**variable**	**description**
non-flow	p	pressure
flow	dm	mass flow
non-flow	h	enthalpy
flow	dE	enthalpy flow
non-flow	λ	air/fuel ratio
flow	$d\Lambda$	air/fuel ratio flow

3.3.2 Medium Model Package

The medium model consists of a thermodynamic state model together with a number of thermodynamic functions. In the medium model, the state and state equations are specified. The included functions calculate, e.g., the enthalpy and the heat capacity.

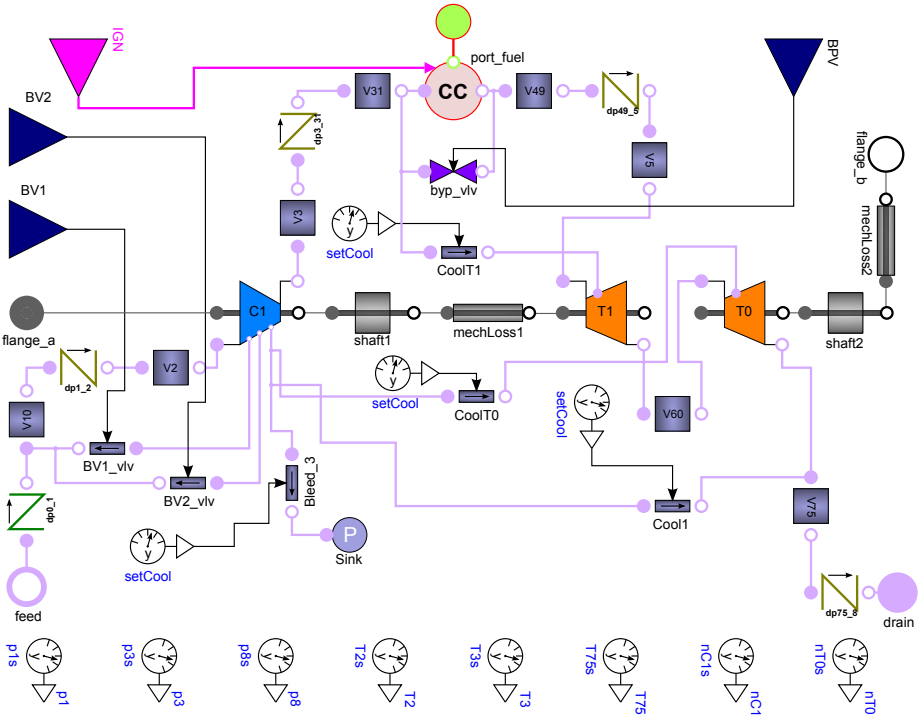

Figure 3.7: In the figure, a model of the two shafted gas turbine presented in Figure 3.1 is shown. The model consists of components from the GTLib package, such as control volumes, valves, turbines, etc. This model can be simulated together with the simulation platform viewed in Figure 1.1 since both gas turbine models have the same environment connections except for the gas sources. This model can be used for dynamic simulations exactly as for the reference model where the accuracy between the two models is high, but with a reduced simulation time. During start-up phases, the actuator signals BV1 and BV2 are used to control the bleed valves. The other actuator signals are IGN and BPV, where IGN control the ignition and BPV the bypass valve through the combustion chamber. The sensors measure pressure and temperature before and after the compressor *C1*, pressure and temperature after the power turbine *T0*, and the shaft speed of the gas generator and the power turbine. Between the output of the compressor and the power turbine there are no measured gas path parameters.

Thermodynamic data charts are available in the Modelica standard library and are used in the gas model package. The tabulated data is the well known NASA polynomial coefficients summarized in McBride et al. (2002).

Thermodynamic Gas State Model

In Modelica, a flexible medium model can be defined due to the object oriented nature of the language. In the start, a basic state model can be specified where the most fundamental relations and variables exist. This fundamental model is common for all used gases. To specify a gas in the package, three states are needed. These states are pressure p, temperature T, and air/fuel ratio λ. In every component in the gas turbine model where the medium model is used, these states must be specified. The medium model consists of a number of additional help variables which are always calculated. These additional help variables with their associated equations are:

$$h = h(T, \lambda) \tag{3.5a}$$
$$R = R(\lambda) \tag{3.5b}$$
$$u = h - RT \tag{3.5c}$$
$$d = p/(RT) \tag{3.5d}$$

where the additional variables are the enthalpy h, the gas constant R, the internal energy u, and the density d. The functions that are used in the gas model are described in the following sub-section.

Function – `lambda2mass`(λ)

The function `lambda2mass` makes a conversion between the air/fuel ratio λ, and the mass fraction vector X. The output vector X consists of the mass fraction of species in the exhaust gas for a given air/fuel ratio. This function is central since it is used everywhere the gas properties are calculated. The function is an implementation of (2.33) and is reviewed here:

$$X(\lambda) = \frac{(A/F)_s \lambda x_a + S x_f}{(A/F)_s \lambda + 1}$$

where $(A/F)_s$ is the stoichiometric air/fuel ratio, S is the stoichiometric matrix, x_a is the mass concentration of the ambient air, and x_f is the mass concentration of the fuel. All of these parameters are defined in a global environment component.

Function – `humidAirCalc`(p_0, T_0, RH)

To imitate more realistic environment conditions, a moist air model is introduced in the function `humidAirCalc`. The function calculates the mass fraction vector of species x_a in the ambient air for the input variables: ambient pressure p_0, ambient temperature T_0, and ambient relative humidity RH. These variables are defined as global environment variables and can be reached from all components in the gas turbine model. The function is called every time the vector x_a in function `lambda2mass` is needed.

In the ambient gas model, the saturation pressure of water is described by Buck (1981). This expression is well used in the meteorological context and has high accuracy in the region of -80 to 50 ^oC. The saturation pressure of water is described by:

$$p_{(H_2O)_s} = 6.1121 \cdot \left(1.0007 + 3.46 \cdot 10^{-3} p\right) \exp\left(\frac{17.502T}{240.97 + T}\right) \tag{3.6}$$

where the ambient temperature T is expressed in Celsius and the absolute pressure p is expressed in bar. The saturation pressure of water $p_{(H_2O)_s}$ is expressed in hectopascal. The relative humidity is defined according to:

$$RH = 100 \frac{p_{H_2O}}{p_{(H_2O)_s}} \tag{3.7}$$

so it is possible to calculate the partial pressure of water vapor. Here, it is assumed that the moist air consists of dry air and water steam, so the partial pressure of dry air p_{air} is simply equal to the difference in atmospheric pressure p and the partial pressure of water vapor p_{H_2O}, i.e., $p = p_{H_2O} + p_{air}$. This, together with ideal gas law (2.40) gives an expression for the mass fraction of water according to:

$$x_{H_2O} = \frac{p_{H_2O} R_{air}}{p_{H_2O} R_{air} + p_{air} R_{H_2O}} \tag{3.8}$$

Since the mass fraction of species in the dry air is known, the mass fraction of the moist air is also determined. When the moist air medium is known, it is possible to calculate thermal properties such as enthalpy and heat capacities as a function of temperature and air/fuel ratio throughout the gas path. It can be noted that a change in the absolute humidity in the ambient air affects the stoichiometric air/fuel ratio for a given hydrocarbon fuel. How the amount of water depends on the ambient condition such as relative humidity and temperature can be seen in Tab 3.2. It can be seen in the table

Table 3.2: Mass of water vapour, in gram, for 1 kg moist air at datum pressure, at temperature T, and relative humidity RH.

T (C^o)	RH = 40 %	RH = 60 %	RH = 80 %
15	4.21	6.33	8.45
20	5.78	8.69	11.61
25	7.85	11.80	15.78
30	10.53	15.85	21.20
35	13.99	21.08	28.22

that the amount of water in the air increases drastically with temperature and humidity. In the medium model, the ambient conditions affect the gas properties instantaneously in every gas turbine component. This depends on the fact that the ambient variables are declared as global and all medium models use these global variables when the mass fraction of species in the ambient air is calculated. The ambient air concentration is then used when the actual gas properties are calculated.

Function – AFS(p_0, T_0, RH)

The function `AFS` calculates the stoichiometric air/fuel ratio $(A/F)_s$ for the input variables: ambient pressure p_0, ambient temperature T_0, and ambient relative humidity RH. The stoichiometric air/fuel ratio is called from the above function `lambda2mass` when the actual air/fuel ratio is calculated. The stoichiometric air/fuel is calculated according to (2.34) and is reviewed here:

$$(A/F)_s = \left(\frac{m_a}{m_f}\right)_s = \frac{2\frac{x_{f,CH_4}}{M_{CH_4}} + 3.5\frac{x_{f,C_2H_6}}{M_{C_2H_6}} + 5\frac{x_{f,C_3H_8}}{M_{C_3H_8}}}{\frac{x_{a,O_2}}{M_{O_2}}}$$

where $x_{f,j}$ is the mass concentration of each species in the fuel, x_{a,O_2} is the mass concentration of oxygen in the air, and M_i is the mole mass of each species.

Function – h(T, λ)

The enthalpy function `h` makes the calculation according to (2.45a), and is reviewed here:

$$h(T,\lambda) = h_s(T)^T X(\lambda) \tag{3.9}$$

where h_s is a vector with enthalpies of the species for a given temperature. The data element in h_s is calculated according to the NASA polynomials. The input variables to the function are the gas temperature T, and the air/fuel ratio λ of the gas. The output of the function is the gas mixture enthalpy.

Function – s(p, T, λ)

The entropy function `s` makes the calculation according to (2.21), and is reviewed here:

$$s(T,p,\lambda) = s^o(T,\lambda) - R\ln\left(\frac{p}{p^o}\right) \tag{3.10}$$

where the absolute entropy $s^o(T,\lambda)$, and p^o is the pressure for the datum state and is defined in a global environment component. The absolute entropy can be separable and is calculated according to:

$$s^o(T,\lambda) = s_s^o(T)^T X(\lambda) \tag{3.11}$$

where s_s^o is a vector with absolute entropy of the species for a given temperature. The data that is included in the absolute entropy vector is calculated according to the NASA polynomials. The input variables to the function are the gas pressure p, the gas temperature T, and the air/fuel ratio λ of the gas. The output of the function is the gas mixture entropy.

Function – T_s(p, s, λ)

The function `T_s` calculates the temperature T of an isentropic compression, or expansion process, for the input variables: pressure p, entropy s, and air/fuel ratio λ. The function solves the entropy expression in (2.21) numerically with respect to the temperature T.

Function – R(λ)

The function R calculates the specific gas constant for the gas. For each species of the gas, the specific gas constant R (in mass basis) is tabulated in the standard Modelica package. This gas constant is simply calculated according to $R = \tilde{R}/\tilde{m}$, where $\tilde{m}$ is the mole mass of the species. The specific gas constant of the gas mixture is calculated according to (2.45c):

$$R(\lambda) = R_s^T X(\lambda) \tag{3.12}$$

where R_s is a vector with the specific gas constants of the species.

Functions – c_p(T, λ) and c_v(T, λ)

The functions c_p and c_v calculate the heat capacities of the gas. The input variables to the function are the gas temperature T and the air/fuel ratio λ. The heat capacity function c_p is calculated according to (2.45d) and reviewed here:

$$c_p(T, \lambda) = c_{p,s}(T)^T X(\lambda) \tag{3.13}$$

where $c_{p,s}$ is a vector with the specific heat capacities of species, that depends on temperature. Since the gas is an ideal gas, the heat capacity function c_v is calculated according to:

$$c_v(T, \lambda) = c_p(T, \lambda) - R \tag{3.14}$$

where R is the specific gas constant.

Function – gamma(T, λ)

The function gamma calculates the isentropic exponent γ. The input variables to the function are the gas temperature T, and the air/fuel ratio λ. The isentropic exponent is calculated according to:

$$\gamma = \frac{c_p(T, \lambda)}{c_v(T, \lambda)} \tag{3.15}$$

where heat capacities functions c_p and cv are called.

3.3.3 Components

In GTLib, a number of standard gas turbine components are implemented and the most characteristic components are presented in this sub-section.

Control Volume

The governing state equations of the control volume component are:

$$V\frac{dp}{dt} = dmRT + m(R\frac{dT}{dt} + T\frac{\partial R}{\partial \lambda}\frac{d\lambda}{dt}) \tag{3.16a}$$

$$mc_v\frac{dT}{dt} = dE - udm - m\frac{d\lambda}{dt}\frac{\partial u}{\partial \lambda} \tag{3.16b}$$

$$m\frac{d\lambda}{dt} = d\Lambda \tag{3.16c}$$

where flow quantities are defined as previous:

$$dm = \sum_i dm_i \tag{3.17a}$$

$$dE = \sum_i dE_i = \sum_i h_i dm_i \tag{3.17b}$$

$$d\Lambda = \sum_i d\Lambda_i = \sum_i \left[\frac{(A/F)_s \lambda + 1}{(A/F)_s \hat{\lambda}_i + 1} \left(\hat{\lambda}_i - \lambda \right) \right] dm_i \tag{3.17c}$$

where the calculation of dE_i and $d\Lambda_i$ is performed by the component that connects the control volumes according to Figure 2.6. The summation is performed by the control volume. The $\hat{\lambda}_i$ is:

$$\hat{\lambda}_i = \begin{cases} \lambda_i & \text{When gas stream } i \text{ flows into the control volume } (dm_i > 0) \\ \lambda & \text{When gas stream } i \text{ flows out from the control volume } (dm_i \leq 0) \end{cases}$$

The partial derivatives (2.62), according to the air/fuel ratio are calculated as:

$$\frac{\partial u}{\partial \lambda} = \frac{(A/F)_s}{(A/F)_s \lambda + 1} (u_{air} - u) \tag{3.18a}$$

$$\frac{\partial R}{\partial \lambda} = \frac{(A/F)_s}{(A/F)_s \lambda + 1} (R_{air} - R) \tag{3.18b}$$

where derivation of the partial derivative of the mass fraction function (2.61) is used together with (2.33). The final equation, connecting mass and density is:

$$m = Vd \tag{3.19}$$

where the density is available in the gas model description.

Compressor

In the compressor component, energy is transformed from mechanical energy to thermodynamic energy through a compression. This gives a component that consists of a mechanical and a thermodynamic part. During the compression, the temperature and pressure of the gas are increased. In an isentropic compression the entropy is constant, see Figure 3.2. So if the compression is ideal, it is possible to calculate the temperature or enthalpy at the high pressure side of the compressor. This is done according to the previous defined function `T_s` and can be written:

$$T_{2s} = T_s(p_2, s_2, \lambda_1) \tag{3.20}$$

The isentropic temperature T_{2s} increases the enthalpy Δh according to:

$$\Delta h = \frac{h(T_{2s}, \lambda_1) - h(T_1, \lambda_1)}{\eta_{is}} \tag{3.21}$$

where η_{is} is the isentropic efficiency. The air/fuel ratio is not changed during the compression, therefore $\lambda_1 = \lambda_2$. The thermodynamic power can be written:

$$P_{thermo} = \left[m_{flow} + \sum_i (1 - r_i) m_{flow,r_i} \right] \Delta h \tag{3.22}$$

where r_i is the enthalpy ratio for the cooling ports, where compressed air is extracted. The mechanical power is:

$$P_{mech} = \frac{P_{thermo}}{\eta_m} \tag{3.23a}$$

$$P_{mech} = \frac{d\varphi}{dt}(\tau_1 + \tau_2) \tag{3.23b}$$

where η_m is the friction constant, $\dot{\varphi} = \omega$ is the angular velocity, and τ_i is the applied torque. Finally, the mass and the energy balance must also be considered but is not shown here.

The performance parameters such as isentropic efficiency η_{is} and mass flow m_{flow} are calculated according to previous defined look-up tables in (3.3), together with the normalized corrected parameters in (3.2), where all gas variables are calculated at the low pressure side of the compressor.

Turbine

The turbine component is analogue with the compressor component, except that no cooling air is extracted from the gas expansion. Instead, compressed air from the compressor is injected in the first turbine blades to protect the material from high temperatures. Because the look-up tables are valid for the hot gases, before cooling air is injected, it is necessary to mix the hot and cool gases after the characteristic calculations are made.

Since exhaust gases and cooling air have different air/fuel ratio λ the mixed gas has the air/fuel ratio concentration according to:

$$\lambda_{mix} = \frac{(\lambda_a m_{flow,a} + \lambda_c m_{flow,c}) + \lambda_a \lambda_c (A/F)_s (m_{flow,a} + m_{flow,c})}{(\lambda_c m_{flow,a} + \lambda_a m_{flow,c})(A/F)_s + (m_{flow,a} + m_{flow,c})} \tag{3.24}$$

where (2.39) is repeated. The air is denoted with indices a, and the combustion gas is denoted with indices c.

The performance parameters for the turbine are the turbine flow capacity and the isentropic efficiency that are presented in (3.2), together with the look-up tables in (3.4) with their associated reference values. The mass flow of the exhaust gases is calculated from the relation:

$$C_T = \frac{m_{flow}\sqrt{T}}{p} \tag{3.25}$$

where the total mass flow m_{flow} through the turbine is the sum of exhaust gases and cooling air.

Combustor

In a gas turbine, the combustion is a constant pressure process. This results in a summation of reactant enthalpies of fuel and air that is equal to the summation of enthalpies of the products species in the exhaust gas. After that, the adiabatic flame temperature can be calculated according to (2.23). It is not necessary to calculate this temperature in the combustor component since this is automatically calculated in all control volumes for a given temperature and air/fuel ratio. Instead, the enthalpy at the exhaust port of the combustor component calculated is according to:

$$h_b = h_a \chi_a + h_f (1 - \chi_a) \tag{3.26}$$

where h_f is enthalpy of fuel, h_a is enthalpy of air, h_b is enthalpy of the exhaust gas, and the mass fraction of air χ_a is simply:

$$\chi_a = \frac{m_{flow,air}}{m_{flow,air} + m_{flow,fuel}} \tag{3.27}$$

The air/fuel ratio λ of the exhaust gases is:

$$\lambda = \frac{m_{flow,air} / m_{flow,fuel}}{(A/F)_s} \tag{3.28}$$

directly according to the definition in (2.25). A pressure loss model through the combustor is defined according to Saravanamuttoo et al. (2001):

$$PLF = \frac{2A^2 \rho_1 \Delta p}{m_{flow}^2} \tag{3.29}$$

where PLF is the pressure loss factor, Δp is the pressure drop, A is the maximum cross-sectional area of the chamber, and ρ_1 is the density for the incoming air.

Other Components – Pressure Losses, Valves, and Sources

In the gas turbine package, a number of common used components are implemented. These components are pressure losses, sources, and valves. Two kind of pressure losses are implemented, i.e., a simple pressure loss component (3.30a), and a turbulent pressure loss component (3.30b), according to

$$m_{flow} = m_{flow,ref} \sqrt{\frac{\Delta p}{\Delta p_{ref}}} \tag{3.30a}$$

$$m_{flow} = A \sqrt{\frac{2 \rho_1 \Delta p}{\xi}} \tag{3.30b}$$

where ξ is a pressure loss factor, Δp is the pressure loss, p_1 is the pressure of the upstream gas, ρ_1 is the density for the upstream gas, and (ref) denotes reference constants.

Two kinds of valves are implemented. The first is a simple, but not a physical based valve that depends on the pressure difference. Instead, the mass flow through the valve is

specified by the user as a fraction of the mass flow through the compressor. This valve is used to extract cooling air from the compressor to the first turbine blades. The second valve is more realistic since the mass flow depends on the area restriction that is specified by a characteristic function. The pressure loss model in (3.30b) is used for this valve, but with an extension to have chocked gas flow.

Finally, a gas source component is implemented in the package. The source specifies the boundary conditions, such as pressure, temperature, and air/fuel ratio of the incoming gas. If the source is used as sink, the temperature and air/fuel ratio of the gas are not considered.

3.4 Conclusion

In the chapter, a gas turbine modeling package – GTLib implemented in Modelica is presented. The GTLib package consists of two parts: (1) a medium model library, and (2) a gas turbine component library. The medium model handles the calculation of thermodynamic properties of the fluid, and the gas turbine component library consists of the gas turbine components. Later on in the chapter, a gas turbine model is constructed from the components in the GTLib package. In the GTLib, the air/fuel ratio concept is introduced which reduces the number of equations and variables in the gas turbine model. The constructed model can be simulated together with the existing simulation platform. The gas turbine model can handle different changes in ambient conditions. These ambient conditions are the pressure, the temperature, and the relative humidity.

The benefit with using GTLib package is the reduction in model equations compared to the reference model implemented by the company. The accuracy of the two models is similar, when transients in atmospheric concentrations of species have declined. In GTLib, the air properties are updated simultaneously in all control volumes in the gas turbine model which gives the behaviour. A disadvantage with GTLib is the loss in generality, here the only gases that are admitted to be used are the air, and fuel gases. The consequence is that an injection of, e.g., pure oxygen somewhere in the gas path is not allowed. An advantage with GTLib is that the reduced number of equations gives a decreased simulation time when the simulation platform is simulated. The main propose with GTLib is that a diagnosis and supervision system can be constructed with the GTLib gas turbine model as a base.

Chapter 4

Diagnosability Analysis and Test Selection Procedure

The idea with the introduced GTLib package presented in the previous chapter is the ability to use the same modeling package to investigate models used for performance calculations and diagnosis statements. The question is how the performance model can be used for diagnosis purposes or which of the equations, in the performance model, are necessary to consider in the diagnosis tests? Therefore, the objective of this chapter is to present a systematic method that can be used to choose a subset of equations from the gas turbine model. These equations are then analyzed and transformed to a suitable form that can be implemented in a diagnosis test used for diagnosis and supervision of the gas turbine application. To simplify the equation selection procedure and introduce estimation parameters, a diagnosis model is developed and introduced in Section 4.2. The diagnosis model, presented in Section 4.7, is similar to the performance model introduced in the previous chapter but the main differences are; (1) bleed valves in the compressor are removed and (2) estimation parameters used to capture health deterioration are introduced. The estimation parameters, used throughout the gas path are called health parameters in the literature. These health parameters are typical correction factors of efficiencies and flow capacities in the gas turbine components. Here, the model is augmented with health parameters in the components; (1) compressor, (2) compressor-turbine, and (3) power-turbine. The equations that are used in the diagnosis tests are selected carefully from the diagnosis model using structural methods shown in Section 4.3. Here, the Dulmage-Mendelsohn decomposition is chosen to select relevant parts of the model. In Section 4.4, a DAE-index analysis of the test equations is investigated and an index reduction is performed since the DAE-index is higher than one. Finally, in Section 4.5 a structural observability analysis of the test equations is investigated.

In Section 4.7, a number of parsers used for an automatic extraction of the test equations are presented. These parsers are used to convert the Modelica models constructed in GTLib package into runnable Matlab code. This is done because the model properties

and the diagnosability of the test equations can be analyzed in the Matlab environment. An automatic extraction is also desirable since the size of system is large. The output, when all parsers are utilized, is the equations in state space form which can be used in a diagnosis test.

4.1 Gas Turbine Monitoring

In industrial gas turbines, deterioration of components throughout the gas path is commonly occurring and contributes to the overall performance degradation of the engine. Monitoring and supervision of performance degradation in the application is a widely studied topic in the gas turbine diagnosis research field, see, e.g., Aker and Saravanamuttoo (1989); Volponi et al. (2003); Doel (2003) where the performance parameters are estimated with different methods. If reliable performance estimations are available, it can be easier for the service engineers to efficiently plan service and maintenance of the gas turbine. In Aker and Saravanamuttoo (1989), it is investigated how compressor fouling affects the performance parameters using a linear fouling model. For a medium fouled compressor, the estimations appear to be reasonably accurate for the linear fouling model.

In papers Diakunchak (1992); Kurz and Brun (2001); Kurz et al. (2009), several mechanisms which cause degradation in gas turbines are presented. The major contribution of degradation mechanisms in an industrial gas turbine is *fouling*. The fouling is caused by small particles and contaminants in the air that are caught by the compressor. These particles increase the roughness of the rotor and stator surface. Another effect that results in performance degradation is the *tip clearances*, which is a common diagnosis for aged gas turbines. Tip clearances denote an increasing gap between the rotating blades and the stationary casing. Fouling due to increased roughness can partially be restored by washing the compressor, while a component replacement is often needed for tip clearances. In the paper Brekke et al. (2009), compressor fouling in two different off-shore gas turbine applications is investigated. The fouling analysis showed that a considerable amount of contaminants appeared at the compressor inlet, at the inlet guide vanes, and at the first rotor stage of the compressor. In this case, the main contaminant in the samples was sodium-based salts which indicate that the gas turbine performance can be restored by a compressor wash.

Experimental data of a fouled compressor, on a large industrial gas turbine site, results in a 5 % reduction in inlet mass flow and 1.8 % reduction in compressor efficiency. This gives a reduction in the output power by about 7 % and increases the heat rate by about 2.5 % (Diakunchak, 1992).

4.1.1 Gas Path Analysis

One of the most famous and pioneering tool of gas turbine engine monitoring and sensor diagnosis is the *gas path analysis* (GPA). The gas path analysis tool was introduced by Urban (1969) and an investigation of the method in a gas turbine engine application was presented in Urban (1972). The GPA method is based on thermodynamic relationships,

and the main objective is to estimate deterioration in gas path components from a number of measured sensor signals which are denoted as *measurement deltas* (Δ). In Urban (1969), a chart that contained the most commonly occurring gas turbine engine parameter interrelationships in a general matrix form was presented. These equations could be used to estimate steady state and transient variations in the performance parameters for an arbitrary gas turbine engine during most conceivable sets of input conditions. The chart is also re-printed in Giampaolo (2009) and the linear relationship between the measured signals and the engines health parameters can be written:

$$\Delta Z = H\Delta h + e \tag{4.1}$$

where ΔZ is the measured parameter deltas, Δh is the deviation in performance, H is the influence coefficient matrix presented in Urban (1969), and e is the measurement noise. Elements in Δh are efficiencies $\Delta\eta$, and flow capacities $\Delta\Gamma$ of the gas path components such as; compressors, turbines, and fans. Elements in ΔZ are typically spool speeds ΔN, temperatures ΔT, and pressures ΔP. The matrix H can be divided into two parts; an engine fault influence matrix H_e, and a sensor fault influence matrix H_s, where the previous matrix H is extended with the sensor fault dependencies.

The primary goal with the gas path analysis framework is to estimate the health parameter delta vector Δh. Depending on the size of the H matrix, different approaches are relevant to consider. If the engine's health is considered and not the sensor faults, the equation system (4.1) is often over-determined, i.e., the number of measurement deltas are larger than the number of health parameter deltas. This results in an optimization problem and, e.g., least-square methods can be applied to solve the optimization problem. In Doel (1994), the commercial gas path analysis program TEMPER is presented, where equation (4.1) is solved using a weighted least-squares technique. If also the sensor faults are considered in the equation system (4.1) the Δh vector is extended with the sensor faults and the matrix H is extended with the influence of the faults. This results in an under-determined system.

The Measurement Delta Vector

The measurement delta vector describes the deviation, from a nominal baseline in percent, for a number of known signals (or combination of known signals). These deviations (or deltas) are then assembled in the ΔZ-vector in (4.1). For example, the measurement delta ΔZ_P of the gas path parameter P is defined:

$$\Delta Z_P = 100\frac{P_{corr} - P_{nominal}}{P_{nominal}} \tag{4.2}$$

where P_{corr} is the normalized value according to the actual ambient conditions and $P_{nominal}$ is the nominal value under the chosen reference state. The nominal value is often calculated using a model of the actual gas turbine engine where the inputs are, e.g., the ambient conditions, the mass flow of fuel, and the generated power by the application. A sketch of the calculation procedure is shown in Figure. 4.1. A typical diagnosis algorithm uses the measurement deltas to automatically detect abnormal changes in the component according deteriorations or sensor faults, e.g., in Ganguli and Dan (2004) a recursive

filtering approach is utilized to filter the measurement deltas to recognize an abnormal change in the supervised components.

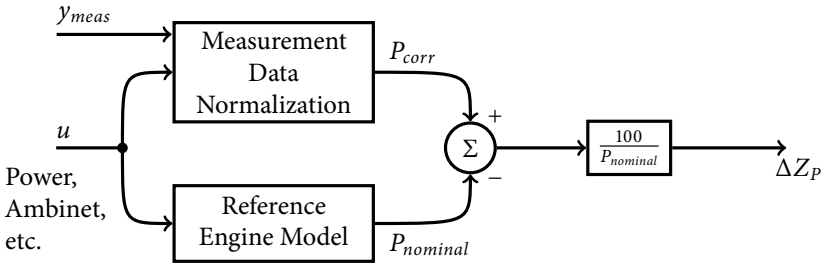

Figure 4.1: Measurement delta ΔZ_P calculation of the gas path parameter P. The reference engine model is typically the performance model described in Section 1.2 on page 2 or in subsection 3.2.2 on page 41.

4.1.2 Engine Health Monitoring

A common approach in the gas turbine diagnosis research field to capture performance degradation is to introduce a number of physical based quantities named *health parameters*. In the equation system (4.1), the deteriorations of components are the only unknown variables in the model. A natural extension of the static model in (4.1) is to introduce the health parameters in the dynamic gas turbine model. As in the static case, these health parameters are typically corrections, or deviations from a nominal baseline, of efficiencies and flow capacities. The considered health deterioration appears in the compressors, in the turbines, in the fans, and in the nozzles. The introduced health parameters can be estimated with a number of techniques, see, e.g., Luppold et al. (1989); Kobayashi and Simon (2003); Borguet and Léonard (2008). In the first two papers, Kalman filters are utilized to estimate the considered health parameters. In the third paper, a quadratic programming approach is used to estimate the health parameter values.

Since performance degradation in the gas turbine is naturally occurring, it can be difficult to avoid sensor fault alarms if the diagnosis system does not compensate for the degradation. This depends on the fact that the error in the performance model gets larger with a high degree of deteriorated components. This can result in estimated sensor values that differ too much from the measured sensor value to trigger a sensor fault alarm (Kobayashi and Simon, 2003).

4.2 Gas Turbine Diagnosis Model

The gas turbine model that is used in the developing phase of the test quantities, which are included in the diagnosis system, is a *reduced* and a *simplified* version of the reference gas

turbine performance model viewed in Figure 1.1. This reduced and simplified model is called the *diagnosis model* and an overview of the diagnosis model is shown in Figure 4.2. In this chapter, the diagnosis model is transformed into smaller subsets that are called *test equations* which are used in the diagnosis tests. In Chapter 5, these test equations are implemented and evaluated on experimental data. Here, the word reduced means that the number of equations and states has decreased according to the utilization of the GTLib package in the model. The term simplified means that some model simplifications have been done. In this case, the bleed valves in the compressor and the bypass over the combustor are assumed to be closed so they can be removed in the model. The bleed valves are usually used during start-up phases (to avoid surge in the compressor) and at full load operations these valves are fully closed. The bypass valve is usually used during partial base loads but does not affect the performance calculations so much. Hence, these two types of valves are removed in the diagnosis model. Since the bleed valves are removed, the model is only valid during operational conditions, and not valid during starts and stops. In the performance model, heat capacities in components after the combustor are considered but in the diagnosis model these heat capacities are removed. However, heat losses in the combustor are still considered in the diagnosis model.

Finally, the direction of the gas flow has to be specified throughout the gas path and the combustor has to be *turned on*. This leads to a diagnosability analysis with higher accuracy, i.e., the structural model presented in Section 4.3 gets sparser.

4.2.1 Input and Output signals

All industrial gas turbines are equipped with a number of actuators, and instrumentation sensors. These sensors measure the temperatures, the pressures, and the shaft speeds of the gas turbine. These quantities are measured in different cross-sectional areas throughout the gas path and are primarily used by the control system to maintain correct actuator values. The actuators are mainly used to control valves which were showed in Figure 3.7. In the diagnosis model, all actuator signals are removed. Instead are the input signals, to the diagnosis model, represented by physical quantities which are the ambient temperature T_0, the ambient pressure p_0, the mass flow of fuel $m_{f,flow}$, the torque τ, and the output pressure p_{out}. These input signals are shown in Figure 4.2. The output signals are the same as in the reference model described in sub-section 1.2.1 and shown in Figure 3.7.

4.2.2 Health Parameters

The health parameters that are introduced in the diagnosis model are; efficiency and mass flow of the compressor *C1*, efficiency and flow number of the compressor turbine *T1*, and the efficiency of the power turbine *To*. These considered health parameters are

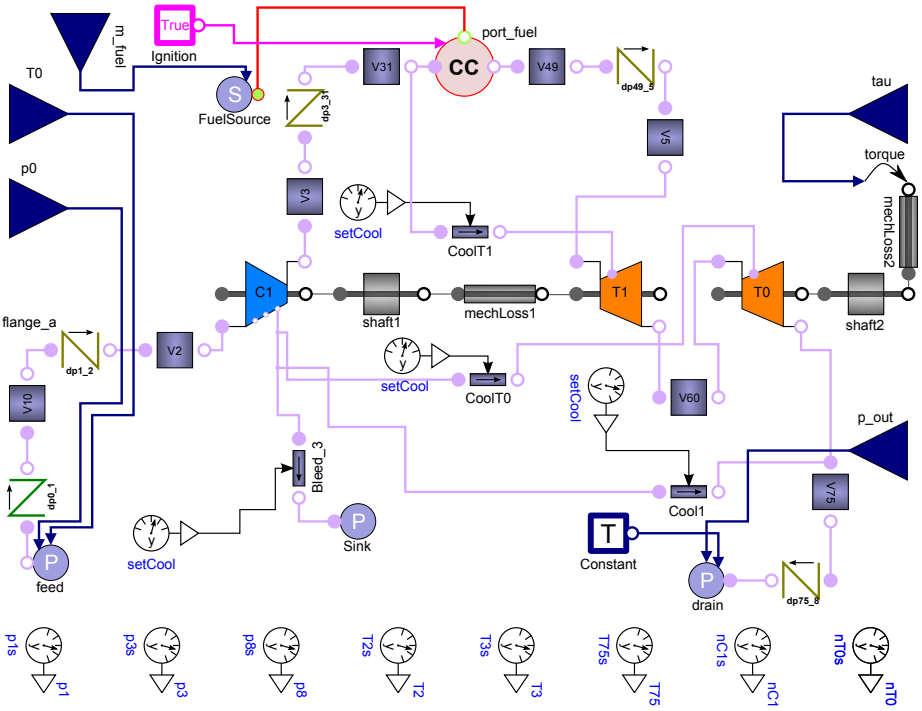

Figure 4.2: The figure gives an overview of the gas turbine diagnosis model. To get the diagnosis model, some of the components from the reference gas turbine model are removed. These components are the bleed valves and the combustor bypass valve. The diagnosis model is valid only during operational conditions. The input signals to the diagnosis model are; the ambient temperature T_0, the ambient pressure p_0, the mass flow of fuel $m_{f,flow}$, the torque τ, and the output pressure p_{out}. The output ambient gas temperature in component `drain` has to be specified, but is not used explicitly in the calculation. Thus, the value of the signal is considered to be a constant. Since the model has no physical based connections to the environment, it is possible to simulate the diagnosis model with the given input signals.

utilized in the actual performance equation and are:

$$\begin{aligned} \eta_{C1} &= f_{C1,\eta}(\ldots) + \Delta\eta_{C1} \\ m_{flow,C1} &= f_{C1,\Gamma}(\ldots) + \Delta\Gamma_{C1} \\ \eta_{T1} &= f_{T1,\eta}(\ldots) + \Delta\eta_{T1} \\ C_{T1} &= f_{T1,\Gamma}(\ldots) + \Delta\Gamma_{T1} \\ \eta_{To} &= f_{To,\eta}(\ldots) + \Delta\eta_{To} \end{aligned} \tag{4.3}$$

where $f_{i,j}$ is a function that represents the nominal characteristics of respective component. In function $f_{i,j}$, the concept of corrected and normalized parameters are utilized according to the presentation in sub-section 3.1.2. The characteristic functions $f_{i,j}$ are implemented as look-up tables.

Since the component deterioration is slow with respect to time, it is assumed that the derivatives of the health parameters are equal to zero. Thus, these constraints are added to the model:

$$\begin{aligned} \Delta\dot{\eta}_i &= 0 \\ \Delta\dot{\Gamma}_i &= 0 \end{aligned} \tag{4.4}$$

were i represents the components; *C1*, *T1*, or *To*. For the component *To*, only the first equation exists.

4.2.3 Sensor Faults

A faulty instrumentation sensor can be defined as a sensor that shows an abnormal behaviour of the measurement signal. The abnormal behaviour can be interpreted as the sensor characteristic specified by the manufacture that is no longer maintained. The abnormal behaviour can result in different kind of faulty behaviour, e.g., these faulty behaviours can appear as:

- Abrupt changes – the sensor fault changes behaviour immediately.
- Incipient faults – the sensor fault appears, and gradually increases in amplitude.
- Intermittent faults – the sensor fault appears, and disappears with a time interval.
- Bias faults – the sensor fault is constant, i.e., the sensor value has a constant offset.

In most cases, the faulty behaviour of the sensor is unknown. In this case, the sensor signal can be modeled with an unknown variable f_i added to the measured quantity. The sensor fault in the gas turbine model are modeled as:

$$\begin{aligned} y_{p_1} &= p_1 + f_{p_1} \\ y_{p_3} &= p_3 + f_{p_3} \\ \vdots &= \vdots \quad \vdots \end{aligned} \tag{4.5}$$

where y_i is the known measurement signal, and p_i is the measured quantity.

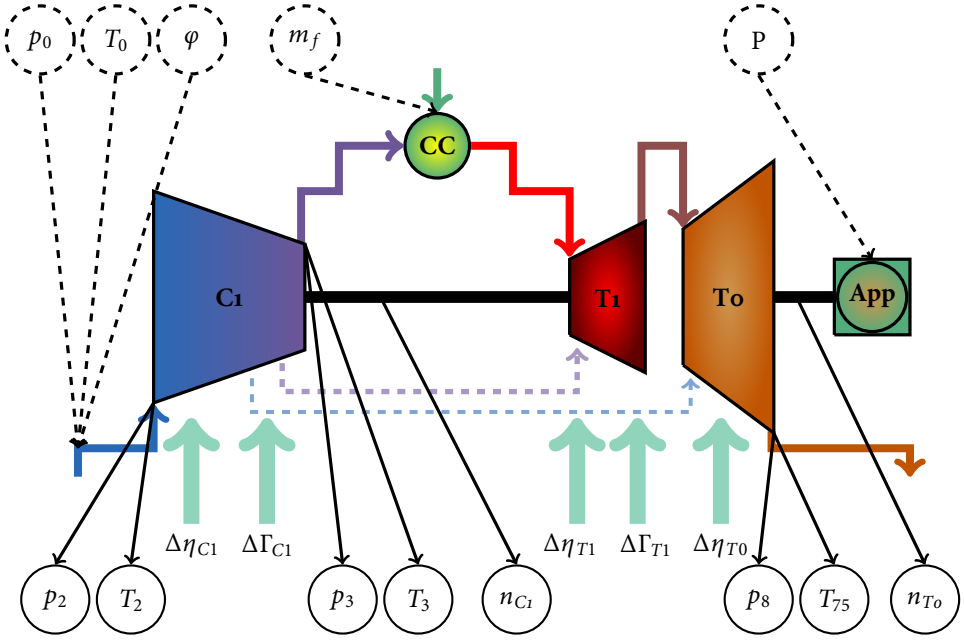

Figure 4.3: The gas turbine with the input signals (dashed circles), the sensor signals (solid circles), and health parameters (arrows). The secondary air flow, used to cool the first turbine blades, are shown with dashed arrows.

4.2.4 Differential Algebraic Equation Form

The diagnosis gas turbine model, with the added health parameters, has the general form:

$$F(\dot{x}, \Delta\dot{h}, x, \Delta h, u) = 0 \tag{4.6a}$$

$$y = h(x) + f \tag{4.6b}$$

where x consists of the unknown variables, Δh consists of the unknown health parameters, y consists of the known measurement signals, u consists of the known input signals, and f consists of the unknown sensor faults. The functions F and h together with their arguments are vector valued functions with appropriate dimensions. Eq. (4.6) is a general mathematical description where the algebraic and the dynamic constraints are mixed together. The expression in (4.6) is the starting point for the model analyses performed in the following chapters.

4.3 Diagnosability Analysis

The goal with the present work is to achieve a systematic method to construct a diagnosis system from an available performance model used for simulations. The performance model considered here is the model constructed from the GTLib package described in Chapter 3. Before a diagnosis system is designed, it is relevant to investigate how introduced faults, or component deteriorations, affect the *detection* and *isolation* performance. For example, is it possible to detect and isolate a drift in the health parameters introduced in the sub-section 4.2.2 with a given set of measurement sensors? Here, detection of a fault f_1 means that it is possible to distinguish between a non faulty system behaviour and a faulty sensor behaviour affected by the fault f_1. The detectability depends on the particular sensor configuration of the system model. The isolability properties can be defined in a similar manner. Instead of distinguishing between a non faulty mode and a faulty mode, it should be possible to distinguish between two different faulty modes. In Frisk et al. (2009), the isolability is formally defined for linear differential algebraic systems, and this class of systems can be written:

$$H(p)x(t) + L(p)z(t) + F(p)f(t) = 0 \tag{4.7}$$

where $x(t) \in \mathbb{R}^{n_x}$ represents the unknown variables, $z(t) \in \mathbb{R}^{n_z}$ represents the known signals, and $f(t) \in \mathbb{R}^{n_f}$ represents the unknown faults. The matrices $H(p)$, $L(p)$, and $F(p)$ are polynomial matrices in the differential operator $p = d/dt$, and they have an appropriate dimension. In the linear case, the isolability properties can be determined through a null-space calculation of the system matrix H and the faulty mode F_j. This can formally be written:

$$N_{HF_j}(p)F_i(p) \neq 0 \tag{4.8}$$

where $F_i(p)$ represents how the fault f_i affects the system and $N_{HF_j}(p)$ is the null-space of $[H(p) \;\; F_j(p)]$. The fault f_i is isolable from fault f_j in (4.7) if, and only if (4.8) is satisfied. The linear filter:

$$r_{\mathrm{NF}}(t) = \gamma N_H(p)L(p)z(t) \tag{4.9}$$

is called a consistency based *residual generator* where the design parameter γ is a vector of suitable dimension. The residual generator should fulfill:

$$\lim_{t\to\infty} r_{\mathrm{NF}}(t) \to 0 \tag{4.10}$$

when the system is in a non-faulty mode.

For non-linear systems, it can be difficult to get an exact characterization of the model equation, i.e., based on consistency relations, which can be used when residual generators are constructed. In most cases, when a residual generator is constructed, the system model together with the measurement equations are transformed into smaller subsets where only the interesting faults are present see, e.g,. Blanke et al. (2003); Chen and Patton (1999); Nikoukhah (1994). The faults that are not present in the sub-models are not detectable by the residual generators, i.e., the faults are decoupled. A common method, to design residual generators, is to construct a state estimation observer. In this

class of residual generators, the state estimations of the observer are compared with the measurement signals to construct a residual equation, i.e., the residual generator. For residual generators based on state observers, see, e.g., Patton and Hou (1998); Martínez-Guerra et al. (2005); Svärd and Nyberg (2008).

To answer questions about detectability and isolability of a model, in a general way, only the model structure can be considered (Blanke et al., 2003). In the present case, an analytic characterization of the gas turbine residual generators is not practical to find due to the size of the system, the non-linear behaviour of the model, and the look-up tables used for performance calculations.

4.3.1 Structural Analysis

The structural model is a coarse model description, where only the variable dependencies in each equation are considered. The analytic model is described by a matrix where each element has a true (1), or a false (0) value. How the variables affect the analytical equations are not considered in the analysis. Whether they affect the expression through, e.g., exponential, logarithmic, or look-up tables they still get the same variable dependencies in the structural model. If a certain variable is included in a specific equation, the matrix element belonging to the certain variable is (1). In the structural model, the rows represent the equations and the columns represent the variables.

To have a model that only consists of the structure gives the opportunity to develop fast algorithms for model analysis, especially for diagnosis purposes. The drawback is that only best-case results are obtained.

Dulmage-Mendelsohn Decomposition

A method that can be useful when relevant subsets of model equations are chosen is the *Dulmage-Mendelsohn decomposition*, presented in Dulmage and Mendelsohn (1958). The Dulmage-Mendelsohn decomposition is an equivalent description of a *bi-partite graph*, which states the calculation chain of a system. The decomposition works on the structural model, and rearranges rows and columns to obtain the structure shown in Figure 4.4. In the figure, the model is divided into an under-determined M^- part, an exactly-determined M^0 part, and an over-determined M^+ part as described below:

- The under-determined part – in this part, the number of equations in M^- is less than the number of variables in X^-. If the underlying analytical model can be simulated, this part never appears. The gas turbine model used in the thesis does not involve this part and is therefore not considered in the analysis.

- The exactly-determined part – in this part, the number of equations is equal to the number of variables. For a component a_i that consists of more than one equation is said to be *strongly connected* which means that the equations contain loops or cycles. For diagnosis purposes, the exactly-determined part of the model provides no extra information. Therefore, this part of the model can be removed without loosing any redundancy.

- The over-determined part – in the last part of the model, the number of equations is more than the number of variables. This indicates that redundancy is available, and the degree of redundancy depends on the number of available measurement sensors. When diagnosis tests are constructed, different subsets of the M^+ can be chosen. In Krysander et al. (2008), a class of these subsets is denoted *Minimal structural over-determined*-sets (MSO sets) and they are constructed using an efficient algorithm. The MSO sets are the smallest over-determined subsets with redundancy, which is possible to obtain.

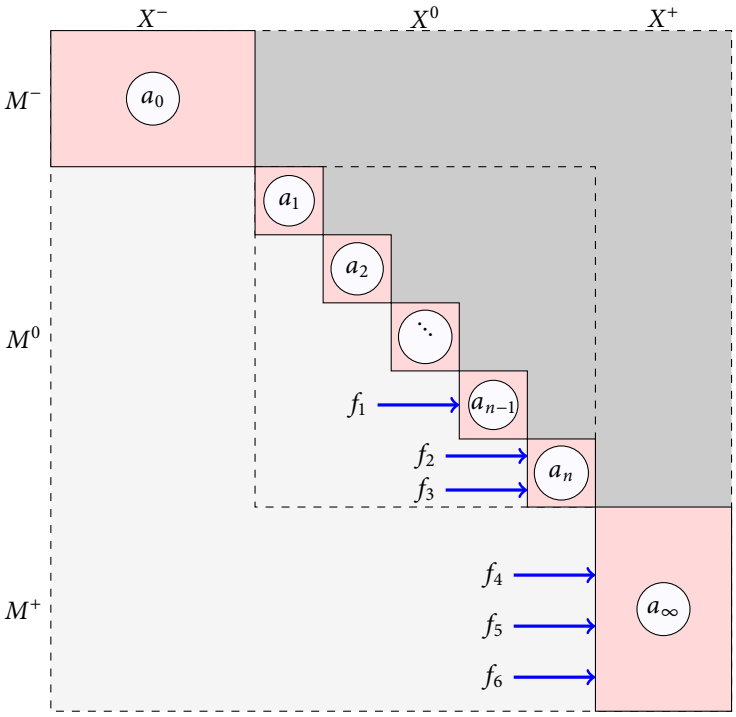

Figure 4.4: The figure shows a Dulmage-Mendelsohn decomposition of a structural model. The light grey shadowed area consists of zero matrix elements. The matrix element in the darker grey area can either be zero or one. The elements that are left span the boxes $a_0 \ldots a_\infty$. Injected faults f_1, f_2, f_3 are not detectable, but faults f_4, f_5, f_6 can possibly be detected.

For diagnosis purposes, it is only necessary to consider the over-determined part M^+ because faults that appear in any equations in the exactly determined part are not detectable because of the lack of redundancy. In Figure 4.4, the faults f_1, f_2, f_3 are not detectable, and the faults f_4, f_5, f_6 are in an ideal case detectable. However, measurement noise can for example disturb the test quantities which can result in a fault which is not detectable in a practical application.

Investigation of Health Parameter Isolation

In the paper Krysander et al. (2008), a method is presented where the over-determined M^+ part is divided into a smaller subset of equations, i.e., *equivalence classes*. The advantage with using these subsets is that if any of the equations in the subset is removed, the remaining equations in the subset get exactly-determined, so the degree of redundancy is 1. In practice, when a diagnosis test (or residual generator) is constructed it is necessary to have at least one redundant equation. In an equivalence class, only one redundant equation is available, and when this equation is removed the faults in the remaining subset are no longer detectable. So, it is not possible to construct two tests that discriminate between two faults (or more) in the same equivalence class, and therefore, they are not isolable from each other. A decomposition of the over-determined M^+ part in Figure 4.4 is shown in Figure 4.5.

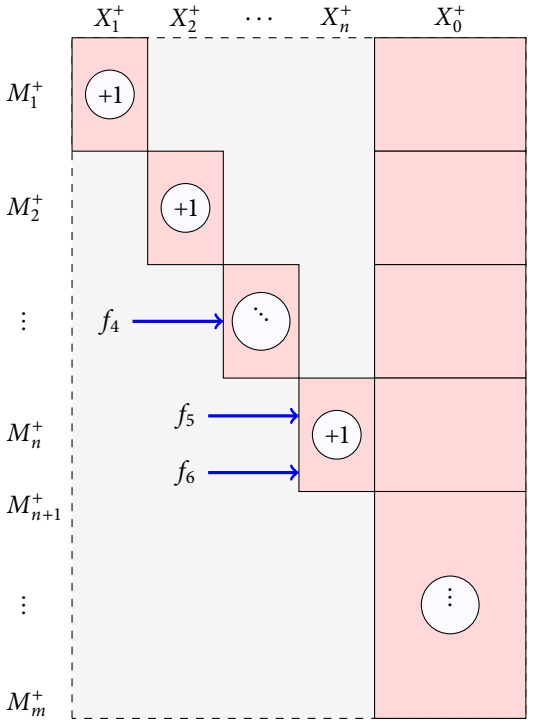

Figure 4.5: In the figure, the decomposition of the over-determined M^+ part from Figure 4.4 into equivalence classes is shown. The equivalence classes are the sets of pair (M_i^+, X_i^+) where $i = 1 \ldots n$. The equivalence classes have one more equation than the number of variables which results in that the faults f_5 and f_6 may be detectable but not isolable from each other. Since f_4 isn't in the same equivalence class as f_5 and f_6, the fault f_4 may be isolable from fault f_5 and f_6.

To analyze how the isolable performance of the health parameters in the gas turbine model (4.6) depends on different sensor configurations, the structural model of the gas turbine with respective sensor configuration is studied. It is assumed that a healthy gas turbine component has an unknown bias in the performance equations, i.e., a derivative of a health parameter that is zero. In an un-healthy gas turbine component, deterioration appears which gives a health parameter with a non-zero derivative. This can be written:

$$\eta_i = f_{i,\eta}(\ldots) + \Delta h_i \tag{4.11a}$$

$$\Delta \dot{h}_i = f_i \tag{4.11b}$$

where $f_{i,\eta}$ is the characteristic, and $f_i = 0$ for a healthy gas turbine component, and $f_i \neq 0$ when a component deterioration is present, i.e., in the faulty case. The fault introduction can be done for each health parameter. In Figure 4.6, the isolable performance of four different sensor configurations is showed. The equivalence classes are plotted as grey boxes in the over-determined M^+ part. The equations where the fault f_i from (4.11) appears is marked with colored lines in the figure, and faults that appear in the same small box are not isolable from each other. With only one measurement sensor, it is not possible to isolate any of the health parameters but all health parameters are detectable as can be seen in subfigure 4.6a. With the measurement sensors y_{p_3} and y_{T_3}, all health parameters except efficiency and flow capacity of the power turbine *To* can be isolated in an ideal case as subfigure 4.6b indicates. If the measurement sensor y_{T_3} is replaced by $y_{T_{75}}$, full isolability is achieved (subfigure 4.6c). Finally, with all measurement sensors, it may be possible to isolate a fault in all the considered health parameters.

4.4 DAE-Index Analysis

The purpose with this section is to transform the system in (4.6) to a system in state space form:

$$\dot{\tilde{x}}_1 = \tilde{f}(\tilde{x}_1, \tilde{u}) \tag{4.12a}$$

$$y = \tilde{h}(\tilde{x}_1) \tag{4.12b}$$

where $\tilde{x}_1$ is the state variables, y is the measurement signals, and $\tilde{u}$ is the input signals. The functions $\tilde{f}$ and $\tilde{h}$ together with their arguments are vector valued functions with appropriate dimensions. For a comprehensive study of DAE systems see, e.g., mathematical reference literature Hairer et al. (1991); Ascher and Petzold (1998).

DAE-index

The first step in the process, to get a system in the form (4.12), is to investigate the so-called *differential-index* of the DAE model. The DAE-index says, in some sense, how easy it is to transform the DAE-model to an ordinary state-space form. In this step, the index of the DAE model (4.6a) is reduced to 1. The index reduced system has the form:

$$\tilde{F}(\dot{\tilde{x}}_1, \tilde{x}_1, \tilde{x}_2, \tilde{u}) = 0 \tag{4.13a}$$

$$y = \tilde{h}(\tilde{x}_1, \tilde{x}_2) \tag{4.13b}$$

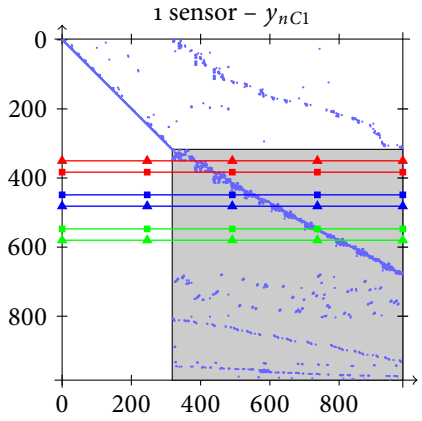

(a) With only one sensor that measures the speed of the gas generator it is possible to detect deterioration in the performance parameters, but it is not possible to discriminate between those deterioration parameters.

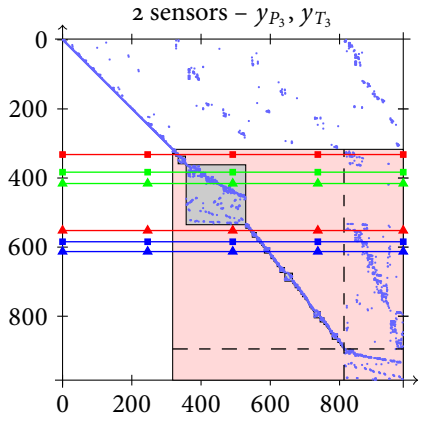

(b) If the compressor discharge temperature and pressure are measured, all health parameters are detectable but it is not possible to discriminate between a deterioration in the efficiency and in the flow capacity of the power turbine.

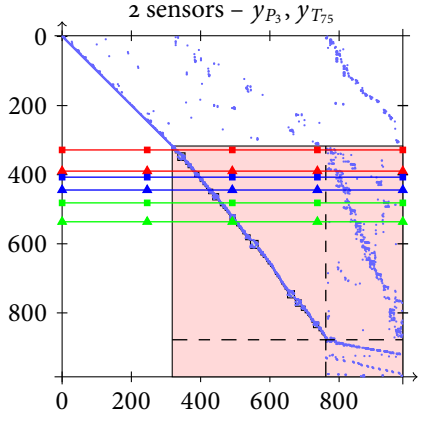

(c) If the temperature sensor y_{T_3} from subfigure 4.6b is replaced with the temperature sensor $y_{T_{75}}$, it is possible to isolate deteriorations in all injected health parameters.

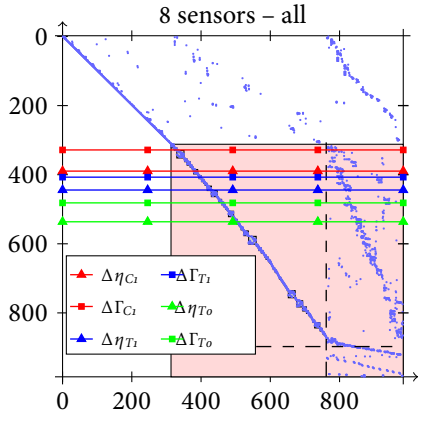

(d) Finally, if all available measurement sensors are used it can be possible to detect and isolate the considered deteriorations in the performance parameters.

Figure 4.6: In the figure, the structural model is shown where the gas turbine model of four different sensor configurations is investigated. In the performance equations, a health deterioration is introduced according to (4.3). The equations, where the injected deterioration appears are marked in respective subfigure. The structural model is divided into two parts, where the first part is the exactly-determined M^0 part and consists of the first 340 equations. The second part is the over-determined M^+ part and consists of the remaining equations. It is not necessary to considered the M^0 part for diagnosis purposes since the absence of redundancy and this part can be removed in the diagnosis tests.

where the dynamic variables $\tilde{x}_1$ and the algebraic variables $\tilde{x}_2$ are separated.

Semi-Explicit DAE Form

In the second step, the index reduced DAE system is written in a semi-explicit form. A DAE-index 1 system has a non-singular Jacobian:

$$\tilde{J} = \frac{\partial \tilde{F}}{\partial(\dot{\tilde{x}}_1, \tilde{x}_2)} \tag{4.14}$$

where $\tilde{x}_1$ is the state variables, and $\tilde{x}_2$ is the algebraic variables. The function $\tilde{F}$ represents the index reduced system from previous step. The system can now be written in the form:

$$\dot{\tilde{x}}_1 = \tilde{\tilde{f}}(\tilde{x}_1, \tilde{x}_2, \tilde{u}) \tag{4.15a}$$
$$0 = \tilde{\tilde{g}}(\tilde{x}_1, \tilde{x}_2) \tag{4.15b}$$
$$y = \tilde{\tilde{h}}(\tilde{x}_1, \tilde{x}_2) \tag{4.15c}$$

where the Jacobian $\partial\tilde{\tilde{g}}/\partial\tilde{x}_2$ is non-singular.

Ordinary State Space Form

In the last step, the algebraic constraints (4.15b) are solved with regard to the algebraic variable $\tilde{x}_2$. This solution of $\tilde{x}_2 = \tilde{G}(\tilde{x}_1)$ and is then inserted into the state equation (4.15a) to get the ordinary state space form:

$$\dot{\tilde{x}}_1 = \tilde{\tilde{f}}(\tilde{x}_1, \tilde{G}(\tilde{x}_1), \tilde{u}) \tag{4.16a}$$
$$y = \tilde{\tilde{h}}(\tilde{x}_1, \tilde{G}(\tilde{x}_1) \tag{4.16b}$$

The expression (4.16) is the same as (4.12).

4.4.1 DAE-Index Reduction

The *flat* DAE model (4.6), exported from Dymola, can be written in the form:

$$\bar{E}\dot{x} = \bar{f}(x, u) \tag{4.17a}$$
$$y = \bar{h}(x) \tag{4.17b}$$

where $\bar{E}$ is a constant matrix that has not full column rank (is singular), x consists of the unknown variables, and u consists of the known actuator signals. The functions $\bar{f}$ and $\bar{h}$ are non-linear vector valued functions of appropriate dimensions. Here, the phrase flat means that all object oriented declarations are transformed to plain equations. Thus, the resulting model consists of only equations and variables. In the model formulation (4.17) it can be difficult to say which of the variables in x that are state variables before an index analysis and index reduction are performed.

In general, a model with a DAE-index 1 (or lower) is easier to handle in practice than a system with a higher index. In the present case, an index analysis of the gas turbine system in (4.17a) shows that the DAE has index 2. One way of handling this situation is to employ index reduction techniques (Takamatsu and Iwata, 2008). A common index reduction technique is to differentiate well chosen model equations a suitable number of times to obtain a low index DAE. In the analysis, the algorithm presented in the paper of Pantelides (1988) is incorporated. The algorithm works on the structural model of the sub-system (4.17a), and the algorithm suggests which equations that needs to be differentiated to receive a system that has a DAE-index of order 1, or lower.

The Mechanical Rotational library, that is a part of the Modelica standard package, uses torque τ and angle φ sharing connections between the connected components. The torques are summed to zero, and angles are set equal in a connection point. The high DAE-index property of the gas turbine model is a consequence of the angles dependencies in the connection points. Pantelides algorithm differentiates the equations in the form: $\varphi_1 = \varphi_2, \varphi_2 = \varphi_3, \ldots$ to receive: $\dot{\varphi}_1 = \dot{\varphi}_2, \dot{\varphi}_2 = \dot{\varphi}_3, \ldots$. If the system is replaced with these new differentiated equations, the DAE-index of the system is equal to 1. The original φ-equations have to be treated separately when the system is simulated, e.g., to have proper initial conditions.

The system from (4.17) can now be written:

$$\tilde{E}\dot{\tilde{x}}_1 = \tilde{f}(\tilde{x}_1, \tilde{x}_2, \tilde{u}) \tag{4.18a}$$

$$0 = \tilde{g}(\tilde{x}_1, \tilde{x}_2, \tilde{u}) \tag{4.18b}$$

$$y = \tilde{h}(\tilde{x}_1, \tilde{x}_2) \tag{4.18c}$$

where $\tilde{E}$ is a constant matrix which have full column rank (but can have more rows than columns), $\tilde{x}_1$ represents the dynamic variables where also the health parameters are included, $\tilde{x}_2$ represents the algebraic variables, $\tilde{u}$ is the known actuator signal vector, and y consists of the known measurement signals. The non-linear function $\tilde{f}$ describes the dynamic behaviour, and the non-linear function $\tilde{g}$ describes the algebraic constraints. If the matrix $\tilde{E}$ is non-quadratic, it must be transformed to a quadratic matrix through variable manipulations. This is possible since the model equations (4.18a)–(4.18b) have DAE-index 1, i.e., $\tilde{E}$ has full column rank.

4.4.2 Algebraic Manipulation of the $\tilde{E}$ matrix

The purpose with this sub-section is to sketch the procedure to transform the non-quadratic $\tilde{E}$ matrix in (4.18a) to a quadratic matrix E where the structure is preserved in a specific manner.

To describe the variable manipulation of the $\tilde{E}$ matrix, the first step is to make a Dulmage-Mendelsohn decomposition of the $\tilde{E}$ matrix structure. If this decomposition results only in an exactly-determined $\tilde{E}^0$ part, the matrix is quadratic and can be inverted and the procedure below is not needed. In the present case, the decomposition gives an exactly-determined $\tilde{E}^0$ and an over-determined $\tilde{E}^+$ part. The exactly-determined part is removed and the over-determined part is shown in Figure 4.7, where also the elimination procedure of the algorithm is sketched. The elimination order can be performed with

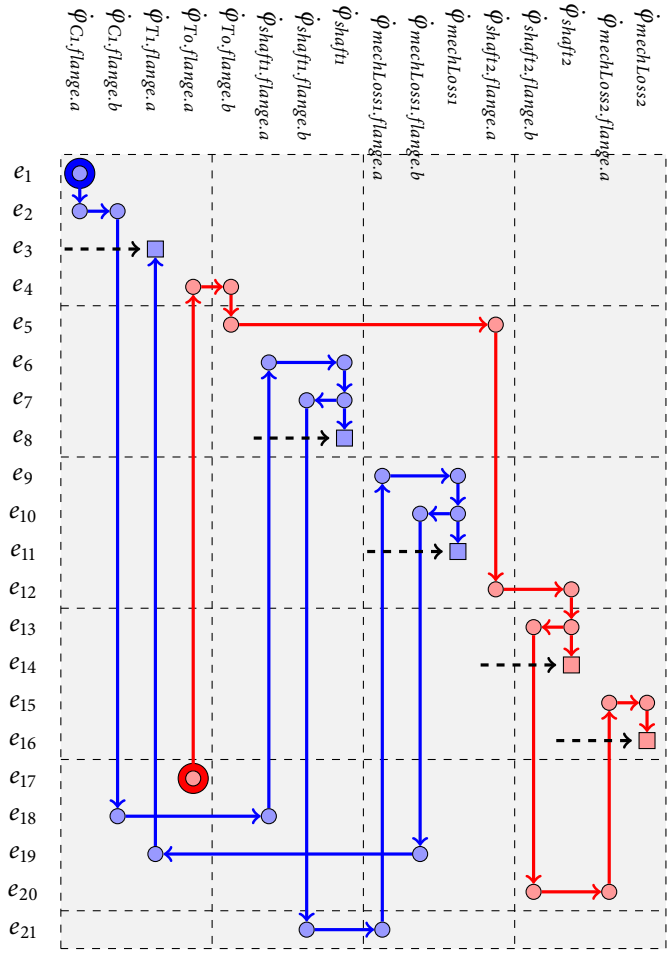

Figure 4.7: In the figure, the variable elimination scheme of the over-determined $\tilde{E}^+$ part of the $\tilde{E}$ matrix is shown. If the Dulmage-Mendelsohn decomposition is performed on the structure where the equation set $\{e_3, e_8, e_{11}, e_{14}, e_{16}\}$ is removed, the calculation order is the same as for the blue line and is shown in Figure 4.8.

different kinds of approaches. The receiving model structure of the system depends on the chosen approach, since variables can be eliminated in different ways. Here, the considered approach in this gas turbine application is according to the following algorithm:

1. Start with an equation that consists of only one differentiated variable, i.e., equation $e_1 : \dot{\varphi}_{C1.flange.a} = \omega_{shaft1}$ in Figure 4.7.

2. Remove all other equations that consists of only one differentiated variable, i.e.,

the equation set $\{e_3, e_8, e_{11}, e_{14}, e_{16}\}$. The system is now un-determined since the number of equation is 15, and the number of variables is 16.

3. Make a Dulmage-Mendelsohn decomposition of the structure to receive the variable substitution order that is showed in Figure 4.8, which is the same that is viewed in Figure 4.7.

4. Make the substitution described in Step 3 above, and now are all the derivatives of the angle variables expressed in angular velocities only.

5. These derivatives are now inserted into the removed equations, i.e., inserted into the equation set $\{e_3, e_8, e_{11}\}$, to get the algebraic constraint such as $\omega_{C1} = \omega_{shaft1}$. These equations are then moved to the algebraic constraint part of the gas turbine model.

6. The remaining equations from the removed equation set in Step 2, i.e., $\{e_{14}, e_{16}\}$ are moved back to the model, and the algorithm is restarted from Step 1 above.

7. The exactly-determined $\tilde{E}^0$ part, that was removed before the algorithm was started, is now moved back to get the quadratic matrix E.

Other methods that can be used to sort elements in the $\tilde{E}$-matrix are, for example, QR-factorization and SVD-decomposition. The disadvantage with these methods is that the received algebraic constraints aren't in the simple form: $\omega_{C1} = \omega_{shaft1}$.

4.4.3 Semi-Explicit Index-1 DAE

After the algebraic manipulation of (4.18a) is performed, the model can be written in the semi-explicit form:

$$\dot{\tilde{x}}_1 = E^{-1}\hat{f}(\tilde{x}_1, \tilde{x}_2, \tilde{u}) \tag{4.19a}$$

$$0 = \hat{g}(\tilde{x}_1, \tilde{x}_2, \tilde{u}) \tag{4.19b}$$

$$y = \tilde{h}(\tilde{x}_1, \tilde{x}_2) \tag{4.19c}$$

where the E-matrix is invertible, and the Jacobian $\partial\hat{g}/\partial\tilde{x}_2$ is non-singular. This means that the algebraic constraint $\hat{g}$ is invertible (at least locally), and can be solved for $\tilde{x}_2$.

State-Space Form

The state-space form, of the semi-explicit DAE model (4.19), can be written:

$$\dot{\tilde{x}}_1 = E^{-1}\hat{f}(\tilde{x}_1, \hat{G}(\tilde{x}_1, \tilde{u}), \tilde{u}) \tag{4.20a}$$

$$y = \tilde{h}(\tilde{x}_1, \hat{G}(\tilde{x}_1, \tilde{u})) \tag{4.20b}$$

where $\tilde{x}_2 = \hat{G}(\tilde{x}_1, \tilde{u})$ is the inversion of the constraint $\hat{g}$. This is possible since the Jacobian matrix $\partial\hat{g}/\partial\tilde{x}_2$ is, at least locally, non-singular.

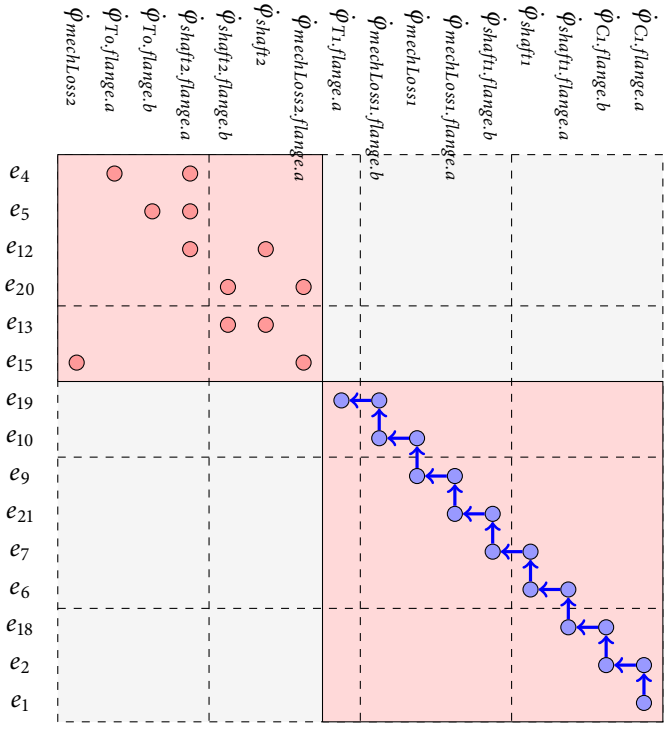

Figure 4.8: Dulmage-Mendelsohn of the structure in Figure 4.7, where the equation set $\{e_3, e_8, e_{11}, e_{14}, e_{16}\}$ is removed. The model is divided into an under-determined, and an exactly-determined part. The first equation e_1 is used to eliminate variable $\dot{\varphi}_{C1.flange.a}$ in equation e_2. The variable $\dot{\varphi}_{C1.flange.b}$ is eliminated in e_{18}, and so on.

4.4.4 DAE-index 1 Conservation in the Over-Determined M^+ Part

In the diagnosis tests, it is only the over-determined part that is of interest since it is only in this part of the model redundancy is available. Therefore, it is of great importance if the over-determined part of the model is a DAE-index 1 system when the index reduced gas turbine model is a DAE-index 1 system. This is true and is shown in Theorem 4.4.1.

Theorem 4.4.1 *The over-determined M^+ part of the DAE-index 1 system in* (4.19) *is also a DAE-index 1 system when the measurement equations are removed.*

Proof The index-1 DAE system:

$$\begin{aligned} E\dot{x}_1 &= f(x_1, x_2, u) \\ 0 &= g(x_1, x_2, u) \\ y &= h(x_1, x_2) \end{aligned} \tag{4.21}$$

has an invertible and constant matrix E, and a non-singular (at least locally) Jacobian matrix $\partial g/\partial x_2$, see e.g., Ascher and Petzold (1998). This can be written structurally:

	$\dot{x}_1$	x_2	x_1
e_1 :	×	×	×
e_2 :	0	×	×
e_3 :	0	×	×

(4.22)

where e_1 represents the set of dynamic equations, e_2 represents the set of algebraic equations, and e_3 represents the set of measurement equations. Since the the matrix E and the Jacobian matrix $\partial g/\partial x_2$ are non-singular, a matching between the pair $\{\{e_1\},\{\dot{x}_1\}\}$ and $\{\{e_2\},\{x_2\}\}$ exists, which results in a matching between the pair $\{\{e_1,e_2\},\{\dot{x}_1,x_2\}\}$ that also exists, independently of the third equation set e_3.

Next step is to make a Dulmage-Mendelsohn decomposition of the system (where $\dot{x}_1$ and x_1 are lumped together) in (4.21). The rows and columns in the Dulmage-Mendelsohn composition can be permuted to obtain the specific structure:

	$\dot{x}_{11}$	x_{21}	$\dot{x}_{12}$	x_{22}
e_{11} :	×	×	×	×
e_{12} :	0	×	×	×
e_{21} :	0	0	×	×
e_{22} :	0	0	0	×
e_3 :	0	0	0	×

(4.23)

where the variables x_1 and x_2 are split into two parts:

$$x_1 = \{x_{11}, x_{12}\}$$
$$x_2 = \{x_{21}, x_{22}\}$$

The equation set $\{e_{21}, e_{22}, e_3\}$ in (4.23) is a redundant set while the equation set $\{e_{11}, e_{12}\}$ has no redundancy. Since the original system (4.22) has a matching in $\{\{e_1,e_2\},\{\dot{x}_1,x_2\}\}$ and matching of variables and equations is not affected by row and column permutations, also $\{\{e_{11},e_{12},e_{21},e_{22}\},\{\dot{x}_{11},x_{21},\dot{x}_{12},x_{22}\}\}$ has a matching. Since the third quadrant has only zeros, a matching in the forth quadrant must exist. Therefore, it is possible to find a matching for the pair $\{\{e_{21},e_{22}\},\{\dot{x}_{12},x_{22}\}\}$ and the sub-system is an index-1 DAE.

□

Remark 4.4.2 *A matching between the pair $\{\{e_i\},\{x_i\}\}$ means that it can be possible to calculated the variable x_i using the equation set e_i. If a matching does not exist, the unknown variables x_i cannot be calculated using the equation set e_i. In a redundant equation set, unknown variables can be matched in several ways.*

4.5 Observability Analysis

If observer based techniques should be considered when the diagnosis tests of the system in (4.20) are designed, it is necessary that the states of the system is observable. To

determine if a non-linear system is observable is in general difficult. A number of different observability criteria is available (Nijmeijer and Fossen, 1999) where also the input signals can affect the observability, in contrast to the observability of linear systems. A starting-point is to check if the non-linear system is locally observable through a linearization in a suitable operating point (x_0, u_0).

$$A = \frac{\partial f}{\partial x_1} + \frac{\partial f}{\partial x_2}\frac{\partial G}{\partial x_1}\bigg|_{\tilde{z}_0}, \; B = \frac{\partial f}{\partial u} + \frac{\partial f}{\partial x_2}\frac{\partial G}{\partial u}\bigg|_{\tilde{z}_0}, \; C = \frac{\partial h}{\partial x_1} + \frac{\partial h}{\partial x_2}\frac{\partial G}{\partial x_1}\bigg|_{\tilde{z}_0}$$

where

$$\tilde{z}_0 = \left(x_0, u_0\right)$$

is the linearization point, and

$$x_2 = G(x_1, u)$$

is the inversion of the static constraint. The linearized system, near the point $\tilde{z}_0$, can now be written:

$$\dot{x} = Ax + Bu \tag{4.24a}$$

$$y = Cx \tag{4.24b}$$

For the linear system in (4.24), the observability can be checked according to the observability matrix $\mathbb{O}(A, C)$ in Theorem 4.5.1.

Theorem 4.5.1 *A pair $A \in \mathbb{R}^{n\times n}$, and $C \in \mathbb{R}^{m\times n}$ is observable if and only if the observability matrix*

$$\mathbb{O}(A, C) = \begin{bmatrix} C \\ CA \\ \vdots \\ CA^{p-1} \end{bmatrix}$$

has full rank n, for a $p \leq n$.

Proof See, e.g., Kailath (1980). □

4.5.1 Structural Observability

If Theorem 4.5.1 is used to determine the observability of the linearization, numerical problems can appear, especially for higher p. To handle the numerical problems, the structural observability presented in Shields and Pearson (1976) can be investigated. In this paper, the structural controllability is presented but it is possible to transpose the matrices to get it on an observability form presented in here. Since the structure of the model is considered, the method only provides a necessary condition for observability. Since the model is physical based, it can be assumed that structural observability implies observability. According to Shields and Pearson (1976), the dual formulation of the controllability theorem can be stated:

Theorem 4.5.2 *A pair $A \in \mathbb{R}^{n\times n}$, and $C \in \mathbb{R}^{m\times n}$ is structural observable if and only if the generalized observability matrix*

$$\mathbb{O}_s(A,C) = \begin{bmatrix} I & A & 0 & \dots & 0 & 0 \\ 0 & I & A & \dots & 0 & 0 \\ \vdots & \vdots & \vdots & & \vdots & \vdots \\ 0 & 0 & 0 & \dots & I & A \\ 0 & 0 & 0 & \dots & 0 & C \\ 0 & 0 & 0 & \dots & C & 0 \\ \vdots & \vdots & \vdots & & \vdots & \vdots \\ 0 & C & 0 & \dots & 0 & 0 \\ C & 0 & 0 & \dots & 0 & 0 \end{bmatrix}$$

with dimension $[n^2 + n(m-1)] \times n^2$ has structural rank n^2.

Proof See Shields and Pearson (1976). □

The structural rank of a matrix can easily be checked using graph theoretical algorithms for matching in bi-partite graphs, e.g., Dulmage-Mendelsohn decomposition. In Matlab, the `sprank` command can be used.

4.5.2 Removing of Unobservable Modes

In the present case, the linearization of the system in (4.20) has unobservable modes, which can be checked using the structural observability method. So, if an observer should be constructed, these unobservable modes need to be removed. As a consequence, when the exactly-determined part M^0 is removed, a number of unobservable modes also disappear, which is stated in Theorem 4.5.3.

Theorem 4.5.3 *An index-1 DAE system, in a semi-explicit form* (4.19)*, has unobservable state variables if they appear in the exactly-determined M^0 part of the structural model shown in Figure 4.4.*

Proof According to Theorem 4.4.1, the semi-explicit index-1 DAE system can be written structurally:

	$\dot{x}_{11}$	x_{21}	$\dot{x}_{12}$	x_{22}	x_{11}	x_{12}
e_{11} :	×	×	×	×	×	×
e_{12} :	0	×	×	×	×	×
e_{21} :	0	0	×	×	0	×
e_{22} :	0	0	0	×	0	×
e_3 :	0	0	0	×	0	×

(4.25)

where $x_1 = \{x_{11}, x_{12}\}$, and $x_2 = \{x_{21}, x_{22}\}$. In (4.25) a Dulmage-Mendelsohn decomposition of the DAE system (where $\dot{x}_1$ and x_1 are lumped) is performed together with an extra rearrangement of the rows and the columns to obtain the specific structure.

According to Theorem 4.4.1, a matching of the pair $\{\{e_{11}, e_{12}\}, \{\dot{x}_{11}, x_{21}\}\}$, and the pair $\{\{e_{21}, e_{22}\}, \{\dot{x}_{12}, x_{22}\}\}$ exists. The system in (4.25) can be written analytically:

$$\dot{x}_{11} = f_1(x_{21}, \dot{x}_{12}, x_{22}, x_{11}, x_{12}) \tag{4.26a}$$
$$x_{21} = g_1(\dot{x}_{12}, x_{22}, x_{11}, x_{12}) \tag{4.26b}$$
$$\dot{x}_{12} = f_2(x_{22}, x_{12}) \tag{4.26c}$$
$$x_{22} = g_1(x_{12}) \tag{4.26d}$$
$$y = h_1(x_{22}, x_{12}) \tag{4.26e}$$

Substitution of the algebraic constraints (4.26b) and (4.26d) into dynamic equations (4.26a) and (4.26c) gives:

$$\dot{x}_{11} = \tilde{f}_1(x_{11}, x_{12}) \tag{4.27a}$$
$$\dot{x}_{12} = \tilde{f}_2(x_{12}) \tag{4.27b}$$
$$y = h_2(x_{12}) \tag{4.27c}$$

System in (4.27) is linearized to give the matrices A and C:

$$A = \begin{array}{c} \begin{matrix} x_{11} & x_{12} \end{matrix} \\ \begin{pmatrix} \times & \times \\ 0 & \times \end{pmatrix} \end{array}, \text{ and } C = \begin{array}{c} \begin{matrix} x_{11} & x_{12} \end{matrix} \\ \begin{pmatrix} 0 & \times \end{pmatrix} \end{array}$$

which gives:

$$CA^k = \begin{pmatrix} 0 & \times \end{pmatrix}$$

for $k \geq 0$. The observability matrix $\mathbb{O}$ in Theorem 4.5.1 cannot have full rank, so differentiated states that appear in the exactly-determined part are not observable. □

In the present case, the consequence of Theorem 4.5.3 is that angles φ states are removed. This means that the actual shaft angle position of the gas generator and the power turbine are not possible to observe in the measurement signals.

4.5.3 Number of Health Parameters in the Model

An important question, when an diagnosis test is constructed, is how many health parameters that can be introduced in the model. The number of health parameters affect the observability of the model, and the maximum number is equal to the number of unique measurement sensors. This necessary condition is summarized in Lemma 4.5.4. Where the health parameters appear in the model also affect the observability.

Lemma 4.5.4 *A pair $A \in \mathbb{R}^{n\times n}$, and $C \in \mathbb{R}^{m\times n}$ is not observable if the number of health parameters is larger then the number of measured states n_c.*

Proof Let $x \in \mathbb{R}^{n_x}$, $h \in \mathbb{R}^{n_h}$, and the number of measured states n_c. The structural rank of a matrix can never be smaller if nonzero elements are added to the element positions of the matrix. This gives the opportunity to investigate the structural rank of the last column in the matrix below:

$$\tilde{\mathbb{O}}_s = \begin{bmatrix} \vdots & & \vdots & \vdots \\ \times & \dots & \times & 0 \\ \times & \dots & \times & A \\ \times & \dots & \times & C \\ \times & \dots & \times & 0 \\ \vdots & & \vdots & \vdots \end{bmatrix}$$

Assume that all element positions in the matrix pair (A, C), except for the health parameter states, are occupied according to:

$$A = \begin{array}{c} \begin{matrix} x & h \end{matrix} \\ \begin{pmatrix} \times & \times \\ 0 & 0 \end{pmatrix} \end{array}, \text{ and } C = \begin{array}{c} \begin{matrix} x & h \end{matrix} \\ \begin{pmatrix} \times & 0 \end{pmatrix} \end{array}$$

where $A \in \mathbb{R}^{n \times n}$, $C \in \mathbb{R}^{n_c \times n}$, and $n = n_x + n_h$. If the structural rank of $\tilde{\mathbb{O}}_s$ should be n^2, the last n columns need to have a structural rank n. Further, the last n columns can be written:

$$\begin{bmatrix} A \\ C \end{bmatrix} = \begin{bmatrix} \times & \times \\ 0 & 0 \\ \times & 0 \end{bmatrix} \tag{4.28}$$

where the zeros are omitted, and has the structural rank $n_x + n_c$. The pair (A, C) is not observable if

$$n_x + n_c < n \tag{4.29}$$

which can be written:

$$n_c < n_h$$

where $n_x = n - n_h$ is used. This gives the matrix pair (A, C) is not observable if $n_c < n_h$. □

Remark 4.5.5 *The same arguments, as in Lemma 4.5.4, can be considered to verify that two health parameters that appear in the same equivalence class in Figure 4.5 are not observable.*

4.6 Diagnosis Test Equations

The equations that should be implemented in each diagnosis test are chosen using the Dulmage-Mendelsohn decomposition described in sub-section 4.3.1. The chosen subset

of equations is the whole over-determined M^+ part of the system in (4.19) which is index reduced with introduced health parameters. The diagnosis test equations can be written:

$$\dot{x}_1 = f\big(x_1, G(x_1, u), u\big) \tag{4.30a}$$

$$y = h\big(x_1, G(x_1, u)\big) \tag{4.30b}$$

where x_1 represents the state variables, u is the input signals, and y is the measurement signals. According to Theorem 4.4.1, the DAE-index of system (4.30a) is the same as for the index reduced system (4.19a) which the tests are based on. This results in algebraic constraints that are invertible, at least locally, which results in the vector G.

When the over-determined M^+ part is considered, unobservable modes which appear in the exactly-determined part are removed according to Theorem 4.5.3. These unobservable modes are the angle position of the shafts, i.e., the φ-states that was shown in Figure 4.7. Before this step, the re-arrangement of the E matrix is necessary to perform to get the algebraic constraints in the form: $\omega_{C1} = \omega_{shaft1}$.

Finally, it is verified that the linearization of (4.30) is structural observable when the exactly-determined M^0 part is removed. This indicates that observer based techniques can be considered when the test quantities are constructed in Chapter 5.

4.7 Parsers for an Automatic Extraction of Sub Systems

Since the number of variables and equations in the gas turbine model is large, a systematic method to select relevant equations automatically is attractive to have. The number of equations is about 1000, as shown in the structural models in Figure 4.6, which is too large for manual processing. It should also be easy to investigate various types of diagnosis setups such as models with different number of sensors and health parameters. Such analyses can be difficult to perform in the Dymola environment, so first a parser for model exportation is desirable.

To analyze model properties, the Matlab environment is preferably practiced since it has available routines for structural methods, model linearization, and Kalman gain calculation. Structural methods are, e.g., Dulmage-Mendelsohn decomposition (`dmperm.m`) and equivalent class decomposition. Another motive to use Matlab is that filtering and other signal manipulations are easier to make than in the Dymola environment. The final goal with the parsers is to transform the flat Modelica gas turbine model to a number of test quantities, based on Kalman filters, that will be presented in Chapter 5. These test quantities have the form shown in (5.2) where f and g are Matlab m-functions.

In this section, a number of parsers that is used to transform the model in Dymola to a suitable form of the diagnosis tests in Matlab is presented. The name *parser* is used because most of the time; there are text strings that are manipulated. For the equation manipulation, the MuPAD symbolic engine is called from the Matlab parsers. The MuPAD symbolic engine is a part of the Symbolic Math Toolbox contained in Matlab. Here, Matlab version 7.11 and MuPAD version 5.5 are used.

4.7.1 Dymola Parser – Automatic Extraction of the DAE Model

To fulfill the requirement, a Dymola parser that can export the diagnosis model to the Matlab environment is developed. The parser is relatively simple, and can handle only a restricted functionality, but the functionality is sufficient to be used together with models constructed in the GTLib package. After the model is exported, the MuPAD symbolic engine is invoked to handle the symbolic transformation of the equations and variables according to the methods described in this section. A description of the Dymola parser is summarized below:

1. Before any symbolic transformation of the model is done in Dymola, it is possible to save the flat Modelica model. The flat Dymola model is a text file that is called `.mof`, and contains information, such as equations, variables, parameters, constants, functions, etc. All this information is needed when the model is simulated outside the Dymola environment. In the `.mof`-file, all the object oriented hierarchies are removed, so the file consists of pure equations and variables. Hence, the `.mof`-file is the input to the Dymola parser.

2. All functions that are called from the Dymola model appear in the beginning of the `.mof`-file. These functions are for example the NASA polynomials, that describe the gas properties in a specific gas and the functions that are implemented in GTLib which are mentioned in sub-section 3.3.2. All of these functions are removed from the `.mof`-file and saved as Matlab functions for future investigations.

3. Next step is to find, save, and remove variables, parameters and constants from the file. The values of the parameters, the constants, and the initial values of the variables are saved. The variables appear with different declarations such as *Real*, *Integer*, and *Boolean* which are handled separately. These variables can also appear as the type *input* and *output*, which also have to be handled separately.

4. Equations that consist of *if*-statements have to be treated with care, since the global equation system changes with the *if*-condition. For example, a model with six *if*-statements (that doesn't has any *elseif* part) gives $2^6 = 64$ different equation systems. This can be difficult to handle in practice, so here it is necessary to state the condition of the *if*-statements. Fortunately, all *if*-statements in the model come from the flow direction of the gas. So here it is assumed that the direction is known, which transforms respective *if*-statement to only one equation.

5. Now the *.mof*-file consists of only pure equations, and the final step is to interpret these equations to a format that is familiar by the MuPAD symbolic engine. The earlier saved variables, parameters, and constants have also to be converted to a format that the MuPAD symbolic engine can understand.

The output of the Dymola Parser is a differential algebraic equation system with attached variables, and given input and output signals. The output DAE system can be treated by the MuPAD symbolic engine available in the Matlab environment.

4.7.2 Structural Model Parser

The structural model of the differential algebraic equation system can easily be acquired through a *variable find approach* by the MuPAD symbolic engine. The acquired DAE system in the previous step consists of a number of functions. These functions can be look up tables, algorithms and mathematical functions. In the structural model, it is not necessary to consider the internal variables in each function. Therefore, it is sufficient to consider the input and the output variables in each internal function. The input and the output signals in the analytical model, as can be seen in Figure 4.2, are not considered in the structural model since they are known quantities.

The output of the Structural Model Parser is the structural model of the differential algebraic equation that is given as an input argument to the parser.

4.7.3 Index Reduction Parser

The structural model, together with the equation system are input to the Index Reduction Parser. Actual rows in the equation system, that are needed to be differentiated, are determined with Pantelides algorithm. These rows are differentiated, and the underlying equations are saved to get proper initial conditions to the differentiated equation system.

The output from the Index Reduction Parser is an equation system that has a differential algebraic index equal to 1. The system is also transformed to a form that the E-matrix in (4.19) has full rank according to the variable elimination procedure described in sub-section 4.4.2.

4.7.4 Ordinary Differential Equation Construction Parser

The intention with this parser is to easily construct a set of runnable Matlab functions that can be used to simulate the index reduced equation system defined previously. For the parser, it is assumed that the input equation system is an index-1 DAE, and can be written in a semi-explicit form. The overall Dulmage-Mendelsohn decomposition of the system is shown in Figure 4.9, where the set of equations e_1 is the differential part, and e_2 is the algebraic part of the system where these equation sets are matched with the variable vectors $\dot{x}_1$ and x_2. This decomposition is done because in each step of the solver, x_1 is the previous state of the system and hence it can be seen as an input signal to the dynamic part b_1.

For the algebraic part b_2 in Figure 4.9, the Dulmage-Mendelsohn is once again utilized, and gives the results shown in Figure 4.10. To solve the overall system, variable $\tilde{x}_n$ is first calculated. This result is utilized in the next equation set $\tilde{e}_{n-1}$ and $\tilde{x}_{n-1}$ is calculated. This solving process goes on until the last variable $\tilde{x}_1$ is calculated. If the set $\tilde{e}_i$ consists of two or more equations, it is said that c_i is a *strongly connected component*. This means that the variables contained in c_i cannot be substituted without transformation, i.e., an inversion of the component is necessary. For linear systems, this can be done easily since Gaussian elimination can be applied to obtain a substitution chain, similar to the structural model. For a non-linear strongly connected component, a numerical solver can preferably be used since an analytic solution can be hard to find.

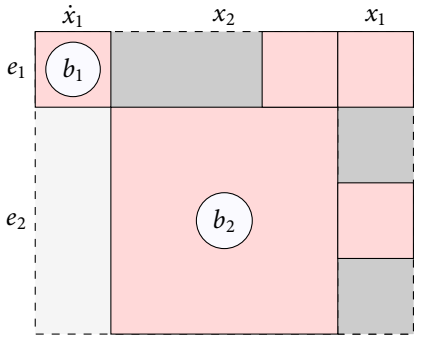

Figure 4.9: Dulmage-Mendelsohn decomposition of a system in semi-explicit form, where $\dot{x}_1$ and x_2 are considered as unknown variables. In each step, when the system is solved, x_1 is the previous state of the system and hence it can be considered as an input signal.

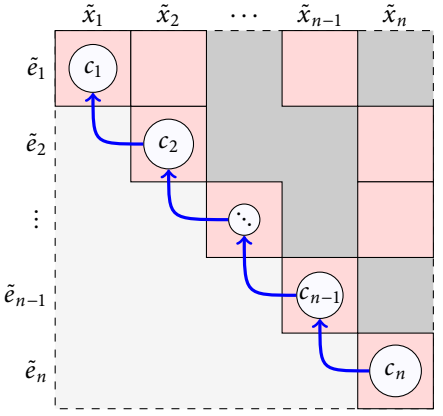

Figure 4.10: In the figure, the Dulmage-Mendelsohn decomposition of the pure algebraic component b_2 from Figure 4.9 is shown. The arrows in the figure illustrate the solution path.

Another interpretation of the behaviour of strongly connected components is to consider a *bi-partite* graph, which consists of loops or cycles, see, e.g., Blanke et al. (2003). A description of the ODE construction parser is summarized in the pseudo algorithm below:

1. First, the equation system is divided in two parts as illustrated in Figure 4.9. The b_1 and b_2 components are located through a DM decomposition, where the sets of unknown variables are $\dot{x}_1$ and x_2. The variable x_1 is considered as known since the previous state of the system is known.

2. The algebraic part b_2 is treated separately, and the structural model is considered when the substitution chain is determined as Figure 4.10 illustrates.

3. For each component c_i, the parser determines if the component consists of only one equation. If this is true, the MuPAD symbolic engine is called and tries to find an analytic solution, i.e., a pure substitution.

4. If the MuPAD symbolic engine failed to find an analytic solution, or if the component is strongly connected, a non-linear Matlab solver is incorporated in the generated file.

5. After the variables in x_2 are calculated, they are inserted in the differential part of the system, together with the previous state x_1. Finally, the state of the system in the next time step can be calculated with a numerical ODE-solver after the component b_1 in Figure 4.9 is inverted.

The outputs from the parser are the two `.m`-files `f` and `G`, that can be interpreted as follows:

$$x_{2,n} = \mathtt{G}(x_{1,n-1}, x_{2,n-1}) \tag{4.31a}$$

$$\dot{x}_1 = \mathtt{f}(x_{1,n-1}, x_{2,n}) \tag{4.31b}$$

where index n means the actual time step, and $n-1$ means the previous time step. Input argument $x_{2,0}$ in (4.31a) is needed by the non-linear solver, to get an appropriate starting point. Eq. (4.31b) can then be called by an ordinary differential equation solver in Matlab.

4.8 Conclusion

In the chapter, a gas turbine diagnosis model is presented that can be used when equations for a diagnosis test are chosen. A number of extra parameters, so-called health parameters are investigated in the gas turbine diagnosis model. The test equations are chosen with structural methods and a DAE-index reduction is performed on the gas turbine model. It is shown that modes that are unobservable are removed from the gas turbine model since the over-determined part is considered.

A number of parsers which is used to convert the Modelica gas turbine diagnosis model into runnable Matlab codes are developed in the chapter. The output, when all parsers are utilized, is a state space form of the chosen diagnosis test equations.

Chapter 5

Estimation of Health Degradation in Industrial Gas Turbines

The performance of an industrial gas turbine degrade gradually due to certain factors such as environment air pollution, fuel content, and ageing to mention some of the degradation factors. Degradation due to compressor fouling can partially be restored by an on-line/off-line compressor wash. Therefore, it is important to supervise the degradation to efficiently plan service and maintenance. The gas turbine fleet consists of a lot of individuals, with different kinds of properties, that have to be monitored by the service engineers. Therefore, it is desirable that it should be easy to construct and evaluate different kinds of test quantities. The main objective of this chapter is to present a methodology that can be used to design diagnosis tests in an automatic manner directly from the gas turbine performance model. The diagnosis tests can later be included in a gas turbine monitoring component, or in the diagnosis system.

In the chapter, three studies are presented where techniques of performance deterioration estimations are investigated. In the first study, four simple approaches to calculate deterioration due to compressor fouling are presented. In the next two studies, the gas turbine model is used as a basis for the estimation techniques. In the second study, the estimations are based on so-called Measurement Deltas, which is generally the difference between the simulated and the measured gas path quantity. In the third study, a non-linear Kalman filter is evaluated on two test cases. In the first test case, simulated data from the reference platform is evaluated for different operational points and different atmospheric weather conditions. In the second test case, experimental data from a gas turbine mechanical drive site in the Middle East is evaluated. Finally, to see how the monitoring system reacts on a faulty sensor, an abrupt bias change is added to one of the measurement signals from the Middle East site.

5.1 Background

In industrial gas turbine applications, deterioration of components in the gas path is common and contributes to the overall performance degradation of the gas turbine. Therefore, it is of great importance to supervise the deterioration of these components to efficiently plan service and maintenance. Monitoring of gas turbines, and especially aircraft engines, is a widely studied topic in the gas turbine diagnosis literature, see, e.g., Volponi et al. (2003); Doel (2003).

In papers Diakunchak (1992); Kurz et al. (2009); Kurz and Brun (2001); Brekke et al. (2009), several mechanisms that cause degradation in gas turbines are presented. The major contribution of degradation in industrial gas turbines is fouling, caused by small particles and contaminants in the air. These particles increase the roughness of the rotor and stator surface. Another degradation effect is tip clearances which is a common diagnosis for older gas turbines. Tip clearances denotes an increasing gap between the rotating blades and the stationary casing. Fouling due to increased roughness can partially be restored by washing the compressor, while a component replacement is often needed for tip clearances. In the last paper, performed by Brekke et al. (2009), deterioration effects due to compressor fouling are investigated in an offshore industrial gas turbine application.

A common solution, about how to estimate deviation in performance from a nominal baseline is to introduce health parameters (Luppold et al., 1989; Kobayashi and Simon, 2003; Borguet and Léonard, 2008). In the two first papers, Kalman filters are used to estimate the considered health parameters. The degradation in performance is natural, so if the model does not compensate for this degradation it can be hard to avoid sensor false alarms. In Kobayashi et al. (2005), a non-linear Kalman filter is demonstrated that can be used in a wide operating range for an in-flight aircraft engine diagnosis application, providing an engine model with high accuracy.

One factor that can affect the model accuracy, and especially the performance of the health parameters, is the absolute humidity in the atmospheric air. The humidity effects, for an in-flight application are, e.g., studied in Bird and Grabe (1991) where methods based on parameter correction are considered. In Mathioudakis and Tsalavoutas (2002), a study is performed where humidity effects are investigated in an industrial gas turbine application. An analysis is presented of how the variation in ambient conditions affects the health parameter estimations. It is shown that a compensation for the ambient conditions reduces the undesirable daily variations in the estimated health parameters. In other gas turbine papers, the variation in absolute humidity is often neglected since it increase the complexity of the model and does not vary significantly much at many industrial gas turbine sites.

A fundamental effect of the change in absolute humidity is the change of molecules in the ambient air media. A change in the concentration of molecules in the media affects the thermodynamic gas properties such as enthalpy, heat capacity, and entropy. The thermodynamic properties influence the estimated performance. In the GTLib framework, as described in sub-section 3.2.1, the concentration of the molecules in the gas path media varies quasi-static according to the change in ambient conditions. The change in ambient conditions can be encapsulated by the developed estimators to reduce

undesirable daily variations, mentioned in Mathioudakis and Tsalavoutas (2002), in the estimated health parameters. Therefore, the absolute air humidity is considered in the present work.

5.1.1 Experiment Setup

The measurement data, which is used in the evaluation procedure in the present chapter, comes from a gas turbine site in the Middle East. Because of the difficult environmental conditions at the site, the compressor is washed frequently. At the current site, the gas turbine is a 1-spool and a 2-shafted machine with a mechanical drive application. A notable aspect with this specific gas turbine is the absence of an instrumentation sensor between the gas generator and the output of the power turbine. The lack of these type of sensors makes the diagnosis and monitoring procedure more difficult, since no measurement signals are available in the gas path between the output of the compressor and the output of the power turbine. Similar gas turbines, launched by other manufactures, have thermocouples between the gas generator and the power turbine. Having ideal thermocouples in that cross-section should reduce the uncertainty of the gas path parameters in the gas generator. To also detect deterioration in the power turbine, the engine is extended with thermocouples in the exhaust gas of the power turbine.

Experimental Platform

A schematic view of the experimental platform is shown in Figure 5.1, where the gas turbine and its surrounding components are presented. The dashed arrows in the figure represent physical connections, i.e., mechanical, thermodynamic, and electrical connections. Solid arrows represent signals to and from the controller.

The input signals to the controller are the atmospheric air sensors, the gas path instrumentation sensors, and the power generated by the application. The atmospheric air sensors measure pressure, temperature, and relative humidity of the ambient air. The gas path instrumentation sensors measure pressures, temperatures, and shaft speeds throughout the gas turbine. In sub-section 4.2.1, the exact positions of these sensors are described. Finally, the generated power by the application is not measured. Instead, the signal is estimated using internal sensors in the driven application component. Hence, the power estimation procedure does not utilize any of the gas path measurements, so a sensor fault in some of the gas path measurements does not affect the reliability of power estimation. The power signal is here considered as a reliable measurement signal.

As shown in Figure 5.1, a measurement signal of the mass flow of fuel is available. The controller does not use this measurement signal since a mass flow meter is expensive for the customer to install. Instead, a mass flow meter is only installed on request by the customer. In the diagnosis module at the present site, a model that include the fuel system together with the fuel pressure and the the fuel valve positions is considered when the mass flow of fuel is calculated. At the sites where a mass flow meter is available, more information about the process is available which can be included in the diagnosis system since the estimated signal can be compared, for example, with the measured signal by the mass flow meter.

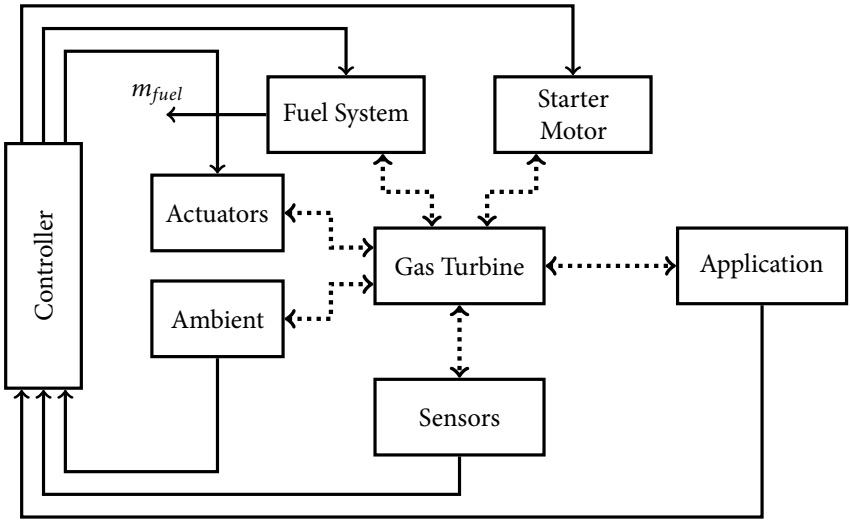

Figure 5.1: Schematic view of the gas turbine experimental platform. The dashed double arrows represent a physical connection, while solid arrows in the figure represent ordinary signals. In, e.g., Modelica, physical based connections are represented by equations and ordinary signals have only one direction.

One Year of Measurement Data

The considered sequence of available experimental data came from one year of operation. During the operation, the gas turbine is started and stopped a number of times. These starts and stops are removed from the measurement sequence when the test quantities are evaluated since the model is not valid during start and stop. During the operation, the compressor is washed five times (middle of November, end of December, end of March, end of June, and middle of September). Where the compressor washes are performed are shown with arrows in the coming evaluation figures, e.g., Figure 5.4 and Figure 5.8.

5.2 Introductory Methods to Determine Compressor Fouling

The objective with this section is to investigate four simple methods that can be used to detect compressor fouling. These methods are summarized in Table 5.1. The three first methods are based on estimation of mass flow in different ways. The first, second, and fourth methods are based on pure measurement signals, which means it is easy to make an investigation of fouling with these methods. The third method is based on the performance model, and is presented here for comparison. Estimation based on the performance model will be presented in Section 5.3. In all methods, the goal is to find a so-called *baseline*. The baseline is determined for a number of time samples of a cleaned

compressor. It is necessary to have the samples in a number of various operational points to get a proper baseline. Time samples that are collected after that are assumed to appear below the baseline. When the distance between the samples and the baseline is too large, it is time to wash the compressor. The baselines in the Figure 5.2 are only sketched by hand and the purpose with the introduced baseline is not to get the perfect position of the baseline through minimization of some criteria. Instead, the baseline should symbolize where a possible position could be in a simplified manner.

Table 5.1: In the table, four methods to detect compressor fouling are presented. It is shown if the method relies on the measurements and/or the physical model.

	Method	Measure-ments	Physical model	Mass flow estimation
(a)	Bell-Mouth Based Estimation	x		x
(b)	Pressure Ratio Based Mass Flow Estimation	x		x
(c)	Performance Model Based Mass Flow Estimation	x	x	x
(d)	Power versus Mass Flow of Fuel	x		

The measurement sequence that is used in the investigation of compressor fouling is collected between two compressor washes. The length of the sequence is about three months, where the first 40 samples start in January, and the last 40 samples end in March. These samples are marked in Figure 5.2, together with all the available points. The first samples (clean compressor) should be used to span the baseline, and the last samples (fouled compressor) should be used to detect compressor fouling.

5.2.1 Bell-Mouth Based Estimation

In Diakunchak (1992), three methods to detect deterioration due to compressor fouling are presented. One of these methods descends from an estimation of the mass flow through the compressor, and a common approach to calculate the mass flow is to measure the static pressure drop over the inlet duct of the compressor, i.e., over the *bell-mouth*. To get a reliable estimation of the absolute mass flow amplitude, the bell-mouth measurements need to be calibrated, together with the inlet pressure and the inlet temperature. For monitoring purposes, it is enough to consider the relative changes in mass flow, and according to Scott (1986), bell-mouth based measurement is a good technique to detect compressor fouling. It is assumed that the mass flow is proportional to the square root of the pressure drop over the bell-mouth. Thereby a decreased pressure drop over the bell-mouth, for a given normalized rotational speed can be interpreted as an increasing deterioration due to compressor fouling. To find when it is time to wash the compressor, a baseline of a cleaned compressor need to be constructed. This can be done by

running the gas generator for a number of different rotational speeds, and then plot the actual baseline for these speeds. Points that appear below this baseline indicate a fouled compressor, and when these points have dipped to a certain value, it is time to wash the compressor.

In subfigure 5.2a, the pressure loss measurement over the bell-mouth is plotted versus the normalized speed of the gas generator. In the figure, it is shown that it can be difficult to find a proper baseline, since the cloud of points are lumped, scattered, and cover nearly the same area. So for this specific sequence the bell-mouth measurements are no good to determine compressor fouling.

5.2.2 Pressure Ratio Based Mass Flow Estimation

For the case with a constant compressor pressure ratio together with fixed ambient conditions, the compressor need to rotate faster to compensate for the degradation in efficiency due to fouling (Kurz et al., 2009). At the same time, the compressor will also consume more power and fuel. Therefore it is interesting to study the pressure ratio versus the normalized rotational speed of the compressor. In subfigure 5.2b, the same measurement sequence is plotted as for the bell-mouth measurement, but the compressor ratio is instead considered. As subfigure 5.2b shows, it is easier to find a baseline in the pressure ratio plot than in the previous plot based on bell-mouth measurements. All the points that should represent a fouled compressor appear in the lower interval in subfigure 5.2b, which is desirable. It is undesirable that points that appear in the upper interval are not representative for a clean compressor. Finally, a considered baseline is sketched in the figure together with all available points.

5.2.3 Performance Model Based Mass Flow Estimation

According to Meher-Homji (1987), a mass flow meter is preferred against a mass flow estimation based on bell-mouth measurement, as an indicator of fouling. For the case where the mass flow through the compressor is not measurable, model based techniques can be utilized to calculate the actual mass flow. These techniques utilize the thermodynamic heat and mass balances. Here, the performance model constructed in GTLib package is simulated with the actual input signals shown in, e.g., Figure 4.3, to determine the mass flow of air. The result of the study is presented in subfigure 5.2c, and shows good result where all samples before the compressor wash appear in the lowermost layer seen from the baseline.

5.2.4 Power versus Mass Flow of Fuel

In the final subfigure 5.2d, the power generated by the application is plotted versus the mass flow of fuel. Also in this case, the points that symbolize a fouled compressor appear in the lowermost layer seen from the baseline. In all subfigures 5.2(a)–(d), normalized quantities from (3.2) in sub-section 3.1.2 are used.

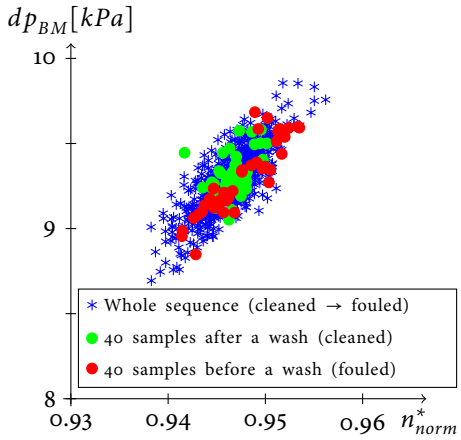

(a) Bell-mouth pressure loss versus normalized speed of the compressor.

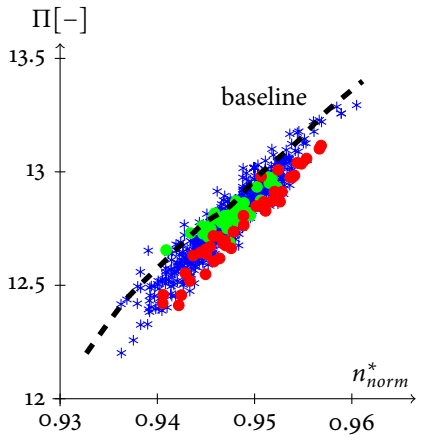

(b) Pressure ratio versus normalized speed of the compressor.

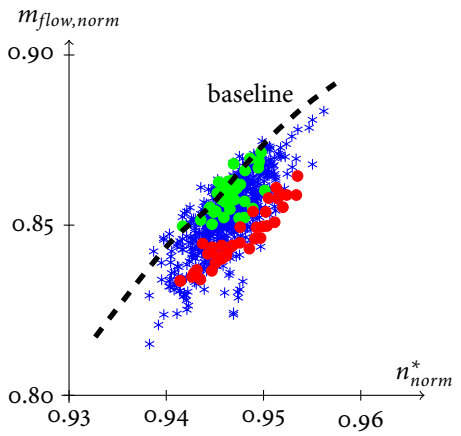

(c) Normalized mass flow of air through the compressor versus the normalized speed.

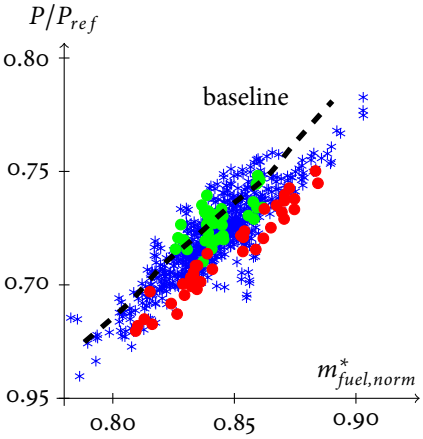

(d) Generated power by the application versus the normalized mass flow of fuel.

Figure 5.2: In the figure, four techniques of performance deterioration estimation due to fouling are presented. The considered measurement sequences are collected between the two compressor washes that are performed in the beginning of January, and in the end of March. All presented signals are based on measurements except the signal of the normalized airflow rate through the compressor. The mass flow of air is calculated by the gas turbine model, which is based on mass and heat balances. The normalized quantities are defined in (3.2). The objective with the study is to find a so-called baseline that can be determined for a clean machine (green points) for a number of different operational points. In the subfigures, the baseline is only sketched by hand to illustrate the principle. Before the compressor wash, the measurement points should be below the baseline (red points). According to this principle, subfigure (c) gives the best result and subfigure (a) gives the worst result.

5.3 Measurement Delta Calculation

In Urban (1972); Volponi (2003b); Simon et al. (2008), the so-called *Measurement deltas* are introduced. A brief introduction of these measurement deltas is available in subsection 4.1.1. The deltas are an important part of the gas path analysis and they are assumed to capture the deviation from a nominal baseline for a given number of known signals (or combination of known signals). Later on, the deltas can be supervised to detect trends or abrupt changes that can indicate a unhealthy behaviour. Since the reference model, that is used in the sequel, consists of a number of corrected parameters and performance maps, the delta calculation in Figure 4.1 can be replaced with the diagram in Figure 5.3:

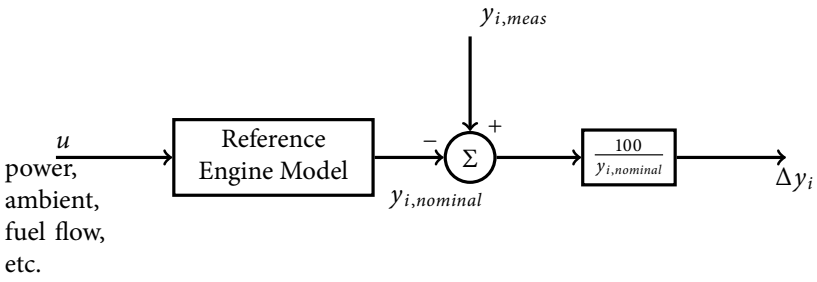

Figure 5.3: Delta Δy_i calculation of the measured quantity i.

and the delta calculation can then be written:

$$\Delta y_i = 100 \frac{y_{i,meas} - y_{i,nominal}}{y_{i,nominal}} \tag{5.1}$$

where $y_{i,meas}$ is the actual measurement, and $y_{i,nominal}$ is the predicted model output for the measured quantity i. Results of the delta calculation for the measured discharge temperature T_3 after the compressor, and the exhaust temperature T_{75} after power turbine are shown in Figure 5.4, and in Figure 5.5.

It can be difficult for the user to know which of the deltas that should be considered, since it is possible to combine signals to construct "infinitely many" deltas. Here, only deltas of measured quantities are constructed, and the temperature deltas give the best plot results of these measured quantities. It is possible to separate trends due to compressor washes in Figure 5.4, and Figure 5.5. These trends can be monitored by a diagnosis system to decide when a compressor wash is necessary to perform. A drawback with the delta trends is that the ambient conditions, e.g., the atmospheric air temperature shown in Figure B.1 impact the estimations.

It is desirable to obtain a static threshold of compressor fouling detection, because the compressor should be washed regularly when a certain degree of fouling has occurred. In Figure 5.4 and Figure 5.5, an upper static threshold is introduced, and the level should be different for summer and winter for best performance. These figures can be misleading, because the status of fouling before each washing is not exactly known, so the degree of

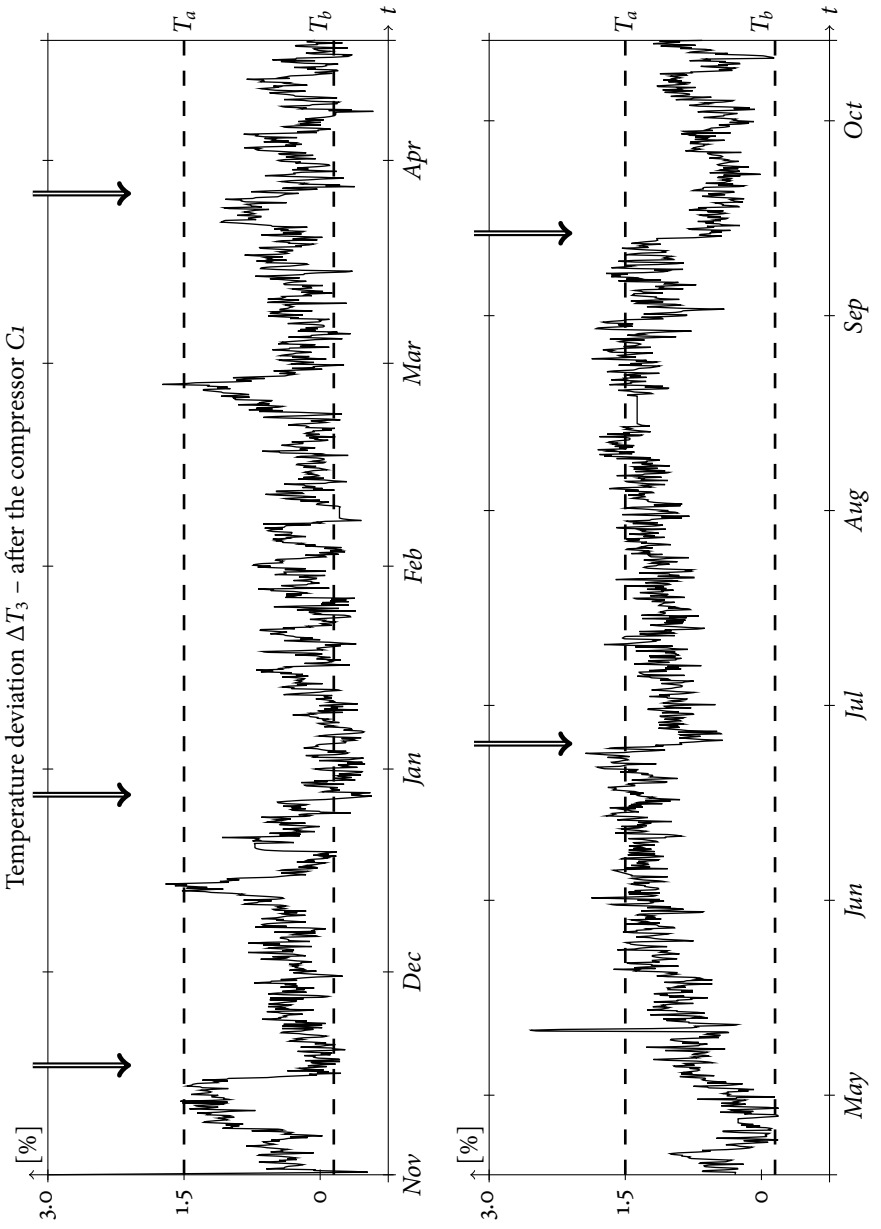

(a) ΔT_3 for the first six-month period.

(b) ΔT_3 for the second six-month period.

Figure 5.4: In the figure, the delta calculation ΔT_3 together with the given static thresholds are shown. The upper static threshold is used to detect compressor fouling, while the lower static threshold should indicate the performance level of a cleaned compressor.

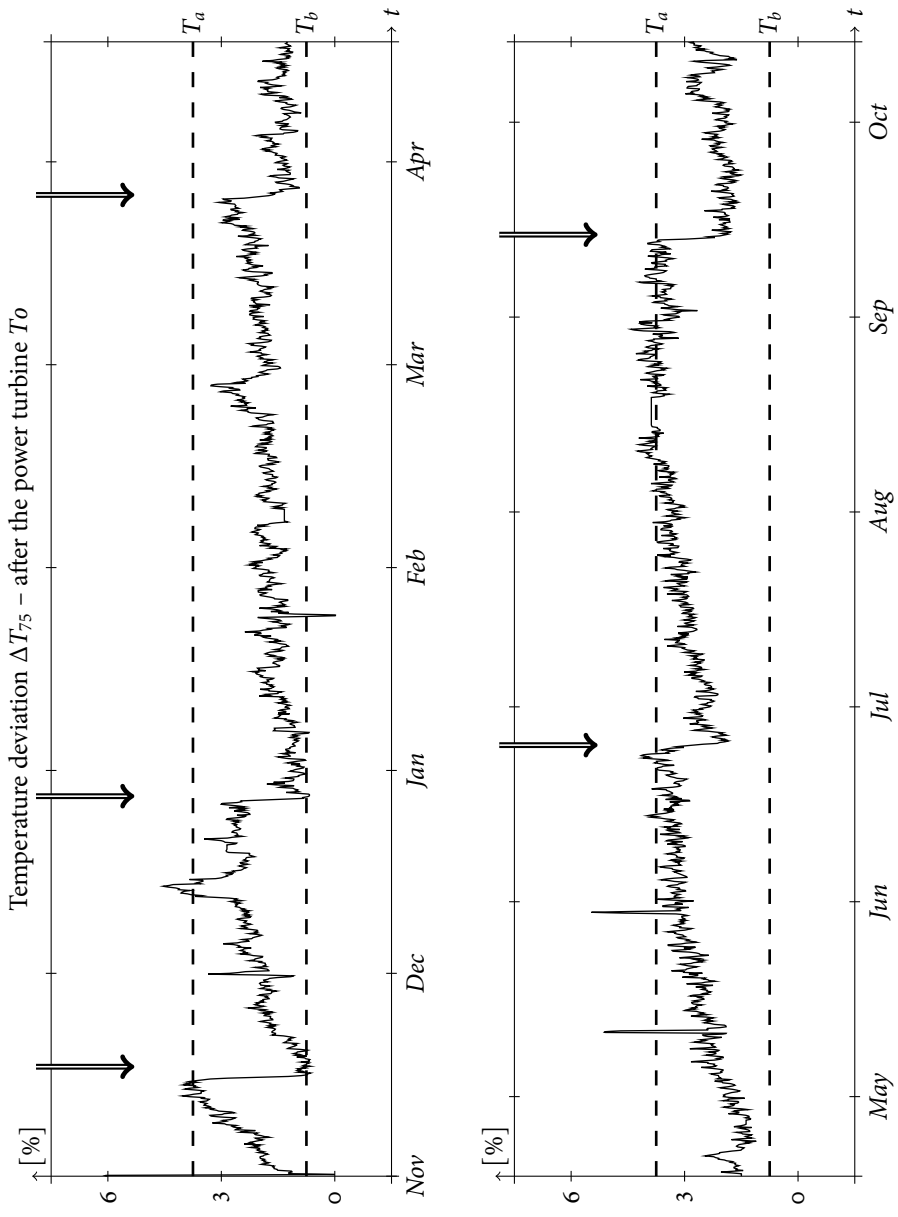

(a) ΔT_{75} for the first six-month period.

(b) ΔT_{75} for the second six-month period.

Figure 5.5: In the figure, the delta calculation ΔT_{75} together with the given static thresholds are shown. The upper static threshold is used to detect compressor fouling, while the lower static threshold should indicate the performance level of a cleaned compressor.

fouling can be different before each wash. On the other hand, after a compressor wash the degree of fouling should be the same independently of the winter or the summer period. The lower threshold in the figures suggests that the estimations are not independent of the ambient air condition. Especially, slow changes in increasing atmospheric air temperature can be difficult to be discriminated from a cleaned compressor, and vice versa. This can clearly be seen in the end of February in the figures where the deltas have increased abnormally much, which can be misunderstood as a fouled compressor.

5.4 Constant Gain Extended Kalman Filters

A common solution in the gas turbine diagnosis literature, to estimate health deterioration, is to use observers. The observers are often Kalman based, and linear in: Luppold et al. (1989); Volponi (2003a), non-linear in: Borguet and Léonard (2008); Dewallef et al. (2006); Rausch et al. (2007). In all of these papers, the application is for in-flight sensor or actuator diagnosis and supervision of performance.

The main objective in this section is to design an observer in the form:

$$\dot{\hat{x}} = f(\hat{x}, u) + K(y - \hat{y}) \tag{5.2a}$$

$$\hat{y} = g(x) \tag{5.2b}$$

where the functions f and g can be non-linear, $u \in \mathbb{R}^{n_u}$ is the input signal vector, $y \in \mathbb{R}^{n_{\hat{y}}}$ is the measurement signal vector, and $K \in \mathbb{R}^{n_{\hat{x}} \times n_{\hat{y}}}$ is the observer gain which can be considered as a design parameter that is specified by the user. The estimation error, or the residual, $r = y - \hat{y}$ is amplified through the K matrix. Thus, if the observer gain K is large, the observer relies more on the measurements than the model equations, and if the observer gain K is small the observer relies more on the model equations than on the measurements. This means that a large K results in state estimations that are more sensitive to measurement noise than if a small K is used. On the other hand, a small K corresponds to estimation errors where model uncertainties get more significant. Thus, when the observer is designed, it is possible for the user to choose between a *fast and noisy* and a *slow and filtered* estimator.

A special type of a non-linear Kalman filter are a so-called *Constant Gain Extended Kalman Filter* (CGEKF), presented in Safonov and Athans (1978), where also the robustness and stability of the observer concept are investigated. The CGEKF is a special case of an *Extended Kalman Filter* (EKF) (Kailath et al., 2000). In the EKF, a new observer gain is calculated for each time step where the results rely on the the Jacobian calculation of f in the system (5.2). The calculation of the Jacobian is performed on-line since the state of the system updates in each time step. In the CGEKF, the observer gain is calculated in advance for a given operating point and can thus be calculated off-line. A state-of-the-art survey of the EKF and the CGEKF is presented in Misawa and Hedrick (1989). In the gas turbine application papers Kobayashi et al. (2005); Sugiyama (2000) the CGEKF concept is considered. In these papers it is demonstrated that the CGEKF observer can be used in a wide operating range for an in-flight aircraft engine diagnosis application. These studies indicate that it is not necessary to calculate a new Kalman gain for each operational

point during a flight program. Instead, it is more important that the engine model, used in the observer, has high accuracy. In Andersson (2005), a CGEKF is constructed for state estimation in a turbocharged automotive application, where the feedback gains are calculated off-line in a number of operating points and stored in a tabular. Interpolation techniques are then applied to calculate the global observer gain K, used in the actual observer in the on-line application.

In the present gas turbine application, the CGEKF methodology is chosen instead of, e.g., the EKF methodology. The motive to choose the CGEKF concept depends on the simplicity of the observer since the observer gain is constant. Usually works a CGEKF well for a suitable choice of the operating point where the observer gain is calculated. The advantage is that the observer gain can be determined off-line which is attractive for an estimator that is used in a real time application.

The observer gain is calculated in the operating point where the ambient air conditions are at the datum state. The power, generated by a 50 Hz generator, is 21 MW and the speed of the power turbine is given by the generator. In the present case, a mechanical drive application is studied, which results in a power turbine speed that can be varied. The chosen fuel is a standard natural gas fuel with a lower heating value (LHV) of about 50 MJ/kg. The CGEKF observer, together with the gas turbine platform, is shown in Figure 5.6. The output signals from the observer component are the estimated measurement signal $\hat{y}$, estimated health parameters $\hat{h}$, and finally an estimation of all the other states variables $\hat{x}$.

5.4.1 Observer Design

The starting point of the observer construction methodology is the gas turbine diagnosis DAE model defined in (4.30). How the equations, used in the observer, are selected is shown in Chapter 4 and in Larsson et al. (2010). Before a summary of the observer design procedure is presented, the equations of the linear/non-linear Kalman observers are shown, and important steps such as observability and observer tuning are discussed.

Kalman Filter

A linear dynamic system, expressed in state space form, can be written:

$$\begin{aligned} \dot{x} &= Ax + Bu + Gw \\ y &= Cx + Du + v \end{aligned} \tag{5.3}$$

where $A \in \mathbb{R}^{n_x \times n_x}$, $B \in \mathbb{R}^{n_x \times n_u}$, $C \in \mathbb{R}^{n_y \times n_x}$, and $D \in \mathbb{R}^{n_y \times n_u}$ are system matrices, $G \in \mathbb{R}^{n_x \times n_w}$ is a gain matrix of the process noise, u is the input signal, w is white process noise, and v is white measurement noise. The noise signals satisfy:

$$\begin{aligned} E[w(t)w(s)^T] &= Q\delta(t-s), \quad & E[v(t)v(s)^T] &= R\delta(t-s), \\ E[w(t)] &= E[w(s)] = 0, & E[v(t)] &= E[v(s)] = 0, \end{aligned} \tag{5.4}$$

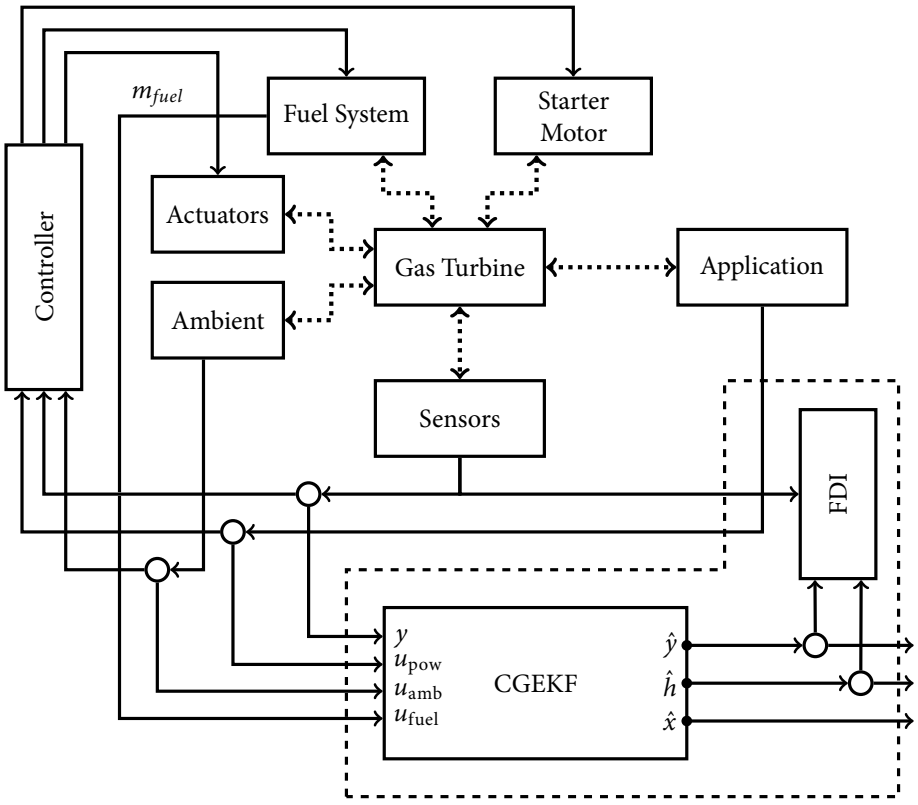

Figure 5.6: Schematic view of the gas turbine experiment platform, where the Constant Gain Kalman filter is introduced to estimate the health h. The Fault Detection and Isolation (FDI) component is also introduced in the experiment platform to detect compressor fouling, and sudden sensor faults. The complete diagnosis system is dashed in the figure.

for the dummy scalar variables t, s and the Dirac function δ. The Kalman filter equations (Kailath et al., 2000) of system in (5.3), are:

$$\begin{aligned} \dot{\hat{x}} &= A\hat{x} + Bu + K(y - C\hat{x} - Du) \\ \hat{y} &= C\hat{x} + Du + v \end{aligned} \tag{5.5}$$

The Kalman gain K is:

$$K = PC^T R^{-1} \tag{5.6}$$

where P is the solution to the Riccati equation:

$$\dot{P} = AP + PA^T + GQG^T - PC^T R^{-1} CP + Q \tag{5.7}$$

for a given initial probability condition $P(0) = E\left[\left(x(0) - \hat{x}(0)\right)\left(x(0) - \hat{x}(0)\right)^T\right]$.

Stationary Kalman Filters

The stationary Kalman filter is obtained by setting $\dot{P} = 0$ in (5.7).

Non-linear Kalman Filters

If the system (5.3) is replaced with a non-linear system in the form:

$$\begin{aligned} \dot{x} &= f(x, u, w) \\ y &= g(x, u) + v \\ w &\sim (0, Q) \\ v &\sim (0, R) \end{aligned} \tag{5.8}$$

where the linearization

$$A = \left.\frac{\partial f}{\partial x}\right|_{\hat{x},u}, \; C = \left.\frac{\partial g}{\partial x}\right|_{\hat{x},u}, \; G = \left.\frac{\partial f}{\partial w}\right|_{\hat{x},u}$$

is applied when the Kalman gain K is calculated. Then it is possible to develop the two non-linear Kalman filters (EKF), and (CGEKF). These filters, or observers can be written:

1. Extended Kalman Filter (EKF):

$$\begin{aligned} \dot{\hat{x}} &= f(\hat{x}, u) + K(\hat{x}, u)(y - h(\hat{x}, u)) \\ \hat{y} &= g(\hat{x}, u) \end{aligned} \tag{5.9}$$

   where the Kalman gain $K(\hat{x}, u)$ is updated in every time step according to (5.6).

2. Constant Gain Extended Kalman Filter (CGEKF):

$$\begin{aligned} \dot{\hat{x}} &= f(\hat{x}, u) + K(y - h(\hat{x}, u)) \\ \hat{y} &= g(\hat{x}, u) \end{aligned} \tag{5.10}$$

   where the Kalman gain K is calculated for the stationary Kalman filter in one operational point according to (5.6).

Observability

In the gas turbine diagnosis model, eight unique measurement positions throughout the gas path are available. According to Lemma 4.5.4, the maximum number of health parameters that can be considered in the model is eight. If more health parameters are used, the observability of the system is not fulfilled. Since the requirement in Lemma 4.5.4 is necessary but not sufficient, the number of health parameters that are observable could be smaller than the maximum number specified in the Lemma. Thus, an observability analysis of the gas turbine diagnosis model is necessary to perform.

To check the observability of the diagnosis model, with different health parameter configurations, the linearized model is studied. According to the numerical problems that can appear for larger models when observability is checked with the criteria in Theorem 4.5.1, the structural observability criteria in Theorem 4.5.2 (Shields and Pearson, 1976) is used. The structural observability analysis shows that the health parameter configuration, described in (4.3), is structurally observable in the linearization point of the chosen CGEKF observer. If another health parameter, i.e., for the mass flow through the power turbine is added, the linearized model is no longer structurally observable which induce unobservability. For the case where the two health parameters for the inlet and outlet duct are added, the structural observability is not affected. A health parameter in the inlet duct can for example be interpreted as a pressure drop in the air filter due to, e.g., fouling. This indicates that it can be possible to supervise the health parameter. Finally, the structural observability of the linearized diagnosis model is strongly connected to the number of health parameters, and where in the model these parameters are introduced.

Observer Tuning

Beside the system matrices, the model uncertainty matrix Q, and the measurement uncertainty matrix R affect the estimation of the state vector $\hat{x}$ in the observer. If the uncertainties of the measured signals are independent, the R matrix is diagonal. The diagonal elements of the matrix represent the variance of respective measurement signal. In the present case, the measurement uncertainty is unknown but it is assumed that all sensors have an uncertainty that is 1 % of the sensor reference value. This gives matrix elements in R as:

$$R_{i,i} = \left(10^{-2} y_{ref,i}\right)^2$$

where $i = 1 \ldots 8$. The model uncertainty matrix Q is determined in a similar manner according to:

$$Q_{j,j} = \left(10^{-2} x_{ref,i}\right)^2$$

where $j = 1 \ldots n$. Since it is the relative relation between Q and R that compromises between the noise sensitivity and the response of the Kalman filter, it is easy to adjust these properties through a constant gain scaling of the Q matrix. A large scaling factor increases the model uncertainty, and the Kalman filter gets a faster response but the influence of measurement noise increases in the state estimation. An advantage with using the gain matrix of the process noise G is that different states can be weighted

independently of each other easily, if also this matrix is diagonal. A small diagonal element in amplitude, that represents the state $\hat{x}_i$, gives slow dynamic, and vice versa. Thus, elements that represent the health parameters are given small values, since the health degradation is slow.

Observer Design Summary

The observer design procedure consists of four important steps. These steps are; the index reduction, the over-determined M^+ part, the state space form, and the CGEKF observer construction. A summary of the design procedure is:

1. Index reduction:
   (a) Start with the model given in Eq. (4.17). Since the measurement signal y in (4.17b) is a known signal vector, the system is over-determined. Thus, remove the measurement equation $y = \bar{h}(x)$ to get a system that is exactly determined.
   (b) Acquire the structural model of the system.
   (c) Check, and reduce the DAE-index of the system (if necessary). For this step, Pantelides algorithm (Pantelides, 1988) is invoked. The input to the algorithm is the structural model. The output of the algorithm is the equations that need to be differentiated to receive a smaller index problem.
   (d) Take back the removed measurement equations from the first step.
2. Find the over-determined M^+ part:
   (a) Once again, acquire the structural model of the system. This time, the measurement equations are also included.
   (b) Find an over-determined part of the structural model. For this step, a Dulmage-Mendelsohn decomposition (Dulmage and Mendelsohn, 1958) is performed, and the whole over-determined M^+ part is chosen.
   (c) The actual test equations are now selected.
3. The state space form:
   (a) Write the semi-explicit DAE-index 1 system in an ordinary state space form through an inversion of the algebraic constraints and a symbolic transformation of the $\tilde{E}$ matrix in (4.18a). Some of the algebraic constraints are non-linear so they are solved with a non-linear numerical solver.
   (b) Linearize the system in a suitable operating point and calculate the matrices A and C.
   (c) Check the structural observability of the linearized system.
4. CGEKF observer construction:

(a) Specify the measurement uncertainty matrix R, and the model uncertainty matrix Q, for the Kalman filter gain with fast dynamic. This Kalman gain is used in the start up phase, and after a compressor wash.

(b) Calculate the Kalman gain K, through solving the Riccati equation (5.7), for the given uncertainty matrices Q and R.

(c) Repeat the two steps above to calculate a Kalman filter gain with slow dynamic. This is the observer Kalman gain which is used most of the time.

(d) Implement the developed observer with the two Kalman gains.

5.4.2 Evaluation of the CGEKF Based Test Quantity

The evaluation of the CGEKF based test quantity is done for two test cases. In the first test case, simulated data gathered from the reference simulation platform shown in Figure 1.1 is evaluated. In this test case the focus is on variation in ambient conditions. In the second test case, experimental data from a gas turbine site in the Middle East is evaluated. The focus here is on compressor fouling detection and an investigation of sensor fault diagnosis.

Bias Compensation in the Measurement Sensors

A constant bias term is added to all measurement signals in the observer. For example, the exact position of the sensors is not known, and the actual absolute pressure can differ from the nominal model, depending on the position in the gas path. A leakage in the turbine, due to increased clearances, also affects the pressure measurement. Thus, the basic idea with the introduced bias terms is to compensate for individual properties in the gas turbine fleet, to get estimated health parameters in the same interval.

The bias terms are calculated once for the cleaned gas turbine. In the experimental data sequence that is investigated, the bias terms are calculated directly after the first compressor wash. The bias terms b_i of measurement sensor i are simply calculated:

$$b_i = \sum_{j=1}^{k} \frac{y_{i,j}^{nominal} - y_{i,j}^{meas}}{k}$$

where k is the number of samples that corresponds to two days of operation, y^{meas} is the measured quantity, and $y^{nominal}$ is the reference value calculated from the nominal model similar to the description in Figure 5.3. This gives an expression for input signal y in the observer (5.2) according to:

$$y = y_{meas} + b$$

where b is the constant sensor bias calculated once. In the present case, the bias compensation is negligible for all sensors except for the discharge pressure sensor p_3 after the compressor. For p_3, the bias compensation is about 10 % from the nominal reference value. The large difference between the measurement and the nominal reference value for the discharge pressure does not depend on the actual sensor calibration since the

discharge pressure is measured with three sensors where all the sensors show values in the same interval. An idea is that the pressure difference came from leakages in the compressor turbine due to clearances.

Simulation studies have shown (e.g., in Figure 5.11) that an introduced sensor bias may affect the estimated health parameters in the same way, i.e., a bias is added to the estimations.

Evaluation 1: Simulated Data – Atmospheric Weather Condition Dependence

The objectives with this evaluation are: (1) assure that the CGEKF observer converges (is stable) to reasonable state values during a sweep in different operating points with introduced health degradation, and (2) investigate the difference between one observer that compensates for changes in absolute humidity in the incoming air, and one that does not compensate for changes in absolute humidity in the incoming air. Incoming gases affect the performance of the gas turbine model; therefore it is interesting to investigate how big the effects, in performance, are when the air humidity is changed. The observer that does not compensate for absolute humidity changes is developed for the datum atmospheric conditions, such as $p_0 = 1.013$ bar, $T_0 = 25\,\mathrm{C}^o$, and $RH = 60\,\%$. These environment values give an amount of water in the incoming air according to the considered air model, and numerical values are shown in Tabular 3.2. The observer that compensates for the absolute humidity in the incoming air is described in subsection 3.2.1.

Input data for the two observers is collected from the reference platform shown in Figure 1.1. In this evaluation case, the ambient temperature is varied according to 15–35 C^o and the relative humidity is varied according to 40–80 %, during the constant pressure at datum state. At the same time, the power generated by the external application, is varied in the interval 16–26 MW. Because of the varied power, the gas generator speed is also varied. In the application here, an electric generator with fix frequency is used. Thus the power turbine has a constant speed, but different generator frequencies are investigated in other studies that have been performed, and with similar results. The objective is to estimate deviation in performance and therefore degradation in the considered performance parameters is injected. These injected degradations, in percent from respective baseline reference value, are presented in Table 5.2.

Table 5.2: Injected degradation in performance equations (in percent of the nominal value).

Health Parameter	Injected Degradation (%)
$\Delta\eta_{C1}$	-3.4
$\Delta\Gamma_{C1}$	-2.5
$\Delta\eta_{T1}$	+2.4
$\Delta\Gamma_{T1}$	+4.6
$\Delta\eta_{To}$	-1.2

The results from the simulation study is presented in Figure 5.7, where the estimated

health parameters are viewed. In the subfigures 5.7(b)–(f) the estimated degradations in the gas path components are shown.

The subfigure 5.7a shows the generated power and the amount of water in 1 kg atmospheric air. The highest and lowest values denote the two extreme cases from Table 3.2. For these two extremes, the observer that does not compensate for absolute humidity has a variation in the health estimation of about 1–2 percentage points for all cases except for the efficiency of the compressor turbine.

The observer that compensates for atmospheric weather conditions follows the injected deterioration in the reference platform nearly perfect even when the ambient conditions are changed, except during transients. One explanation of this phenomenon is that the gas properties, according to the change in atmospheric air, are updated simultaneously in the whole observer. It can also be seen in the figure that different operating points do not affect the estimations so much, which is desirable. In Figure 5.7, the power turbine has a fix speed, but similar simulation studies are performed where also the power turbine speed is varied. The results of these studies are similar with the outcome in Figure 5.7. The conclusion is that the observer that compensates for the different ambient conditions gives better performance estimations and converges to the actual state of the system even if the operational points are changed.

Evaluation 2: Experimental Data – Mechanical Drive Site

The objectives with this evaluation are: (1) estimate the actual health state of the gas turbine over time, (2) see if the observer gives reliable state estimates, (3) check if the observer based concept is suitable to use when the time for compressor wash is determined, and finally (4) detect an injected sensor fault in the measurement sequence.

For this evaluation, two Kalman filter gains for the observer in (5.10) are generated where also the health parameters viewed in (4.3) are included. The Q and R matrices are tuned so the Kalman filter gains represent an observer with a weak feedback term and an observer with a strong feedback term respectively. The two Kalman gains are merged into one observer called a test quantity of performance estimation, i.e., the observer switches between the two Kalman gains. In the start and after a compressor wash the test quantity uses the Kalman gain that represents an observer with a strong feedback term. All the other time, the Kalman gain that represents an observer with a weak feedback term is used in the test quantity. Thus, the test quantity switches between an observer with fast dynamic and an observer with slow dynamic. The CGEKF method is used in the test quantity, instead of the more general EKF filter, since the computation burden is smaller for a CGEKF than an EKF. The test quantity compensates for different ambient conditions according to Evaluation 1 in sub-section 5.4.2.

In Figure 5.8, the health parameter $\Delta\eta_{C1}$ for the isentropic efficiency in the test quantity is shown (dashed line). In the same figure, the health parameter for an observer that only consider the Kalman feedback gain with a fast response is also viewed (solid line). This is done because the actual test is more or less a filtered variant of the observer with the strong feedback Kalman gain. In the figure, two static thresholds are introduced. The purpose with these thresholds is to emphasize the levels of degradation. After a compressor wash, the level of performance should be the same independently if the

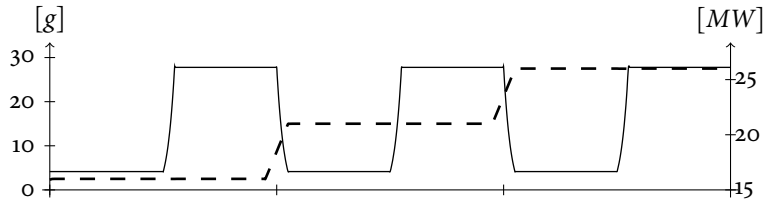

(a) Water steam – solid , Generated power – dashed

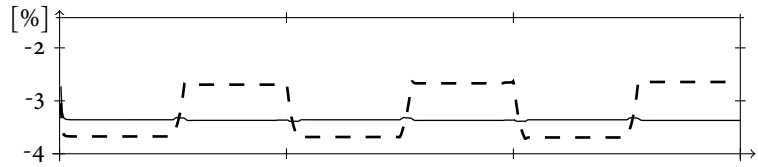

(b) Health parameter: $\Delta\eta_{C1}$

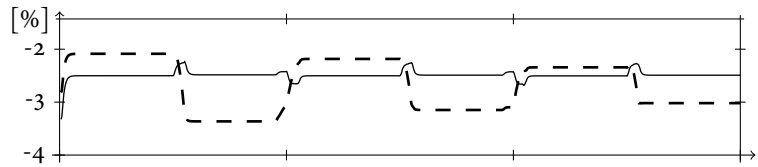

(c) Health parameter: $\Delta\Gamma_{C1}$

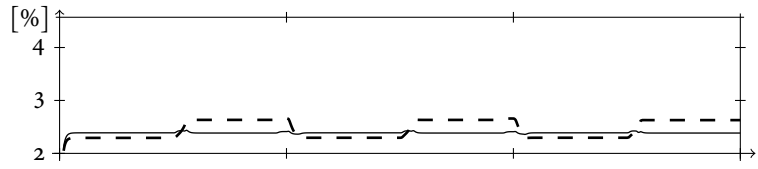

(d) Health parameter: $\Delta\eta_{T1}$

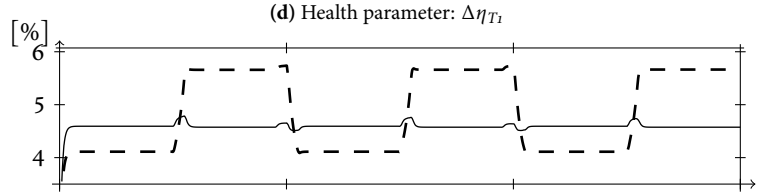

(e) Health parameter: $\Delta\Gamma_{T1}$

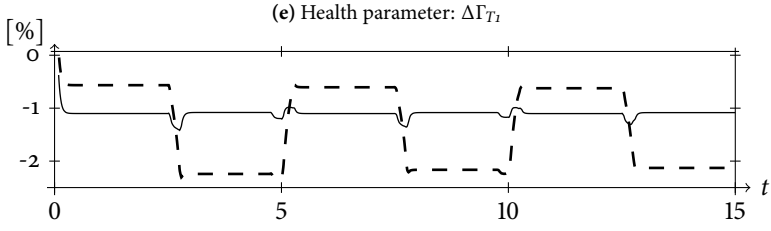

(f) Health parameter: $\Delta\eta_{To}$

Figure 5.7: In the figure, performance estimation of data generated in simulation platform shown in Figure 1.1, with injected degradations according to Table 5.2 (not viewed in the subfigures), are shown. Two CGEKF observers are evaluated, i.e., an observer that compensates (solid lines) and an observer that does not compensate (dashed lines) for the variation in ambient conditions are shown in subfigures (b)–(f). The power of the external application is varied together with changes in the absolute humidity of the incoming air are viewed in subfigure (a).

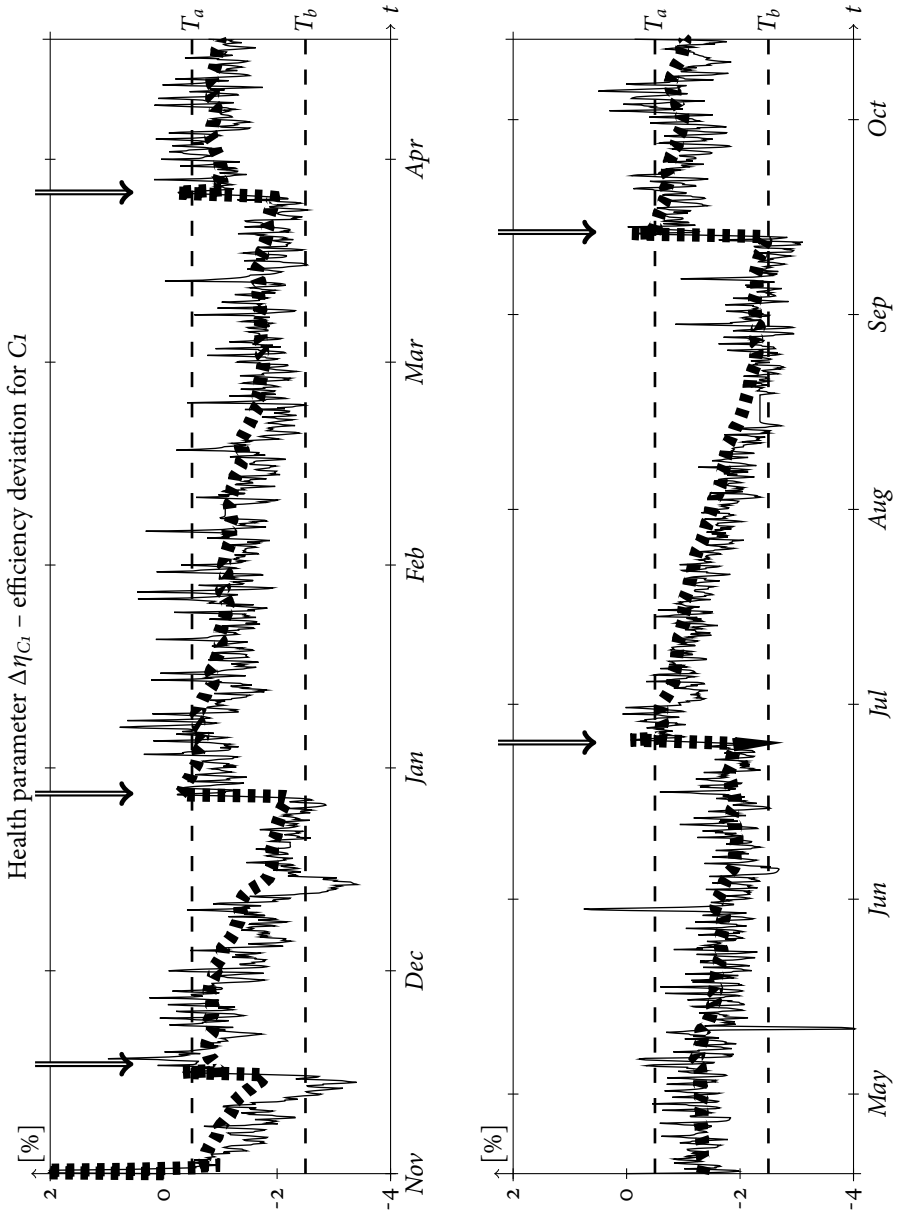

(a) The first six-month period Nov–Apr.

(b) The second six-month period May–Oct.

Figure 5.8: In the figure, the estimated deviation for the compressor efficiency from a nominal reference value is shown for a time interval of one year. Compressor washes are marked with arrows in the two subfigures. The range of degradation in efficiency can be bounded to an interval of about 2 percent as the shadowed area indicates, independent of the atmospheric weather conditions during the year. Then it is possible to use a static threshold to detect when a compressor wash is necessary to perform.

washes are performed in the summer or in the winter which the upper threshold should emphasize. The lower threshold is more important since it is this threshold that should trigger an alarm, and initiate a compressor wash, in the FDI component which is viewed in Figure 5.6. Since the data is from a gas turbine site, it is not known how fouled the compressor was before the compressor wash is performed. Therefore, the comparison between the different washes is a little unfair, but the degradations before a compressor wash are very similar in all cases. The other health parameters that are estimated by the observer are shown in the appendix. These health parameters are more difficult to interpret but needed for the sensor diagnosis to compensate for the trends in the residuals (5.11).

In the FDI component, residuals for each of the eight instrumentation sensors are constructed. These residuals, used for sensor fault detection, are in the form:

$$r_i = y_i - \hat{y}_i \tag{5.11}$$

where y_i is the measured quantity, and $\hat{y}_i$ is the estimated quantity by the observer.

For a good model, these residuals should be centered around zero with a small amplitude since the observer captures the information in the measurement signals. If no health parameters are introduced in the diagnosis model, the residuals are dependent on, e.g., the grade of compressor fouling. If the residuals depend on such factors, it can be difficult to use the residuals to detect and isolate sensor faults. A subset of the actual residuals for the second half year is shown with black lines in Figure 5.9. In these residuals it is not possible to see degradations due to compressor fouling or where the compressor washes are performed.

The red lines in Figure 5.9 represent sequences where a sensor fault is injected in the measurement data of the compressor discharge temperature sensor T_3. The fault is injected in the middle of July and is a step fault with an amplitude of 1 % or ≈ 7 K of the sensor reference value. In an ideal case, all residuals will react but as the figure shows the residual r_5 has the strongest reaction. So, the residuals of the tests are sensitive, in an ideal case, to all abrupt sensor faults but the residual that represents the faulty sensor has higher tendency to react. Therefore, a soft sensor fault isolation decision can be introduced in the gas turbine diagnosis system, or in the FDI component. As can be seen in the figure, the residual r_5 is back to normal after some time and it is not possible to see the sensor fault in the residuals anymore. This phenomenon depends on the health parameters since they capture the faulty sensor value as shown in Figure 5.11. The health parameters think the bad sensor value is correct but the gas path components have deteriorated. According to the figure, it is only the health parameters of the isentropic efficiency that are affected by the introduced sensor fault.

The CUSUM algorithm (Page, 1954), together with the static thresholds J are performed to detect the sensor faults in the residuals. The CUSUM test quantity $T(t)$ can be determined according to:

$$s(t) = |r_i(t)| - v_i \tag{5.12a}$$

$$g(t+1) = g(t) + s(t) \tag{5.12b}$$

$$T_i(t) = g(t) - \min_{0 \le i < t} g(i) \tag{5.12c}$$

where $g(0) = 0$, v_i is a tuning parameter to ensure that $E[s(t)] < 0$ in the fault free case, and $|r_i(t)|$ is the absolute value of residual in (5.11). The test quantity gives an alarm if $T_i(t)$ is larger than the threshold J_i. The design parameters v_i and J_i are tuned so the test doesn't give any unnecessary alarms in the fault free case. The CUSUM algorithm is often more suitable to use, compared to low-pass filtering, to detect changes in signals. The CUSUM based tests, without a threshold J_i, of the residual signals in Figure 5.9 are shown in Figure 5.10 where test $T_5(t)$ stands out from the other tests, i.e., the fault sensor.

5.5 Overall Results of the Performance Estimation Techniques

In this section, a discussion of advantages/disadvantages of the considered performance estimation techniques is presented.

5.5.1 Bell-Mouth Based Estimation

The first standardized method to detect compressor fouling is based on the bell-mouth pressure drop measurement shown in subfigure 5.2a. The method is simple since the model assumption of the mass flow is not so sophisticated. The bell-mouth measurement gives an estimation of the relative mass flow through the compressor. For the available measurement sequence the method indicates poor performance. It is hard to distinguish when a compressor wash is needed, since a baseline for a clean compressor lies in the middle of all points in the diagram. It is desirable that all points in the diagram lie below the baseline, and the distance increases with time. A better baseline estimation is received if a physical model is used to estimate the mass flow as subfigure 5.2c shows.

5.5.2 Measurement Delta Calculation

The second method is based on the so-called measurement deltas. These measurement deltas are more or less, a comparison between an estimated and a measured gas path parameter. A first step is to construct these deltas directly for the measured quantities, i.e., for the pressures, the temperatures, and the shaft speeds throughout the gas path. The benefits with this method are; (1) it is simple to construct deltas because the performance model is already available, and (2) trends due to performance degradation, e.g., compressor fouling, can be detected. The performance model is not augmented with extra parameter or state variables. Therefore, degradation in components is not modeled explicitly which results in residuals that are dependent on, e.g., compressor fouling. Thus, these residuals are not suitable for sensor fault diagnosis. It can also be difficult for the user to determine which of the deltas that can be relevant to study, since it is possible to construct infinitely many deltas. It can also be difficult to associate a number of deltas to a physical fault in the gas turbine.

The disadvantage with the method is the dependency of the ambient weather condition. The deltas appear to detect trends in performance degradation but also in the ambient atmospheric condition. Therefore it can be difficult to know exactly when a

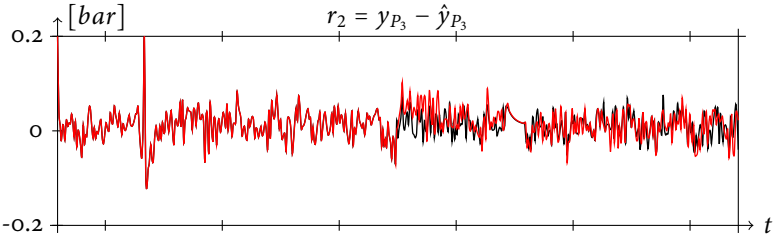

(a) Residual for the discharge pressure P_3 after the compressor.

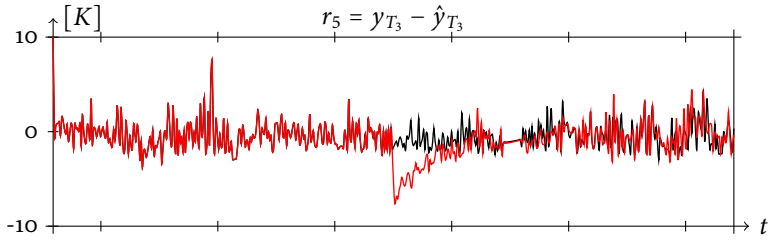

(b) Residual for the discharge temperature T_3 after the compressor.

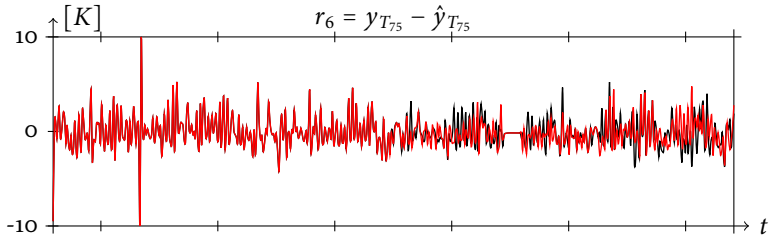

(c) Residual for temperature T_{75} in the exhaust gas.

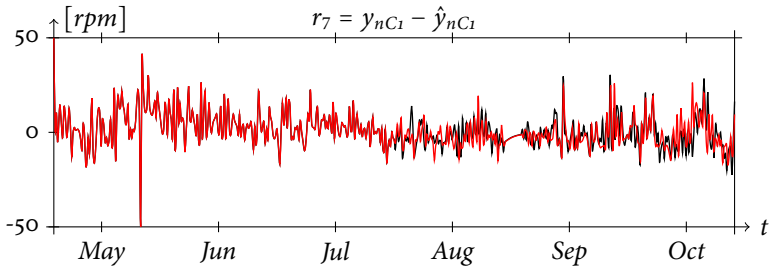

(d) Residual for shaft speed n_{C_1} for the gas generator.

Figure 5.9: In the figure, residuals for four of the eight sensors through the gas path are shown. In the middle of July, an abrupt sensor fault of 1 % ($\approx$ 7 K) of the sensor reference value is injected in the measurement signal. It is possible to see the injected sensor fault in the residual, and a good guess is that the sensor T_3 is faulty. After some days, the faulty sensor behaviour disappears since the health parameters capture the faulty sensor value. The black lines represent the non-faulty behaviour and the red lines represent the faulty sensor sequence.

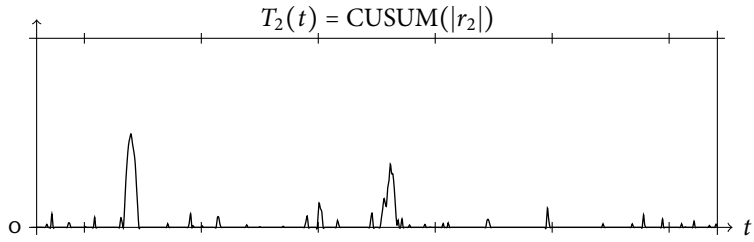

(a) CUSUM test $T_2(t)$ of residual r_2.

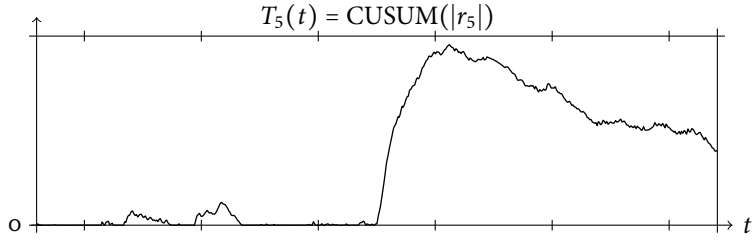

(b) CUSUM test $T_5(t)$ of residual r_5.

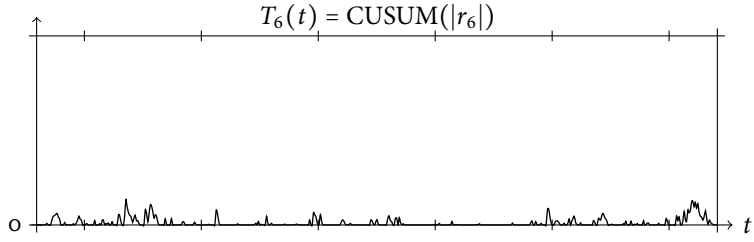

(c) CUSUM test $T_6(t)$ of residual r_6.

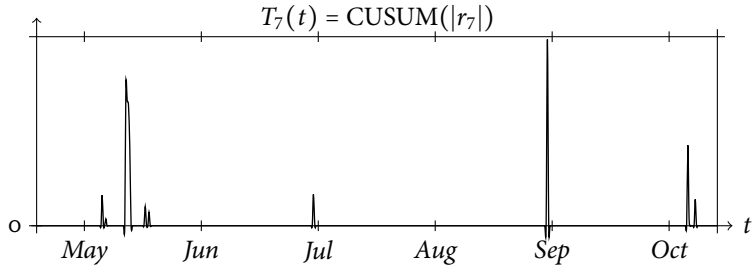

(d) CUSUM test $T_7(t)$ of residual r_7.

Figure 5.10: In the figure, the CUSUM based tests $T_i(t)$ of the residual signals from Figure 5.9 are shown. The test $T_5(t)$ that represents the faulty sensor stands out from the other tests.

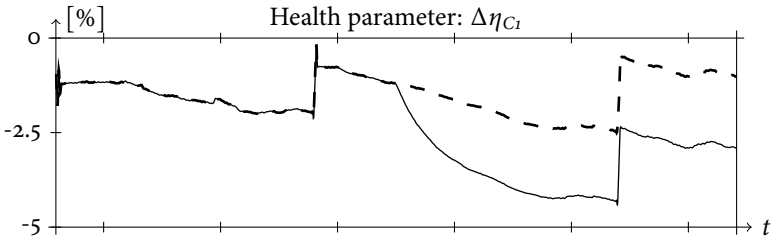

(a) Health parameter $\Delta\eta_{C1}$ for efficiency of compressor.

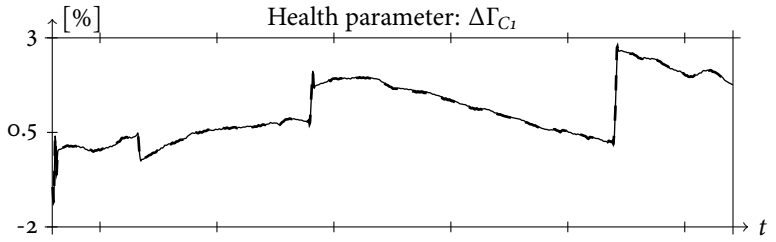

(b) Health parameter $\Delta\Gamma_{C1}$ for mass flow of compressor.

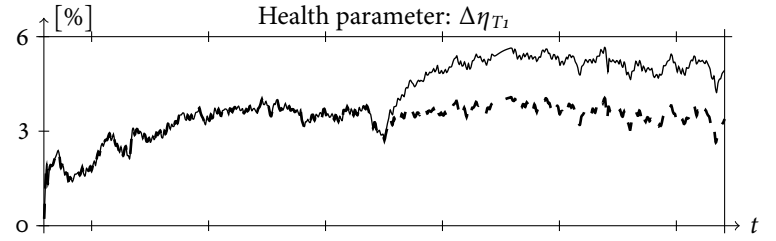

(c) Health parameter $\Delta\eta_{T1}$ for efficiency of compressor-turbine.

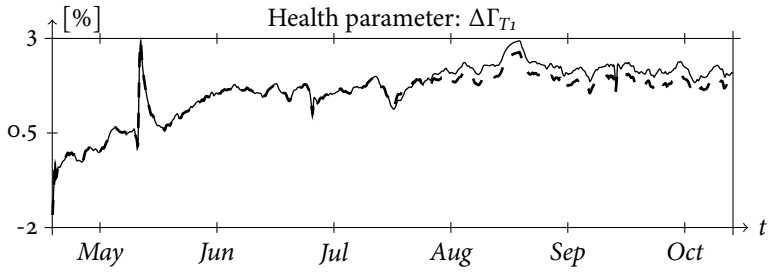

(d) Health parameter $\Delta\Gamma_{T1}$ for swollow capacity of compressor-turbine.

Figure 5.11: In the figure, health parameters of a faulty and a non-faulty sensor y_{T_3} are shown. The fault is introduced in the middle of July. The health parameters of efficiency are affected by the faulty sensor while the health parameters of flow capacity are not affected. The solid lines represent the faulty sensor case while the dashed lines are for the non-faulty sensor case.

service of the gas turbine is necessary to perform, without further normalization of the data.

5.5.3 Constant Gain Extended Kalman Filters

The last method is based on observer state estimations. First, in this method only relevant parts of the original performance model are considered in the observer, which leads to a smaller model. In an observer, the filtering of signals is encapsulated by the feedback term, so an external filter is not necessary. Benefits with this method are; (1) the modeling is more physical based since health parameters can be injected in the performance equations, (2) the efficiency estimation of the compressor is explicitly calculated, (3) this leads to estimation of the efficiency that is independent of the atmospheric conditions, (4) sensor diagnosis can be introduced, both with, and without decoupling sensors, and (5) observers are suitable for real time estimations since it is in an input-output form, (6) when the framework to generate observers is developed it is possible to generate diagnosis test in a relatively easy manner.

A disadvantage with the method is that the number of usable health parameters is limited since it is required that the system is observable. The health parameters injected in the compressor-turbine and power-turbine are difficult to interpret but they are needed for the sensor diagnosis, i.e., to get residuals that are around zero. Finally, it is difficult to know where in the model the health parameters should be injected but a *physical based guess* is to introduce these parameters in the performance equations.

5.6 Conclusion

In the chapter, a framework to develop observer based tests for performance estimation in an industrial gas turbine application is presented. These tests can be generated automatically in a systematic way for a chosen operational point, and for a suitable choice of the noise matrices Q and R. The constructed tests are based on constant gain extended Kalman filters (CGEKF) where the user can add a suitable choice of health parameters to a specified set of performance parameter equations or other relevant equations. The choice of health parameters affects the observability of the system, and a structural observability analysis shows that the considered health parameters in this study are structurally observable. The introduced health parameters have slow dynamic compared to the other state variables, except for the cases where the compressor is washed. The dynamic of the health parameters is slow since the performance degradation is a relatively slow process in general. This is achieved using two Kalman gains in the test quantity. Directly after a compressor wash, a switching between the two Kalman gains occur, and switching back after a number of time samples. The benefit with using slow varying health parameters is the ability to detect abrupt sensor faults in the measurement signals. It is possible to achieve fault isolation for the sensor fault, in a softer way, without decoupling any sensors. This can be achieved through the residual associated with the faulty sensor reacts stronger than in the other residuals.

The performance of the developed observer based test quantity is considered good. Before a compressor wash, the isentropic efficiency of the compressor has deteriorated about 2 % which indicates that a compressor wash can be necessary to perform. The benefit with the observer based method is the ability to separate the efficiency deterioration from other factors, e.g., ambient conditions. This results in test quantity where a static threshold can be used to trigger a compressor wash alarm, independently if it is summer or winter. The efficiency deterioration can also be separated from a deterioration in the other considered performance parameters.

In the chapter, a simulation study with two observers is performed where the ambient atmospheric weather condition is varied and the performance of the observers are investigated. In the study, the first observer compensates for changes in absolute humidity and the second observer does not compensate for changes in absolute humidity. The result of the study indicates that in the most extreme cases, a change in the ambient condition can be misinterpreted as a performance deterioration in the gas turbine. Thereby, using an observer by default that consider ambient conditions can be valuable.

Chapter 6

Conclusion

When designing a diagnosis and supervision system of an industrial gas turbine it is crucial to consider physical relationships such as mass and energy balances; thermodynamic gas properties such as enthalpy, heat capacity, and entropy; and performance characteristics of the gas turbine components. In the developed gas turbine model, the thermodynamic gas properties rely on the gas medium model and here are the NASA Glenn Coefficients used to describe the gas properties. The performance characteristics rely on look up tables, which are based on measurements by the manufacturer. All these gas turbine properties are encapsulated by the gas turbine model, which is constructed using the developed gas turbine library GTLib, implemented in the modeling language Modelica. The benefit with using GTLib is the reduction in model equations and states in the gas turbine model compared to the original gas turbine model developed by the company. The reduction depends largely on the using of the air/fuel ratio concept instead of the mass fraction of species as in the original model. The gas turbine model can be used for performance calculation and in the construction of a diagnosis and supervision system. In the diagnosis model, a number of estimation parameters so-called health parameters are introduced to capture performance deterioration in the gas turbine components; compressor, compressor-turbine, and power-turbine.

With the diagnosis model as a starting-point, diagnosis tests based on Constant Gain Extended Kalman Filters (CGEKF) can be generated automatically in a systematic way for a chosen operational point and for a suitable choice of the noise matrices Q and R using developed parsers for this work. The sub-models, which are considered in the diagnosis tests, are chosen using structural methods. Here, the whole over-determined part is considered in each diagnosis tests. Since the tests are based on observers, an observability analysis is necessary to performed. The observability analysis shows that the diagnosis model is not observable by default, but these unobservable modes disappear when the over-determined part of the diagnosis model is considered.

The constructed observers are evaluated on: (1) simulated data generated from the reference simulation platform when the ambient conditions and demanded power are

varied, and (2) one year of experimental data from a mechanical drive site in the Middle East. The environment conditions at the Middle East site are tough due to contaminants in the air, which results in frequently compressor washes. The conclusion from the simulation study is that large deviation in the ambient conditions affect the estimated health parameter in the same range as a fouled compressor, i.e., a deterioration of 1–2 %. To minimize the error depending on the change in ambient conditions, the observers can compensate for the deviation in ambient conditions. In the second test case, the health parameter that capture compressor efficiency deterioration gives estimation of the degradation within an interval of 2 percent independently of the winter or summer period. This gives the opportunity to have static thresholds for fouling detection in the diagnosis and supervision system. In the diagnosis system, sensor faults with faster dynamic than the introduced health parameters can be detected. Why the sensor faults need to have faster dynamic than the health parameters depends on the fact that the faulty sensor value is captured by the health parameters. If the sensor fault dynamic is faster than the health parameter dynamic the residual can be used for change detection. Here, the CUSUM algorithm, together with a suitable threshold is used to detect the sensor fault.

References

G. F. Aker and H. I. H. Saravanamuttoo. Predicting gas turbine performance degradation due to compressor fouling using computer simulation techniques. *Journal of Engineering for Gas Turbines and Power*, 111(2):343–350, 1989. doi:10.1115/1.3240259. URL `http://link.aip.org/link/?GTP/111/343/1`.

Per Andersson. *Air Charge Estimation in Turbocharged Spark Ignition Engines*. PhD thesis, Linköpings Universitet, December 2005. URL `http://www.vehicular.isy.liu.se/Publications/PhD/05_PhD_989_PA.pdf`.

Uri M. Ascher and Linda R. Petzold. *Computer Methods for Ordinary Differential Equations and Differential-Algebraic Equations*. Society for Industrial and Applied Mathematics, Philadelphia, PA, USA, 1st edition, 1998. ISBN 0898714125.

J. Bird and W. Grabe. Humidity effects on gas turbine performance. In *International Gas Turbine and Aeroengine Congress and Exposition*, Orlando, FL, 1991.

M. Blanke, M. Kinnaert, J. Lunze, and M. Staroswiecki. *Diagnosis and Fault-Tolerant Control*. Springer, 2003.

S. Borguet and O. Léonard. A sensor-fault-tolerant diagnosis tool based on a quadratic programming approach. *Journal of Engineering for Gas Turbines and Power*, 130(2): 021605, 2008. doi:10.1115/1.2772637. URL `http://link.aip.org/link/?GTP/130/021605/1`.

Gary L. Borman and Kenneth W. Ragland. *Combustion Engineering*. McGraw-Hill, 1998. ISBN 0-07-006567-5.

Olaf Brekke, Lars E. Bakken, and Elisabet Syverud. Compressor fouling in gas turbines offshore: Composition and sources from site data. *ASME Conference Proceedings*, 2009 (48869):381–391, 2009. doi:10.1115/GT2009-59203. URL `http://link.aip.org/link/abstract/ASMECP/v2009/i48869/p381/s1`.

Arden L. Buck. New equations for computing vapor pressure and enhancement factor. *Journal of Applied Meterology*, 20:1529, 1981.

E. Buckingham. On physically similar systems; illustrations of the use of dimensional equations. *Phys. Rev.*, 4(4):345–376, Oct 1914. doi:10.1103/PhysRev.4.345.

Francesco Casella, Martin Otter, Katrin Proelss, Christoph Richter, and Hubertus Tummescheit. The modelica fluid and media library for modeling of incompressible and compressible thermo-fluid pipe networks. *The 5th International Modelica Conference 2006*, 2006.

Malcolm W. Chase, Jr, editor. *NIST-JANAF Thermochemical Tables*, volume Part 1 and Part 2 of *Journal of Physical and Chemical Reference Data*. American Institute of Physics, 500 Sunnyside Boulevard, Woodbury, New York, fourth edition, 1998. ISBN 1-56396-831-2.

J. Chen and R.J Patton. *Robust Model-Based Fault Diagnosis for Dynamic Systems*. Kluwer Academic Publishers, 1999. ISBN 0-7923-8411-3.

P. Dewallef, C. Romessis, O. Léonard, and K. Mathioudakis. Combining classification techniques with kalman filters for aircraft engine diagnostics. *Journal of Engineering for Gas Turbines and Power*, 128(2):281–287, 2006. doi:10.1115/1.2056507. URL `http://link.aip.org/link/?GTP/128/281/1`.

I. S. Diakunchak. Performance deterioration in industrial gas turbines. *Journal of Engineering for Gas Turbines and Power*, 114(2):161–168, 1992. doi:10.1115/1.2906565. URL `http://link.aip.org/link/?GTP/114/161/1`.

S.L. Dixon and Cesare Hall. *Fluid Mechanics and Thermodynamics of Turbomachinery*. Elsevier, 6th edition edition, 2010. ISBN 978-1-85617-793-1.

D. L. Doel. Temper—a gas-path analysis tool for commercial jet engines. *Journal of Engineering for Gas Turbines and Power*, 116(1):82–89, 1994. doi:10.1115/1.2906813. URL `http://link.aip.org/link/?GTP/116/82/1`.

D. L. Doel. Interpretation of weighted-least-squares gas path analysis results. *Journal of Engineering for Gas Turbines and Power*, 125(3):624–633, 2003. doi:10.1115/1.1582492. URL `http://link.aip.org/link/?GTP/125/624/1`.

A. L. Dulmage and N. S. Mendelsohn. Coverings of bipartite graphs. *Canadian Journal of Mathematics*, 10:517–534, 1958.

Thomas D. Eastop and Allan McConkey. *Applied Thermodynamics for Engineering Technologists*. Prentice Hall, 5th edition, 1993. ISBN 0-582-09193-4.

Lars Eriksson. CHEPP – A chemical equilibrium program package for matlab. In *Modeling of Spark Ignition Engines*, number 2004-01-1460 in SAE Technical paper series SP-1830, 2004. doi:10.4271/2004-01-1460.

Erik Frisk, Mattias Krysander, and Jan Åslund. Sensor placement for fault isolation in linear differential-algebraic systems. *Automatica*, 45(2):364–371, 2009. doi:10.1016/j.automatica.2008.08.013.

Peter Fritzson. *Principles of Object-Oriented Modeling and Simulation with Modelica 2.1*. Wiley, 2004.

Ranjan Ganguli and Budhadipta Dan. Trend shift detection in jet engine gas path measurements using cascaded recursive median filter with gradient and laplacian edge detector. *Journal of Engineering for Gas Turbines and Power*, 126(1):55–61, 2004. doi:10.1115/1.1635400. URL `http://link.aip.org/link/?GTP/126/55/1`.

Tony Giampaolo. *Gas Turbine Handbook: Principles and Practice*. The Fairmont Press, 4th edition edition, 2009. ISBN 0-88173-613-9.

Sanford Gordon and Bonnie J. McBride. Computer program for calculation of complex chemical equilibrium compositions, rocket performance, incident and reflected shocks, and chapman-jouguet detonations. interim revision, march 1976. Technical Report SP-273, National Aeronautics and Space Administration (NASA), 1971. URL `http://ntrs.nasa.gov/search.jsp?print=yes&R=19780009781`.

Sanford Gordon and Bonnie J. McBride. Computer program for calculation of complex chemical equilibrium compositions and applications i. analysis. Technical Report RP-1311, National Aeronautics and Space Administration (NASA), 1994. URL `http://www.grc.nasa.gov/WWW/CEAWeb/RP-1311.htm`.

A. A. El Hadik. The impact of atmospheric conditions on gas turbine performance. *Journal of Engineering for Gas Turbines and Power*, 112(4):590–596, 1990. doi:10.1115/1.2906210. URL `http://link.aip.org/link/?GTP/112/590/1`.

E. Hairer, S. P. Norsett, and G. Wanner. *Solving Ordinary Differential Equations II: Stiff and Differential-Algebraic Problems*. Springer, Berlin, 2nd revised edition edition, 1991.

John B. Heywood. *Internal Combustion Engine Fundamentals*. McGraw-Hill series in mechanical engineering. McGraw-Hill, 1988. ISBN 0-07-100499-8.

J. H. Horlock. *Advanced Gas Turbine Cycles*. Pergamon, revised edition edition, 2007.

A Idebrant and Lennart Näs. Gas Turbine Applications using Thermofluid. In Peter Fritzson, editor, *Proceedings of the 3rd International Modelica Conference*, pages 359–366. The Modelica Association, May 2003.

Thomas Kailath. *Linear Systems*. Prentice-Hall, Inc, Englewood Cliffs, New Jersey 07632, 1980.

Thomas Kailath, Ali H. Sayed, and Babak Hassibi. *Linear Estimation*. Prentice-Hall, Inc, Upper Saddle River, New Jersey 07458, 2 edition, 2000.

Takahisa Kobayashi and Donald L. Simon. *Application of a Bank of Kalman Filters for Aircraft Engine Fault Diagnostics*. NASA/TM-2003-212526, 2003. URL `http://ntrs.nasa.gov/search.jsp?print=yes&R=20030067984`.

Takahisa Kobayashi, Donald L. Simon, and Jonathan S. Litt. *Application of a Constant Gain Extended Kalman Filter for In-Flight Estimation of Aircraft Engine Performance Parameters*. NASA/TM-2005-213865, 2005. URL http://ntrs.nasa.gov/search.jsp?print=yes&R=20050216398.

Mattias Krysander, Jan Åslund, and Mattias Nyberg. An efficient algorithm for finding minimal over-constrained sub-systems for model-based diagnosis. *IEEE Transactions on Systems, Man, and Cybernetics – Part A: Systems and Humans*, 38(1), 2008.

R. Kurz and K. Brun. Degradation in gas turbine systems. *Journal of Engineering for Gas Turbines and Power*, 123(1):70–77, 2001. doi:10.1115/1.1340629. URL http://link.aip.org/link/?GTP/123/70/1.

Rainer Kurz, Klaus Brun, and Meron Wollie. Degradation effects on industrial gas turbines. *Journal of Engineering for Gas Turbines and Power*, 131(6):062401, 2009. doi:10.1115/1.3097135. URL http://link.aip.org/link/?GTP/131/062401/1.

Emil Larsson, Jan Åslund, Erik Frisk, and Lars Eriksson. Fault isolation for an industrial gas turbine with a model-based diagnosis approach. *ASME Conference Proceedings*, 2010(43987):89–98, 2010. doi:10.1115/GT2010-22511. URL http://link.aip.org/link/abstract/ASMECP/v2010/i43987/p89/s1.

Emil Larsson, Jan Åslund, Erik Frisk, and Lars Eriksson. Health monitoring in an industrial gas turbine application by using model based diagnosis techniques. In *ASME Turbo Expo 2011-GT2011*, Vancouver, Canada, 2011. ASME.

R H Luppold, J R Roman, G W Gallops, and L J Kerr. Estimating in-flight engine performance variations using kalman filter concepts. In *25th Joint Propulsion Conference*, Monterey, USA, 1989. 2584-AIAA.

R. Martínez-Guerra, R. Garrido, and A. Osorio-Miron. The fault detection problem in nonlinear systems using residual generators. *IMA Journal of Mathematical Control and Information*, 22(2):119–136, 2005. doi:10.1093/imamci/dni010.

K. Mathioudakis and T. Tsalavoutas. Uncertainty reduction in gas turbine performance diagnostics by accounting for humidity effects. *Journal of Engineering for Gas Turbines and Power*, 124(4):801–808, 2002. doi:10.1115/1.1470485. URL http://link.aip.org/link/?GTP/124/801/1.

Bonnie J. McBride and Sanford Gordon. Computer program for calculating and fitting thermodynamic functions. Technical Report RP-1271, National Aeronautics and Space Administration (NASA), 1992. URL http://www.grc.nasa.gov/WWW/CEAWeb/RP-1271.htm.

Bonnie J. McBride, Michael J. Zehe, and Sanford Gordon. Nasa glenn coefficients for calculating thermodynamic properties of individual species. Technical Report TP-2002-211556, National Aeronautics and Space Administration (NASA), 2002. URL http://www.grc.nasa.gov/WWW/CEAWeb/TP-2002-21556.htm.

C.B. Meher-Homji. Compressor and hot section fouling in gas turbines – causes and effects. In *Industrial Energy Conference*, Houstion, TX, 1987.

E. A. Misawa and J. K. Hedrick. Nonlinear observers—a state-of-the-art survey. *Journal of Dynamic Systems, Measurement, and Control*, 111(3):344–352, 1989. doi:10.1115/1.3153059. URL `http://link.aip.org/link/?JDS/111/344/1`.

Modelica Association. The Modelica Language Specification version 3.0, 2007. URL `http://www.modelica.org/`.

H. Nijmeijer and T.I. Fossen. *New directions in nonlinear observer design*. Lecture notes in control and information sciences. Springer, 1999. ISBN 9781852331344.

Ramine Nikoukhah. Innovations generation in the presence of unknown inputs: Application to robust failure detection. *Automatica*, 30(12):1851 – 1867, 1994. ISSN 0005-1098. doi:10.1016/0005-1098(94)90047-7.

Per Öberg. *A DAE Formulation for Multi-Zone Thermodynamic Models and its Application to CVCP Engines*. PhD thesis, Linköpings universitet, 2009. URL `http://www.fs.isy.liu.se/Publications/PhD/09_PhD_1257_PO.pdf`.

E.S. Page. Continuous inspection schemes. *Biometrika*, 41:100–115, 1954.

Constantinos C. Pantelides. The consistent initialization of differential-algebraic systems. *SIAM J. Sci. Stat. Comput.*, 9(2):213–231, 1988.

R.J. Patton and M. Hou. Design of fault detection and isolation observers: A matrix pencil approach. *Automatica*, 34(9):1135 – 1140, 1998. ISSN 0005-1098. doi:10.1016/S0005-1098(98)00043-0.

Randal T. Rausch, Kai F. Goebel, Neil H. Eklund, and Brent J. Brunell. Integrated in-flight fault detection and accommodation: A model-based study. *Journal of Engineering for Gas Turbines and Power*, 129(4):962–969, 2007. doi:10.1115/1.2720517. URL `http://link.aip.org/link/?GTP/129/962/1`.

M. Safonov and M. Athans. Robustness and computational aspects of nonlinear stochastic estimators and regulators. *Automatic Control, IEEE Transactions on*, 23(4):717 – 725, aug 1978. ISSN 0018-9286. doi:10.1109/TAC.1978.1101825.

H.I.H. Saravanamuttoo, G.F.C. Rogers, and H. Cohen. *Gas Turbine Theory*. Longman, 5th edition edition, 2001. ISBN 0-13-015847-X.

J.N. Scott. Reducing turbo machinery operation costs with regular performance testing. In *International Gas Turbine Conference and Exhibit*, Dusseldorf, Germany, 1986.

R. Shields and J. Pearson. Structural controllability of multiinput linear systems. *Automatic Control, IEEE Transactions on*, 21(2):203 – 212, apr 1976. ISSN 0018-9286. doi:10.1109/TAC.1976.1101198.

Donald L. Simon, Jeff Bird, Craig Davison, Al Volponi, and R. Eugene Iverson. Benchmarking gas path diagnostic methods: A public approach. *ASME Conference Proceedings*, 2008(43123):325–336, 2008. doi:10.1115/GT2008-51360. URL http://link.aip.org/link/abstract/ASMECP/v2008/i43123/p325/s1.

N. Sugiyama. System identification of jet engines. *Journal of Engineering for Gas Turbines and Power*, 122(1):19–26, 2000. doi:10.1115/1.483172. URL http://link.aip.org/link/?GTP/122/19/1.

Carl Svärd and Mattias Nyberg. Observer-based residual generation for linear differential-algebraic equation systems. In *IFAC World Congress*, Seoul, Korea, 2008.

Mizuyo Takamatsu and Satoru Iwata. Index reduction for differential-algebraic equations by substitution method. *Linear Algebra and its Applications*, 429(8-9):2268 – 2277, 2008. ISSN 0024-3795. doi:10.1016/j.laa.2008.06.025.

Michael Tiller. *Introduction to Physical Modeling with Modelica*. Kluwer Academic Publishers, Norwell, MA, USA, 2001. ISBN 0792373677.

Stephen R. Turns. *An Introduction to Combustion – Concepts and Applications*. Mechanical Engineering Series. McGraw Hill, second edition, 2000.

L. A. Urban. *Gas Turbine Engine Parameter Interrelationships*. Windsor Locks, 1969.

L. A. Urban. Gas path analysis applied to turbine engine condition monitoring. *Journal of Aircraft*, 10(7):400–406, 1972.

A. J. Volponi. Gas turbine parameter corrections. *Journal of Engineering for Gas Turbines and Power*, 121(4):613–621, 1999. doi:10.1115/1.2818516. URL http://link.aip.org/link/?GTP/121/613/1.

A. J. Volponi. *Foundation of Gas Path Analysis (Part I and II)*. von Karman Institute Lecture Series: Gas Turbine Condition Monitoring and Fault Diagnosis, January 2003a.

A. J. Volponi, H. DePold, R. Ganguli, and C. Daguang. The use of kalman filter and neural network methodologies in gas turbine performance diagnostics: A comparative study. *Journal of Engineering for Gas Turbines and Power*, 125(4):917–924, 2003. doi:10.1115/1.1419016. URL http://link.aip.org/link/?GTP/125/917/1.

A.J. Volponi. Gas turbine condition monitoring & fault diagnosis. In *Lecture Series 2003-01*. von Karman Insitute for Fluid Dynamics, 2003b.

Appendix A

Mole/Mass Conversions

A.1 Mole/Mass Fraction Calculation

Mole, and mass fraction conversion appears at different places in the thesis. Here will these calculations be summarized.

Mole Mass

The mole mass of a mixture with mole concentration $\tilde{x} \in \mathbb{R}^n$, is defined as the sum of the elements:

$$\mathrm{M} = \sum_i \mathrm{M}_i \tilde{x}_i \tag{A.1}$$

where M_i is the mole mass for species i, and the sum over all species is $\sum_i \tilde{x}_i = 1$. The mole mass expressed in mass concentration $x \in \mathbb{R}^n$ can be written:

$$\frac{1}{\mathrm{M}} = \sum_i \frac{x_i}{\mathrm{M}_i} \tag{A.2}$$

To convert between mass and mole fraction, following formulas are valid:

Mole fraction → Mass fraction

$$x_i = \frac{m_i}{m} = \frac{\mathrm{M}_i}{\sum_i \mathrm{M}_i \tilde{x}_i} \tilde{x}_i = \frac{\mathrm{M}_i}{\mathrm{M}} \tilde{x}_i \tag{A.3}$$

where m_i is the mass of species i, and m is the total mass. In the last step, (A.1) is used.

Mass fraction → Mole fraction

$$\tilde{x}_i = \frac{n_i}{n} = \frac{1/\mathrm{M}_i}{\sum_i x_i/\mathrm{M}_i} x_i = \frac{1/\mathrm{M}_i}{1/\mathrm{M}} x_i \tag{A.4}$$

where n_i is the number of moles of species i. In the last step, (A.2) is used.

A.2 Stoichiometry Matrix Expressed in Mass

The stoichiometry matrix, expressed in mole, repeated from (2.30) is:

$$\tilde{S} = \begin{pmatrix} 0 & 0 & 0 & 0 & 0 \\ 1 & 2 & 3 & 1 & 0 \\ 2 & 3 & 4 & 0 & 0 \\ 0 & 0 & 0 & 0 & 1 \\ -2 & -3.5 & -5 & 0 & 0 \end{pmatrix}$$

where the rows represent the species: Ar, CO_2, H_2O, N_2, and O_2 according to the air vector x_a in (2.28). The columns represent the species: CH_4, C_2H_6, C_3H_8, CO_2, and N_2 according to the fuel vector x_f in (2.28). Expression (A.3) can now be utilized for each matrix element to get:

$$S = \begin{pmatrix} 0 & 0 & 0 & 0 & 0 \\ \frac{M_{CO_2}}{M_{CH_4}} & 2\frac{M_{CO_2}}{M_{C_2H_6}} & 3\frac{M_{CO_2}}{M_{C_3H_8}} & 1 & 0 \\ 2\frac{M_{H_2O}}{M_{CH_4}} & 3\frac{M_{H_2O}}{M_{C_2H_6}} & 4\frac{M_{H_2O}}{M_{C_3H_8}} & 0 & 0 \\ 0 & 0 & 0 & 0 & 1 \\ -2\frac{M_{O_2}}{M_{CH_4}} & -3.5\frac{M_{O_2}}{M_{C_2H_6}} & -5\frac{M_{O_2}}{M_{C_3H_8}} & 0 & 0 \end{pmatrix} \tag{A.5}$$

where the stoichiometric matrix now is expressed in masses instead of moles.

A.3 Determination of Stoichiometric Air/Fuel Ratio

Reaction formula (2.32) represents a combustion, and is expressed in masses:

$$m_a x_a + m_f x_f \rightarrow m_a x_a + m_f S x_f \tag{A.6}$$

where S is the stoichiometric matrix from (A.5). The stoichiometric air/fuel ratio appears when it is just enough oxygen in the reaction, i.e., the last row in (A.6) that represents oxygen is equal to zero and can be solved. The last line can be written:

$$m_a x_{a,O_2} = m_f \left(2\frac{M_{O_2}}{M_{CH_4}} x_{f,CH_4} + 3.5\frac{M_{O_2}}{M_{C_2H_6}} x_{f,C_2H_6} + 5\frac{M_{O_2}}{M_{C_3H_8}} x_{f,C_3H_8} \right)$$

which can be rewritten in form:

$$\frac{m_a}{m_f} = \frac{2\frac{x_{f,CH_4}}{M_{CH_4}} + 3.5\frac{x_{f,C_2H_6}}{M_{C_2H_6}} + 5\frac{x_{f,C_3H_8}}{M_{C_3H_8}}}{\frac{x_{a,O_2}}{M_{O_2}}} \equiv \left(\frac{m_a}{m_f}\right)_s \tag{A.7}$$

which is the definition of $(A/F)_s$.

Appendix B

Measurement Plots

In this appendix, additional experimental data plots are viewed. These plots are the ambient temperature T_0, the ambient pressure p_0, the shaft speed of the gas generator n_{GG} and the generated power by the external application P.

B.1 Ambient Temperature T_0

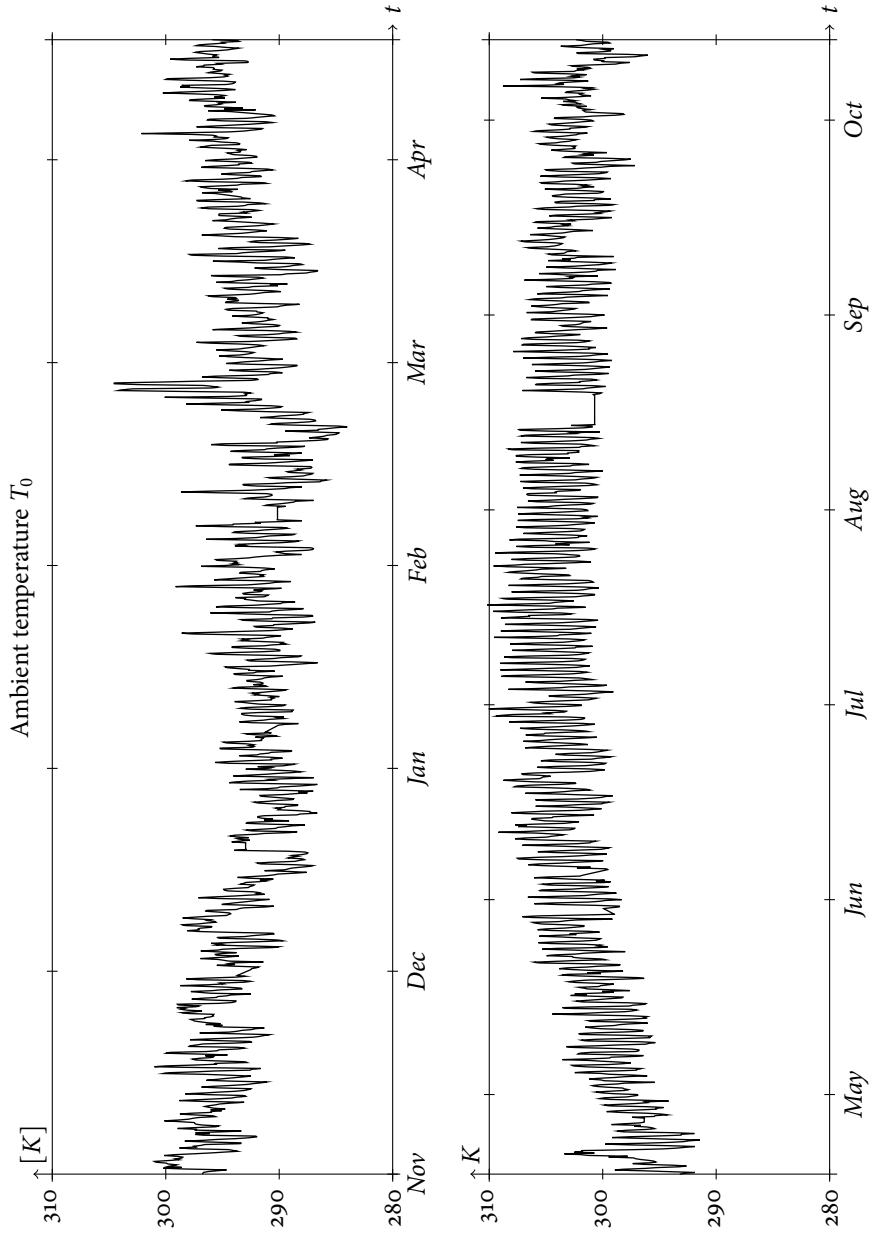

(a) The first six-month period Nov–Apr.

(b) The second six-month period May–Oct.

Figure B.1: The mean ambient temperature varies according to winter and summer. In the end of February, the mean ambient temperature rises for a couple of days, which affect the calculated measurement temperature deltas.

B.2 Ambient pressure p_0

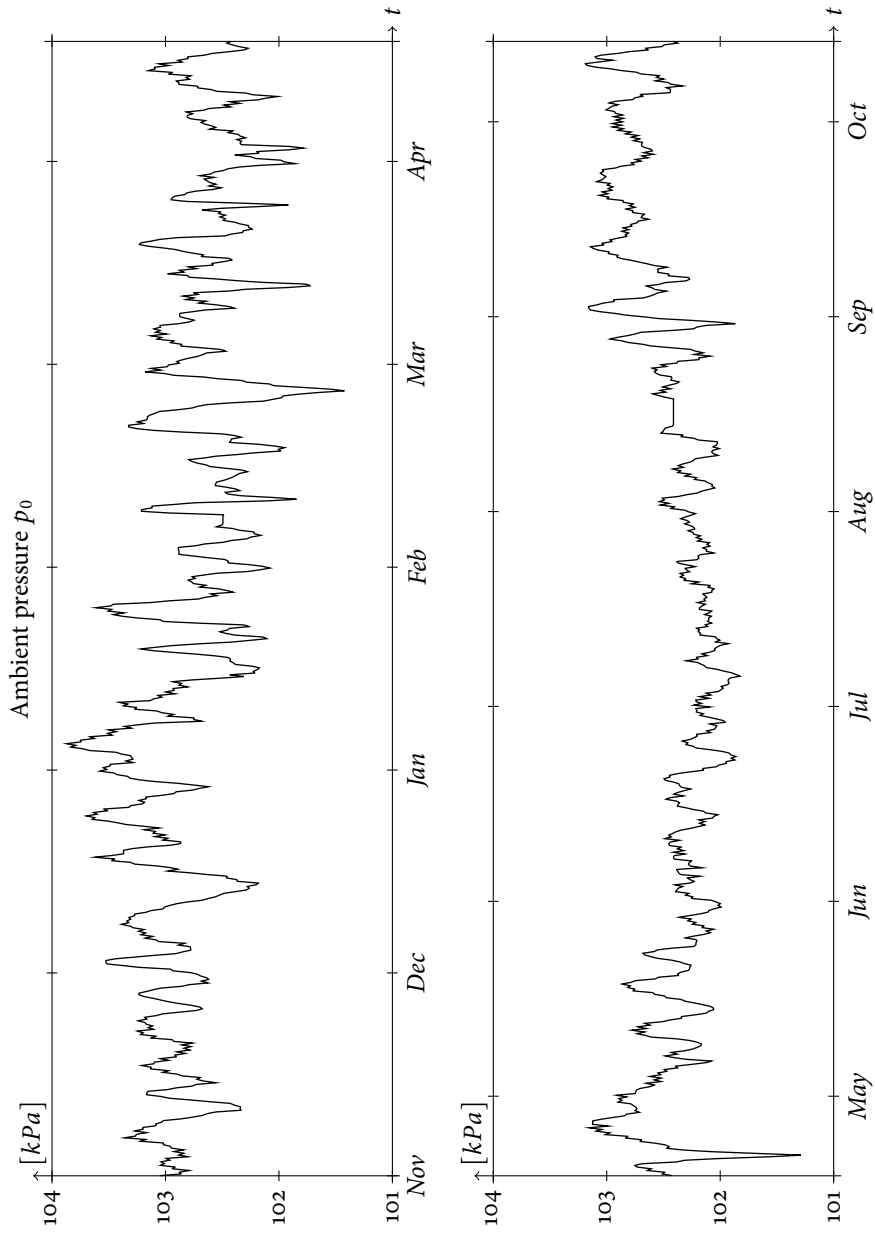

(a) The first six-month period Nov–Apr.

(b) The second six-month period May–Oct.

Figure B.2: Ambient pressure p_0 for one year of experimental data.

B.3 Shaft Speed n_{C1} of the Gas Generator

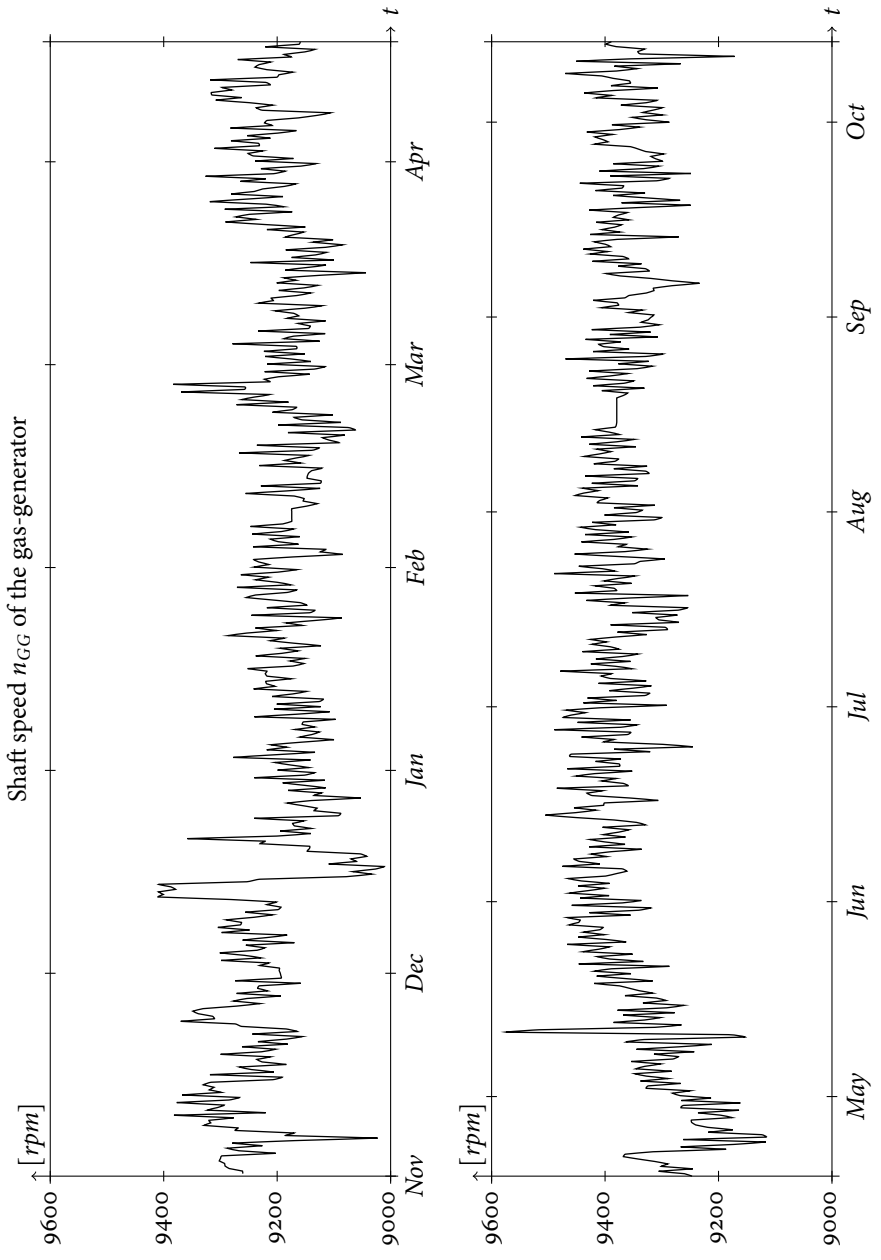

(a) The first six-month period Nov–Apr.

(b) The second six-month period May–Oct.

Figure B.3: Shaft speed n_{GG} of the gas generator for one year of experimental data.

B.4 Generated Power by the Application

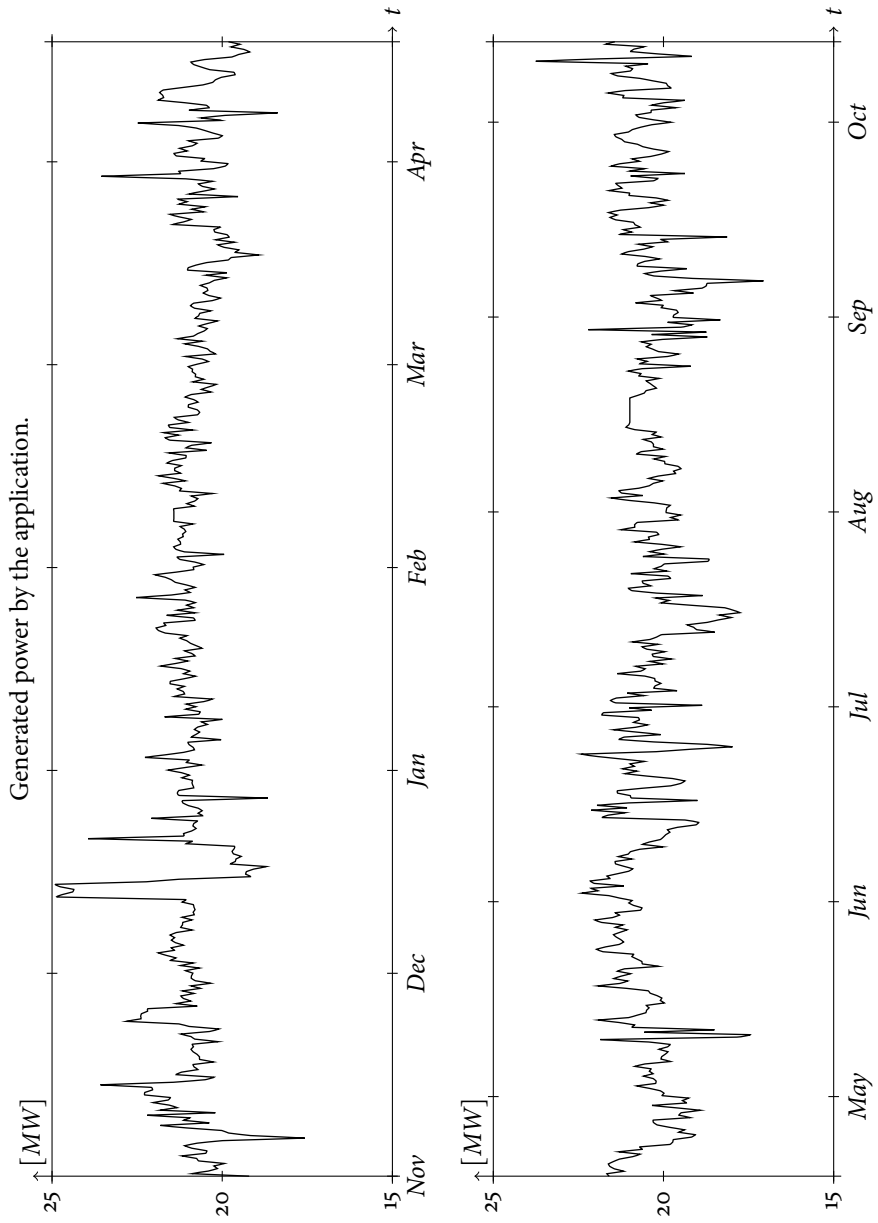

(a) The first six-month period Nov–Apr.

(b) The second six-month period May–Oct.

Figure B.4: Generated power by the application for one year of experimental data.

Appendix C

Health Parameter Plots

In this appendix, considered health parameters in the observers which are not viewed in Chapter 5 are viewed here. These health parameters are; flow capacity of compressor $\Delta\Gamma_{C1}$, efficiency of compressor-turbine $\Delta\eta_{T1}$, flow capacity of compressor-turbine $\Delta\Gamma_{T1}$, and efficiency of power-turbine $\Delta\eta_{To}$. The health parameters are viewed for the two observer cases: (1) fast observer dynamic – solid lines, and (2) slow observer dynamic, except after a compressor wash, – dotted lines. As can be seen in the figures, it can be difficult to interpret what the actual physical meaning of the parameters really is. For the flow capacity degradation of the compressor, the performance increases after a compressor wash. The level of performance reduction varies during the data sequence, which results in thresholds used for fouling detection that are not constant.

For the health parameters of efficiency in the compressor-turbine $\Delta\eta_{T1}$ and in the power-turbine $\Delta\eta_{To}$, a reduction in one of the parameters is compensated with an expansion in the other parameter. It also seems that they are correlated with the ambient temperature.

C.1 $\Delta\Gamma_{C1}$ – Flow Deviation of *C1*

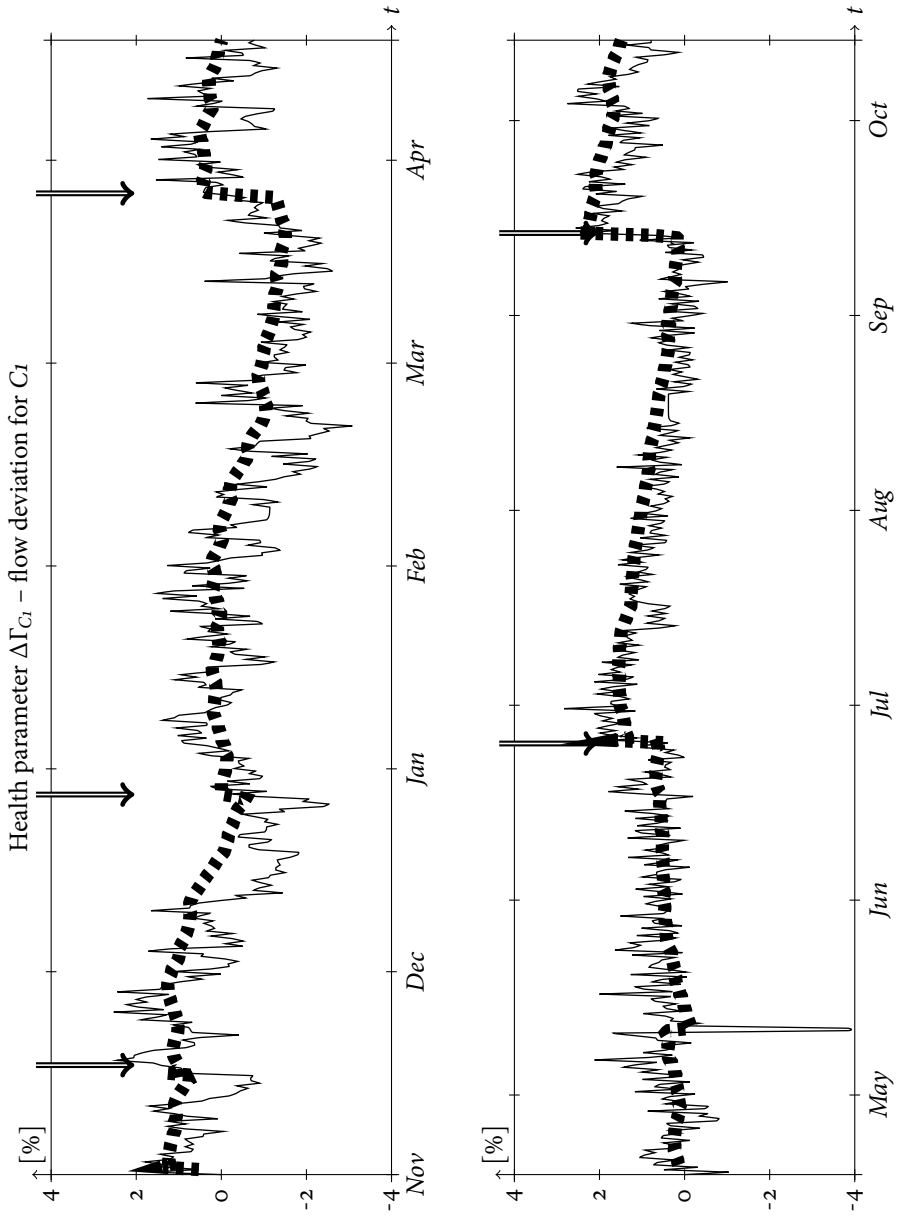

(a) The first six-month period Nov–Apr.

(b) The second six-month period May–Oct.

Figure C.1: In the figure, the estimated deviation for the compressor flow capacity from a nominal reference value is shown for a time interval of one year. Compressor washes are marked with arrows in the subfigures.

C.2 $\Delta\eta_{T1}$ – Efficiency Deviation of *T1*

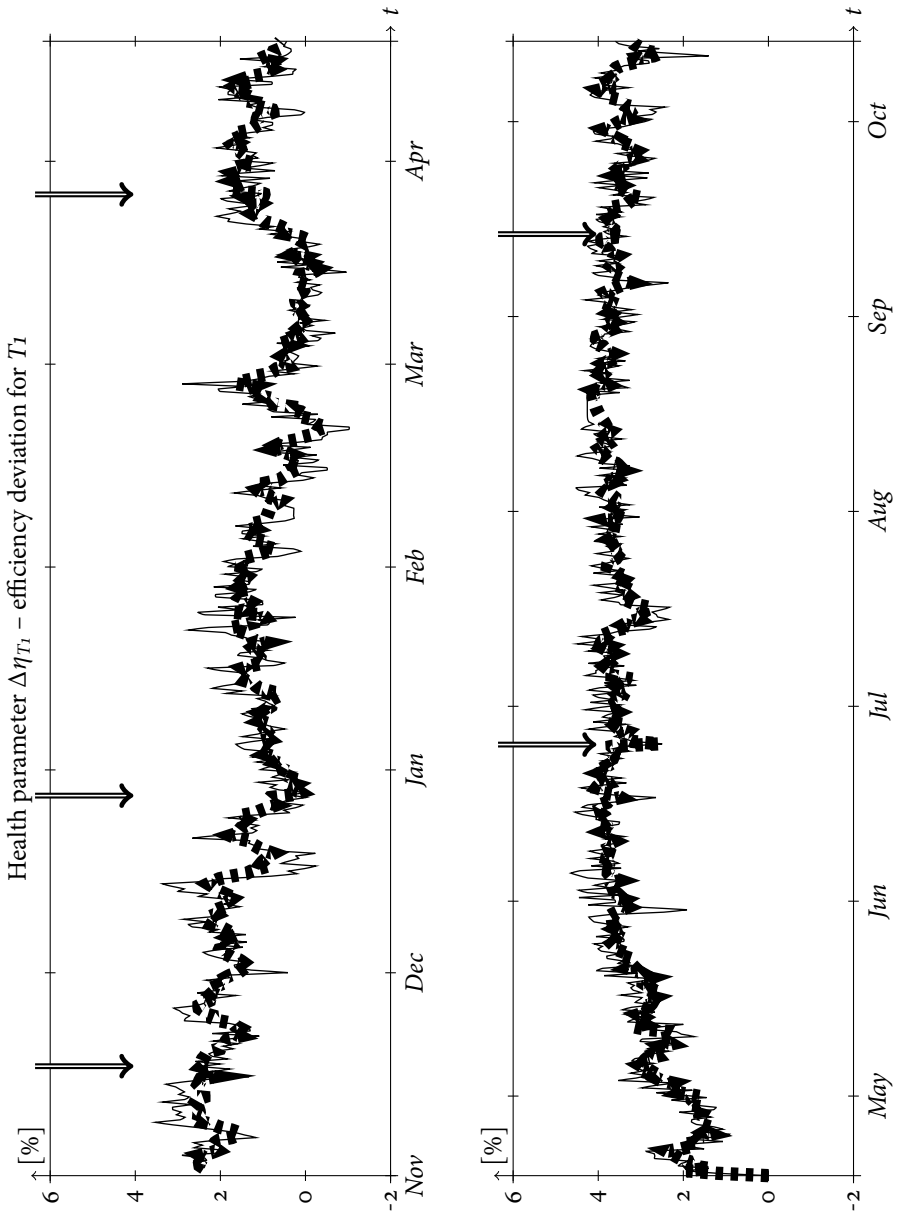

(a) The first six-month period Nov–Apr. **(b)** The second six-month period May–Oct.

Figure C.2: In the figure, the estimated deviation for the compressor-turbine efficiency from a nominal reference value is shown for a time interval of one year. Compressor washes are marked with arrows in the subfigures.

C.3 $\Delta\Gamma_{T1}$ – Flow Deviation of *T1*

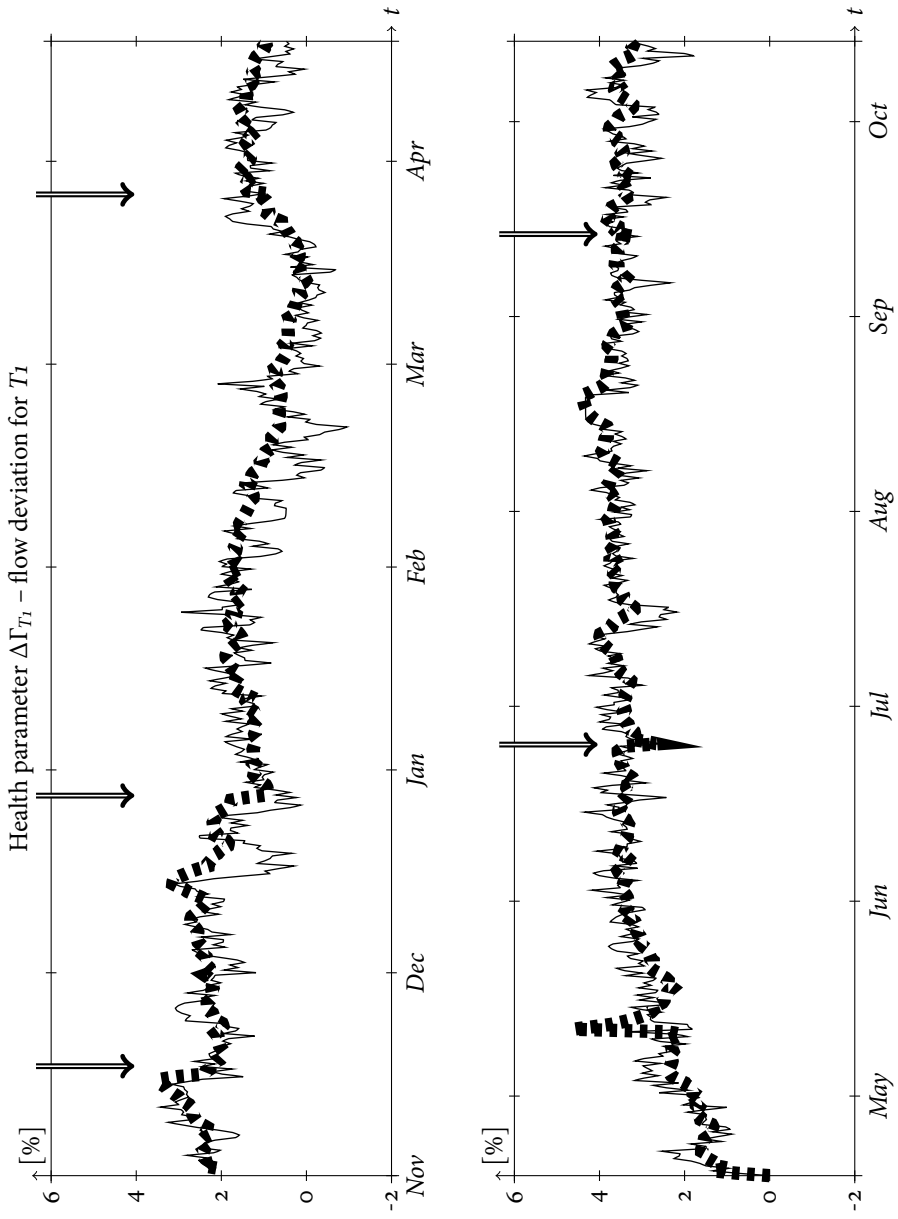

(a) The first six-month period Nov–Apr.

(b) The second six-month period May–Oct.

Figure C.3: In the figure, the estimated deviation for the compressor-turbine flow capacity from a nominal reference value is shown for a time interval of one year. Compressor washes are marked with arrows in the subfigures.

C.4 $\Delta\eta_{To}$ – Efficiency Deviation of *To*

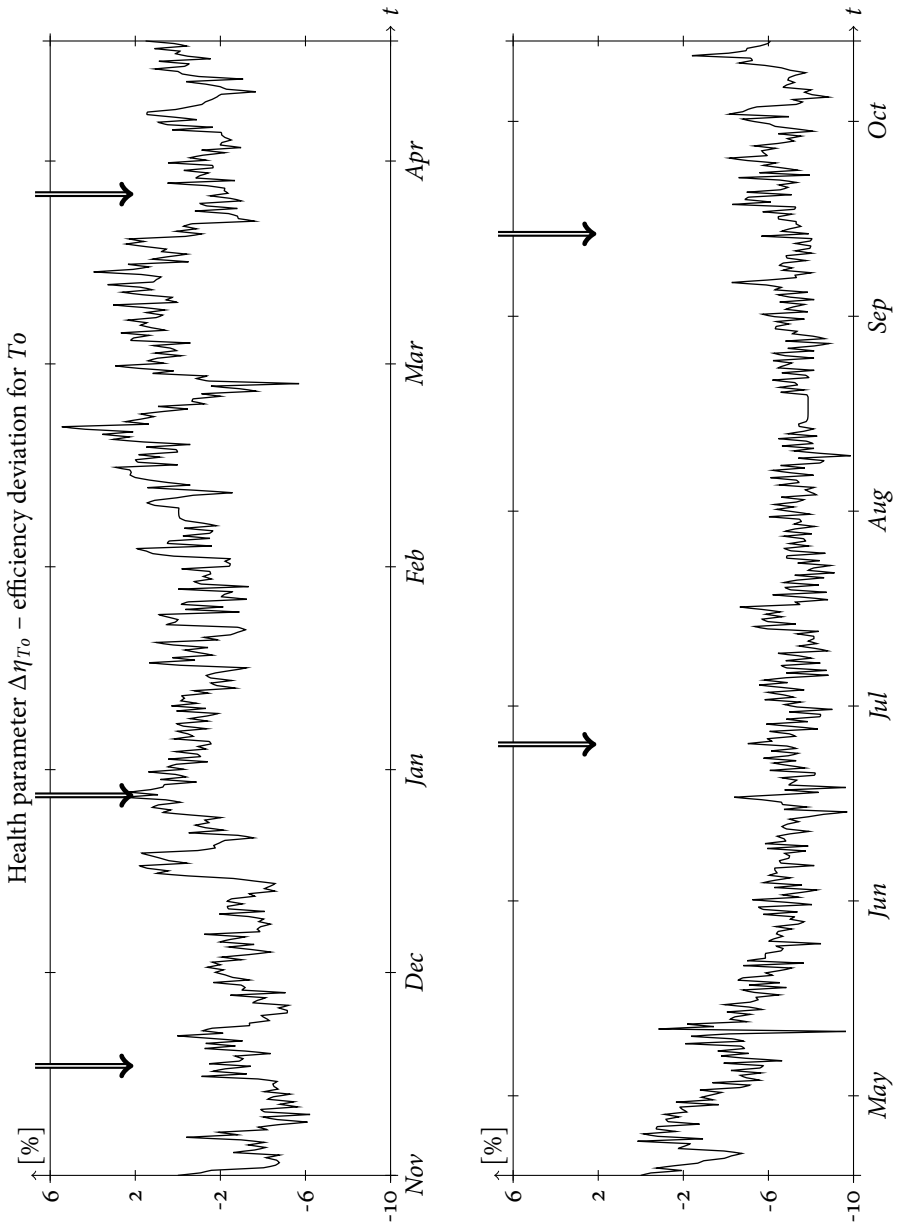

(a) The first six-month period Nov–Apr.

(b) The second six-month period May–Oct.

Figure C.4: In the figure, the estimated deviation for the power-turbine efficiency from a nominal reference value is shown for a time interval of one year. Compressor washes are marked with arrows in the subfigures.